Eight-Step Global Kinetic Mechanism on Methane Oxidation with Nitric Oxide Formation for Lean-Premixed Combustion Turbines

Igor V. Novosselov

A thesis submitted in partial fulfillment of the requirement for the degree of

Master of Science in Mechanical Engineering

University of Washington

2001

Program Authorized to offer Degree: Mechanical Engineering

University of Washington

Graduate School

This is to certify that I have examined this copy of a master's thesis by

Igor V. Novosselov

and have found that it is complete and satisfactory in all respects,
and that any and all revisions required by the final
examining committee have been made.

Committee Members:

_____
Philip C. Malte

_____
John C. Kramlich

_____
David G. Nicol

Date: _____

I presenting this thesis in partial fulfillment of the requirements for a Master's degree at the University of Washington, I agree that the library shall make its copies freely available for inspection. I further agree that extensive copying of this thesis is allowable only for scholarly purposes, consistent with "fail use" as prescribed in the U.S. Copyright Law. Any other reproduction for any purposes or by any means shall not be allowed without my written permission.

Signature_____

Date_____

University of Washington

Abstract

Eight-Step Global Kinetic Mechanism on Methane Oxidation with Nitric Oxide Formation for Lean-Premixed Combustion Turbines

Igor V. Novosselov

Chair of supervisory committee:
Professor Philip C. Malte

An eight-step, pressure-sensitive global mechanism for methane oxidation with nitric oxide formation for CFD simulation of lean-premixed combustion is developed and validated in the present thesis. The global mechanism is based on the detailed chemical kinetic mechanism GRI 3.0 and covers the pressure range from 5 to 20 atmospheres and the fuel-air equivalence ratio range from 0.45 to 0.8. The mechanism includes: three reactions for hydrocarbon oxidation, two reactions for nitric oxide formation via non-equilibrium free radical chemistry, and three reactions for NO formation in zones of the equilibrium free radical chemistry. The four major pathways of NO formation are simulated by the global mechanism: NNH, prompt, nitrous oxide, and Zeldovich.

The new eight step global mechanism is validated by comparing results obtained with it in chemical reactor modeling against the experimental data for high-pressure jet-stirred reactors. The comparison shows that the eight-step global mechanism provides good agreement with GRI 3.0 and with the experimental data for the cases with preheated inlet air (an assumption used in the development of the global mechanism). Additional validation of the eight-step global mechanism is obtained by employing it in a chemical reactor network simulation of a gas turbine combustor. The eight-step

global mechanism is also tested in the CFD simulation of the gas turbine combustor. The results of the CFD modeling show good agreement of CO and NO exit plane emission with the experimental data for premixer fuel-air equivalence ratios in the vicinity of 0.6.

TABLE OF CONTENTS

LIST OF FIGURES

LIST OF TABLES

Acknowledgments

We wish to acknowledge and express appreciation for the financial support and encouragement provided for this research by Ansaldo Ricerche s. r. l., especially Dr. Giulio Mori, and by Solar Turbines, Inc., especially Dr. Kenneth O. Smith. Also thanked are Dr. David G. Nicol and Professor John C. Kramlich for advising on the MSME committee of Mr. Igor V. Novosselov.

Chapter 1

Introduction and Objectives

1.1 Introduction

In light of increasing environmental concerns on one hand and growing energy consumption on the other, human society is moving towards technologies that can be acceptable in the future. While searching for new energy sources, the use of fossil fuels seems to be unavoidable, developing of new energy conversion technologies is also very important.

Land-based gas turbine (GT) engines operate on natural gas and are considered one of the cleanest combustion technologies. Among the fossil fuels that are used today, natural gas the highest hydrogen to carbon ratio, thus produces the least amount of carbon dioxide. Though the carbon dioxide is not viewed as a pollutant by current standards, it is a green house gas that contributes to global warming. There are other environmental advantages of natural gas over the other fossil fuels. In particular, the absence of sulfur in natural gas implies that there are practically no sulfur dioxide emissions present. Sulfur dioxide is a known precursor to acid rain. The other advantage of gas turbine is its high efficiency. The current efficiencies of combined cycle gas turbine (CCGT) approach 60%.

However, the high temperatures associated with combustion can lead to high levels of nitrogen oxides (NOx) emissions. Reducing the NO_x without compromising the low CO levels is one of the main concerns in the design of GT combustors. One of the techniques in reducing nitrogen oxide emission is lean premixed (LP) combustion. By burning the mixture lean, the combustor can avoid high local fuel-air equivalence ratios that increase the flame temperature.

Different methods have been presented in the literature for modeling the combustion process associated with turbulent phenomena. However, there are no computer models available that incorporate the full set of chemical kinetic reactions coupled with turbulent flow modeling. Attempts have been made to include the complex chemistry in turbulent models, but such models are limited to rather simple systems and still require great amounts of computer time (i.e., H_2 combustion, Borghi (1988)). To model the more complex combustion system various simplified global kinetic mechanisms have been developed (see Chapter 2). These mechanisms are limited by their the operating condition and may fail to predict CO and NO emissions accurately out of their range.

1.2 Objectives

The objective of this work is to develop and validate a pressure sensitive global mechanism for methane oxidation with NO formation for lean premixed (LP) combustion in gas turbine engines. In order to model the combustion more accurately all known

mechanisms of NO formation are considered, and the global mechanism is applied to variable pressure.

1.3 Approach and Validation

The global kinetic mechanism is based on the detailed chemical kinetic mechanism GRI 3.0. The research and validation are done in the following order:

1. Study the Computational Fluid Dynamics (CFD) results of Nicol and Malte (2000) to determine typical conditions for the GT combustor; i.e. the sizes and location of the main reaction zones, including flame zone, post-flame zone, and recirculation zone; and the characteristic parameters of the zones, including equivalence ratios, temperatures, residence times, turbulence parameters, and species concentrations.

2. Using the full chemistry of GRI 3.0 in Chemical Reactor Modeling (CRM) representative of the reaction zones, develop a computer-generated database of species concentrations, rates of reactions for various reactor arrangements, pressures, equivalence ratios, and temperatures that are applicable to LP combustion in gas turbine.

3. Perform the regression analysis for the database to obtain the global rate expressions for methane oxidation and nitric oxide formation.

4. Compare the CRM results obtained with global rate expressions versus the full kinetic mechanism GRI 3.0.

5. Validate the global rate expressions in CRM against jet-stirred reactor databases of Teodora Rutar (2000) and Karin U. M. Bengtsson (1998).

6. Validate the global rate expressions using the gas turbine Combustor A database from Nicol and Malte (2000). Combustor A is simulated using a CRM consisting of twelve zones, and a CFD model with k-ε momentum equation closure. In both simulations, the global rate expressions provide the chemical kinetic data.

Chapter 2

Modeling of the Combustor A

2.1 Turbulent Combustion

In industrial applications, combustion is normally associated with turbulence. Large flow rates, enhancing mixing designs, and heat release during combustion increase the turbulence.

Combustion systems can be divided into premixed, partially premixed, and non-premixed. Examples for premixed combustion are the carbureted and post-injected internal combustion engine with spark ignition and the LP combustor for the GT engine. In the GT application, the fuel and air come to the combustor premixed. Turbulence is necessary for such mixing. Partially premixed combustion can be observed in direct injection internal combustion engines. Non-premixed combustion takes place in diesel engines and the other applications where the fuel is injected separately from the air, and in cases where solid or liquid fuels are used.

The rate of chemical reaction during the combustion process depends on the type of combustion and the conditions in the combustor. One can distinguish two different rates at which combustion occurs: the mixing rate, in which case the fuel reacts as fast as the mixing occurs, and the chemical kinetic rate, which assumes that mixing is infinitely fast and the chemistry is slow. This division is described by Damkohler number (Da), which is defined as chemical time divided by mixing time.

2.2 CFD Modeling of Turbulent Combustion

There are a number of ways to model turbulent combustion. CFD modeling has ability to provide valuable insight on the flow and temperature fields of the combustor, which are difficult to obtain experimentally. While CFD is a valuable tool for predicting the flow and temperature fields, this method cannot incorporate complicated chemistry of detailed chemical kinetic mechanisms. Thus CFD cannot always accurately predict the exhaust emissions. CFD solves the Reynolds-averaged Navier-Stokes (RANS) equations coupled with energy and species equations. The commercial CFD package FLUENT is used in the simulations. The momentum equations are closed using standard k-ε, renormalized group (RNG) k-ε, and the Reynolds stress model (RSM). The can-type combustor simulated, hereafter referred as Combustor A, is modeled as a 2-D axi-symmetric flow with swirl. The computational domain is divided into finite volumes, 190 x 81, as depicted in figure 2.1. The previously developed 5-step, 8-atm global mechanism of Nicol (1995) is used as a starting point for the CFD simulations. FLUENT is also able to incorporate mixing controlled reaction rates, by employing the Magnussen and Hjertager model (1976), which is based on the eddy break-up model of Spalding (1970). The code automatically chooses the slower rate of two (chemical or mixing) and defines it as a limiting rate for the reaction.

The CFD results of Nicol and Malte (2000), using the global mechanism of Nicol (1995), are shown in figure 2.2 and 2.3. The results are used to develop the CRM of Combustor A, and to gain insight on the main zones of the combustor and the CRM elements to use for the development of the new global mechanism.

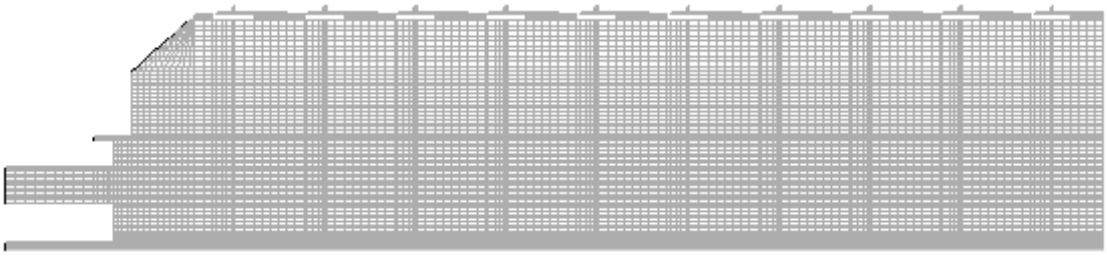

Figure 2.1 computational domain for CFD modeling of combustor A

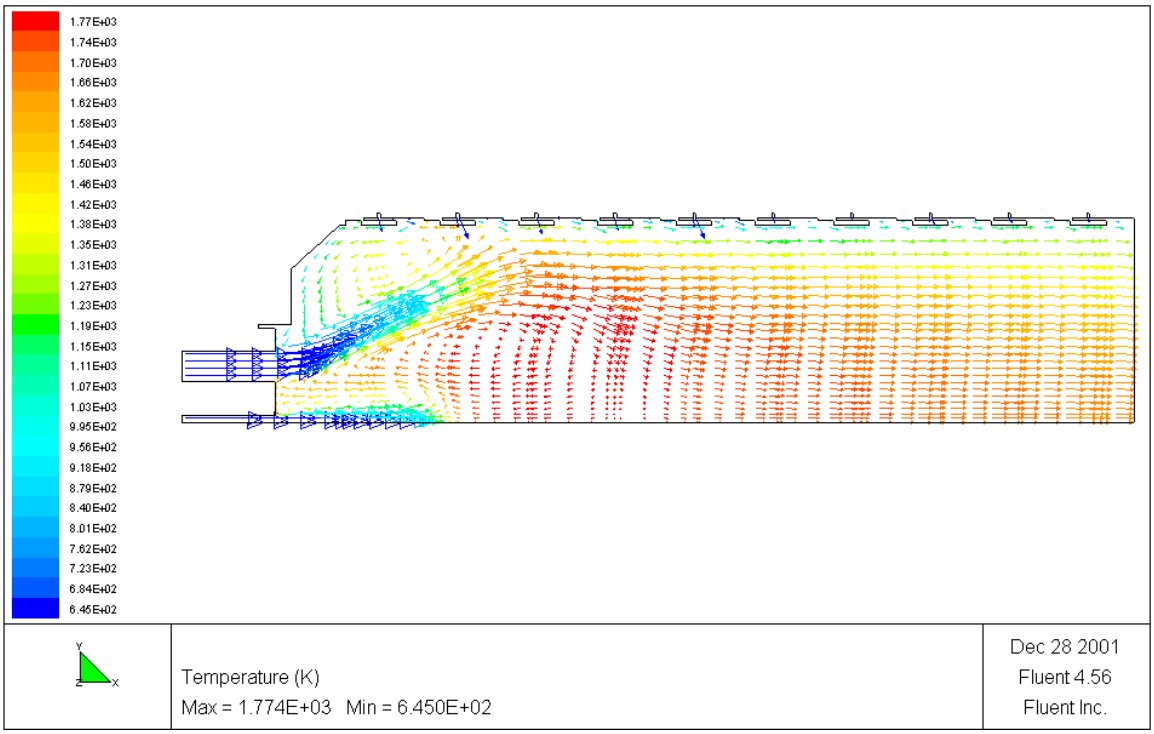

Figure 2.2 Velocity vectors colored by temperature, inlet temperature - 645K. Maximum temperature - 1780 K

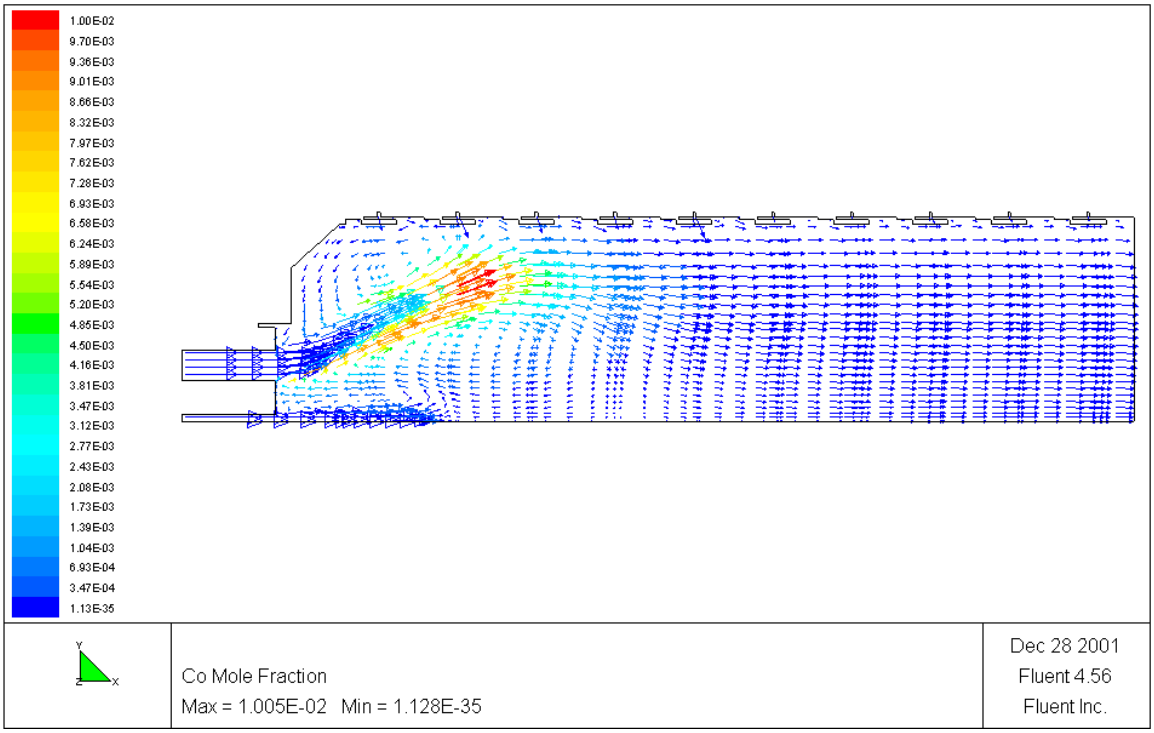

Figure 2.3 Velocity vectors colored by CO mole fraction. Maximum CO - 10 e+4 ppm (1%) CO at the outlet ~3.5 ppm

2.3 Chemical Reactor Modeling

CRM solves the energy and species equations decoupled from the fluid mechanics. The flow information is obtained from experiment, or from the CFD simulation with simplified chemistry. CRM uses the arrangement of perfectly stirred reactors (PSRs) and plug flow reactors (PFRs). For CRM a detailed chemical kinetic mechanism is used, such as GRI 3.0 (1997) or Miller and Bowman (1989)

The computer code MARK3, developed by Dr. Pratt and modified by Dr. Nicol is used for the CRM simulations. MARK 3 solves the system of non-linear partial differential equations. The code solves the system of equations at stationary time step, and uses the convergence of Jacobi-Newton (diagonalized Newton-Raphson) or the predictor-corrector scheme if the Newton-Raphson method fails to converge. The initial guess values for the first iteration are calculated for adiabatic equilibrium for the given condition.

CRM provides very detailed chemistry but does not to predict the flow field for complex systems such as the gas turbine combustor. On the other hand, the methods used in the CFD modeling can compute the flow field to the useful degree of accuracy, but are limited with respect to the chemical kinetics that can be solved.

The 5-step, 8-atm global mechanism of Nicol (1995) is used in the CFD simulations. Results obtained from the CFD computations contain flow field information, species concentrations and the reaction rates. These results show that the reactions of formation and destruction of CO in the flame zone are mixing controlled and do not depend on the chemical rates. Reactions of formation of nitric oxide are kinetically controlled but these reactions do not significantly alter the flow and temperature fields in the combustor. Based on the CFD results, one can develop a CMR model of combustor. That CRM model has the individual reactor elements and the mass exchanges between the elements based on the CFD results.

Figure 2.2 shows the velocity vector colored by temperature from the RSM-CFD solution of Combustor A. Combustor A is a film cooled lean/premixed combustor can, the base case has a premixer fuel-air equivalence ratio (Φ) of 0.61 and overall Φ of 0.33. The overall residence time of the gas in the combustor is about 30 ms, and the peak temperature is about 1800 K. The inlet pressure is 10 atm, the inlet temperature is 650K. The diameter of the combustor can is about 20cm. In figure 2.3, the CO concentration field predicted by the RSM CFD is shown. The chemical kinetics mechanism is the five-step, 8-atm mechanism. From these figures, few distinct regions are seen:

1. A shear layer flame zone between the stream entering from the premixer and the main on-axis recirculation zone of the combustor. The flame zone is narrow and then blossoms into a thicker flame brush, which is about 10 cm downstream from the inlet.

2. A large on-axis recirculation zone which provides the back flow of the hot, reactive combustion products for ignition of the fresh reactants in the upstream shear layer

between inlet premixed stream and the recirculation zone. The small recirculation zone in the dome region also helps to recirculate hot burnt gas and promote ignition in the thicker part of the flame zone.

3. Post-flame, burn-out-zone-combustion is located downstream of the large on-axis recirculation zone as the flow straightens out and flow axially toward the outlet of the combustor can.

4. Post-flame zone, with cooling air addition, is located along the wall of the combustor

From this understanding, a simplified CRM arrangement of elemental reactors is obtained as shown in Figure 2.4, and used in the development of the new global mechanism. The essential reactor elements are:

1. PSR for the flame zone. This PSR is run adiabatically giving the maximum flame temperature, and it is run with assigned temperature, permitting lower temperatures associated with the initial reaction of the premixed reactants.

2. PSR for the recirculation zone. This is PSR2 in figure 2.4

3. PFR for the post flame zone

4. PFR with air addition for further burn-out of the reactants. This is PFR2 in figure 2.4.

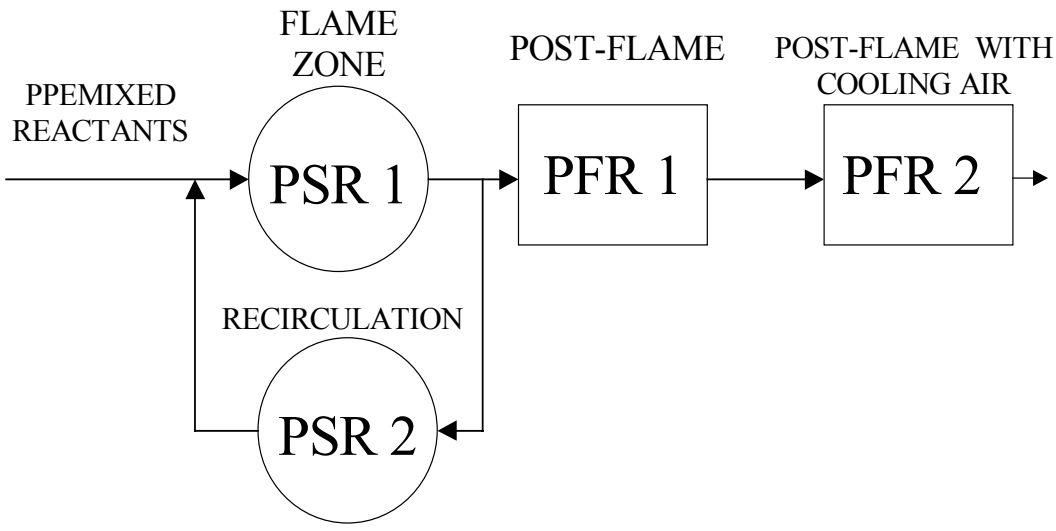

Figure 2.4 Simplified Chemical Reactor Model of the Combustor A

A very detailed CRM arrangement is also obtained for modeling Combustor A. The combustor is divided into several chemical reactor elements. The different types of the elements (MIX, PSR, and PFR) represent each region see figure 2.5: the stream from premixer (MIX 1, PSR2, PSR 3, PSR 6, PSR 10, PSR 14); dome recirculation zone (MIX 4); main recirculation zone (PSR 11 and PSR 12); and post-flame zone (PFR 17). See figure 2.5. The balance of the numbered elements are the small MIX reactors needed to connect the functional elements. The volumes of each element are estimated from the CFD results.

The first element in the detailed CRM arrangement is a MIX element, which represent the inlet into the combustor. About 10% of the fresh mix are ignited in the very short PSR 2 as hot gas approaches from the on-axis main recirculation zone (PSR 12). The freshly ignited gas mixes with additional recirculated and burnt gas in PSR 3. In PSR 6 the burning mixture receives and burns unburned gas from the dome zone (MIX 4) and additional hot products from main recirculation element (PSR 11). From PSR 6, part of the mixture recycles to PSR 11 in the upper part of the main recirculation zone, the other part moves downstream to PSR 14. The other 90% of the fresh methane-air mixture from MIX 1 does not react immediately, rather it mixes with air in the combustor dome area (element MIX 4). This lean mixture enters PSR 10 where it is ignited and burned. Under the very lean conditions the reaction in element 10 sustain a CO concentration of 0.5 - 1%. The CO is destroyed in PSR 14 where the gas from PSR 10 mixes and burns with the products of PSR 6. Part of the gas from element 14 (about 5%) goes to the lower part of the central recirculation zone PRS 12. PSR 12 receives some fresh air from the pilot inlet and recycles to PSR 3. Most of the flow from PSR 14 enters the PFR 17 where it is deluded by secondary air and exits the combustor. Note that in this simulation there is no fuel entering the combustor through the centerline pilot, only a small amount of air enters through this pilot.

The rates of the flow into the elements and their residence times are estimated from the CFD results. The flow rate in an element computed as follows:

$$m_{dot} = \bar{\rho} \times \overline{V} \times A_c,$$

where:
ρ = average density in the element, kg/m^3
V = average velocity in the element, m/s
A_c = cross area of the element, m^2

Figures 2.6, 2.7, and 2.8 show the flow rates in the jet and the recirculation zones of the Combustor A calculated for different fuel-air equivalence ratios.

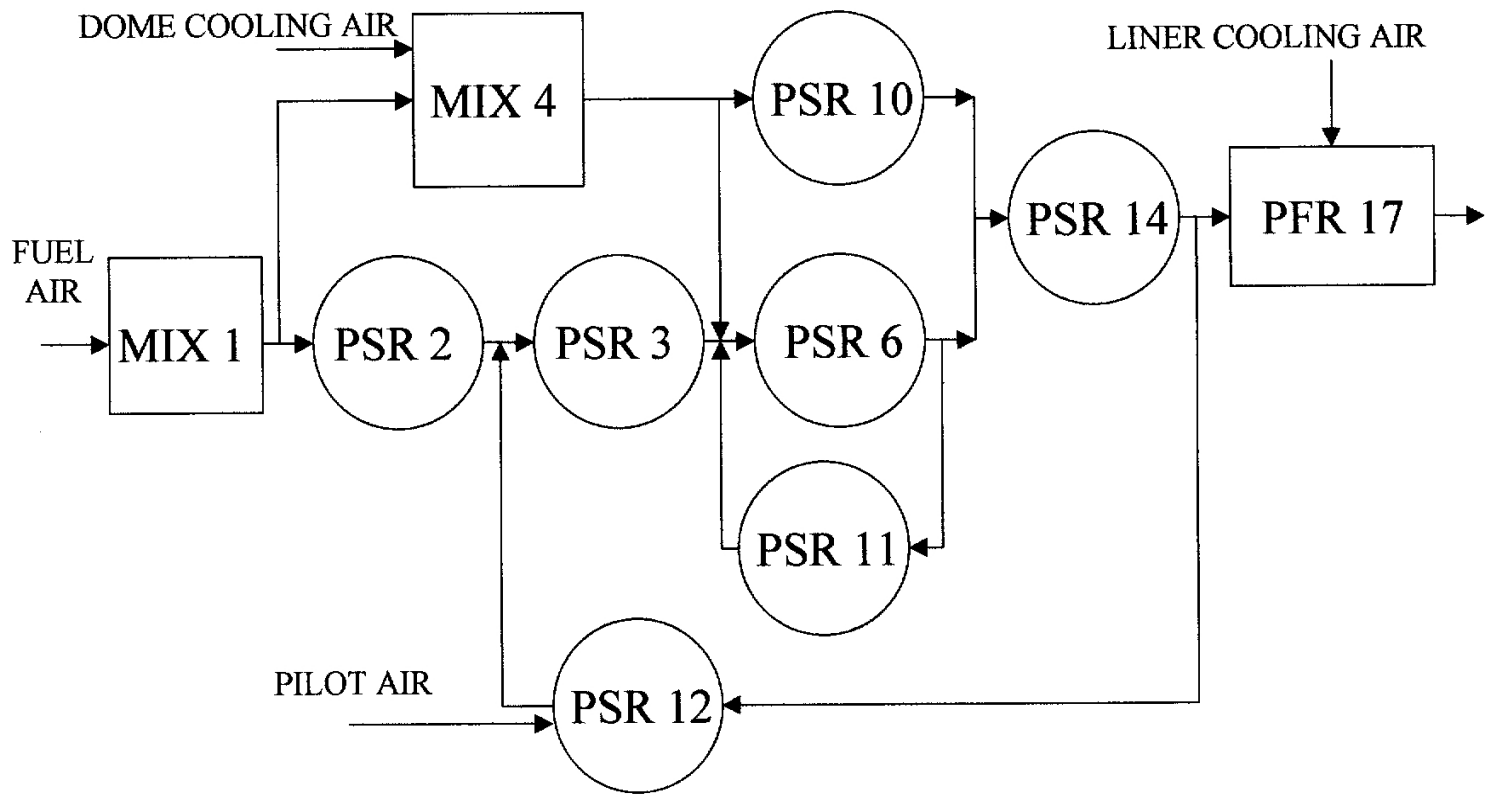

Figure 2.5 Detailed CRM of combustor A

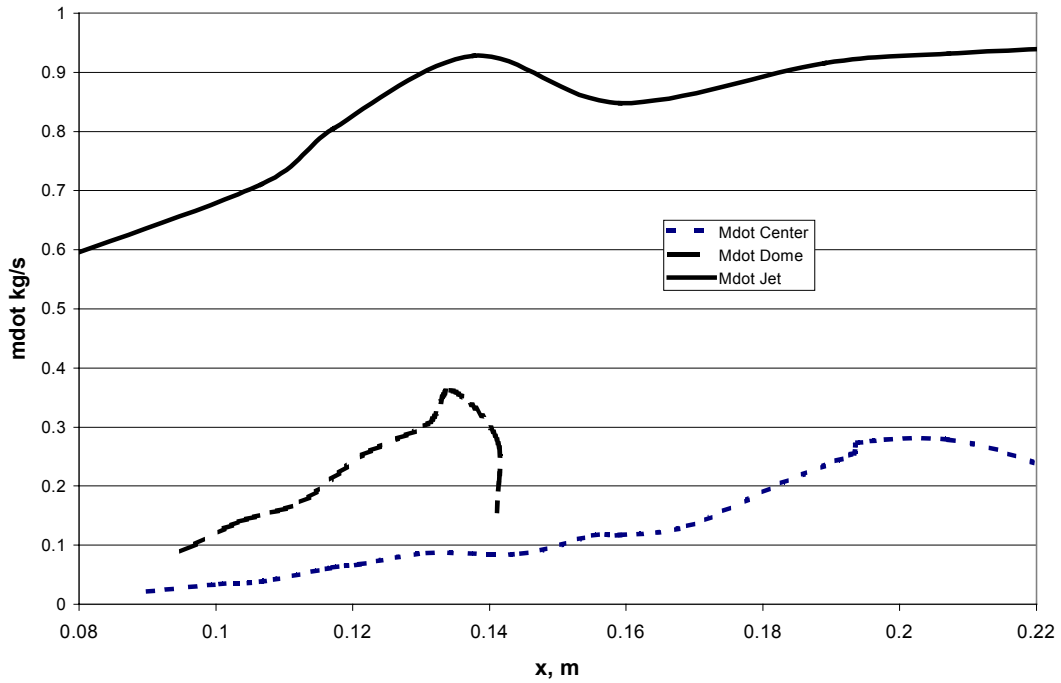

Figure 2.6 Flow rates in the center recirculation zone, dome recirculation zone, and the stream from the premixer ("jet") for the Combustor A operated with premixer fuel-air equivalence ratio of 0.49. The distance from the front of the combustor = x.

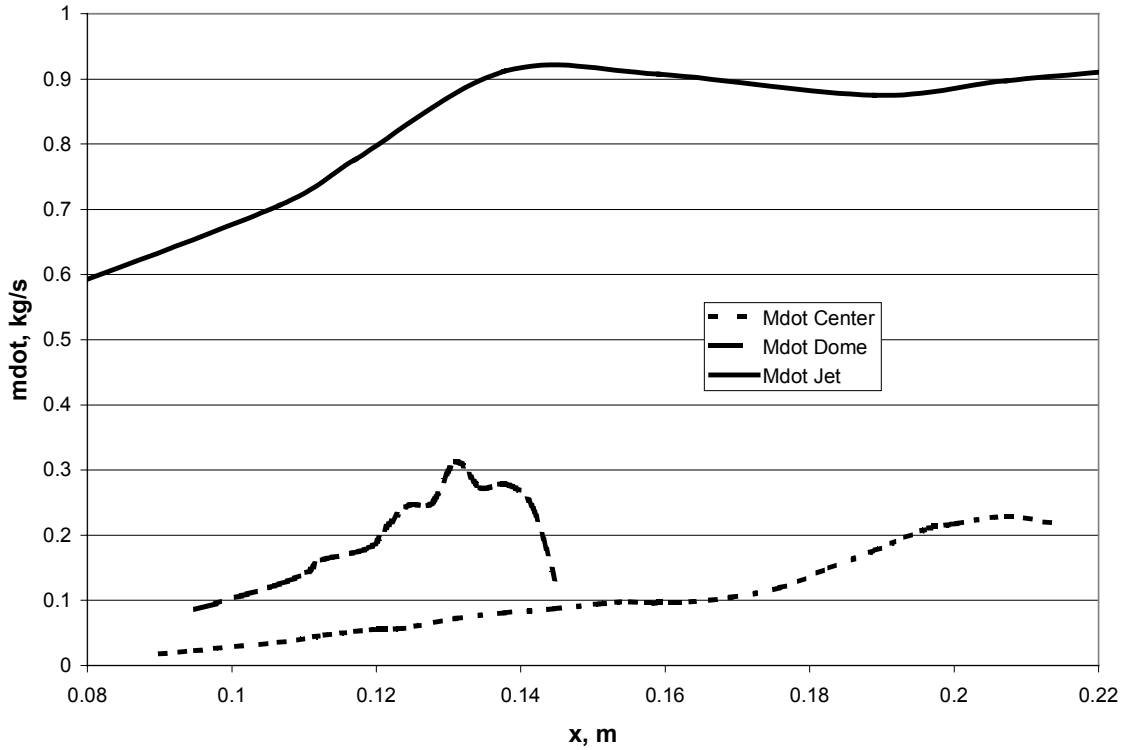

Figure 2.7 Same as figure 2.6, except the premixer Φ = 0.61

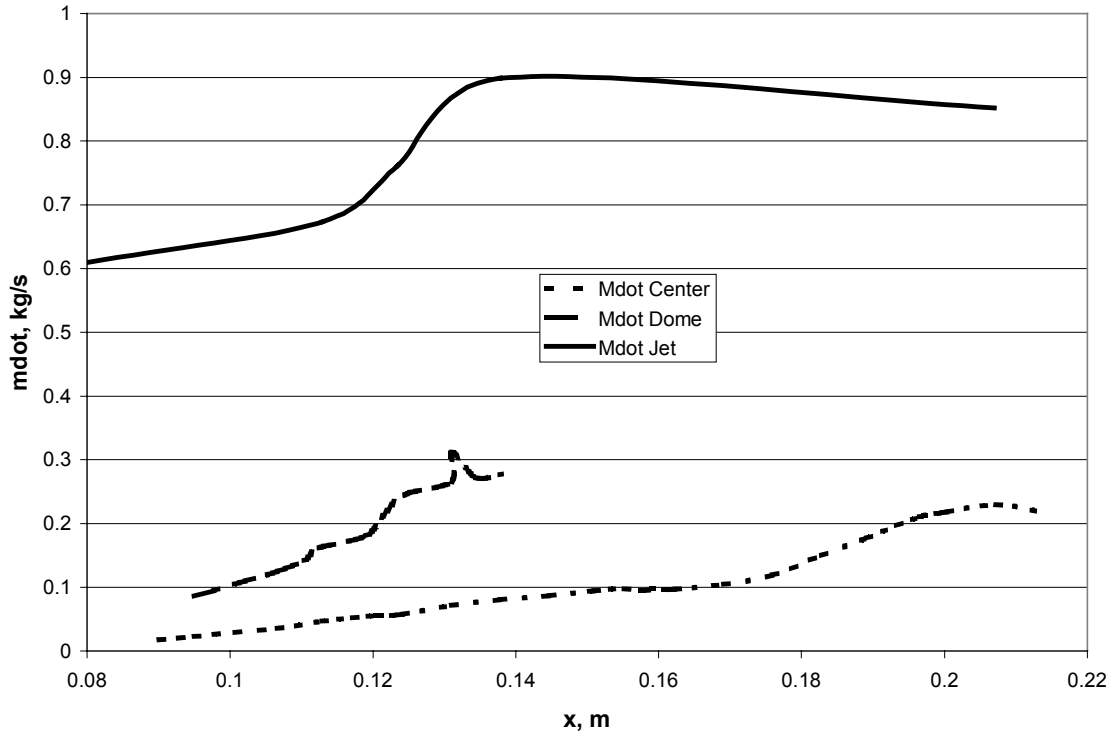

Figure 2.8 Same as figure 2.6, except the premixer Φ = 0.87

2.4 Determining the Coefficients for Mixing Controlled Reaction Rates

The MARK 3 code does not take into account mixing controlled reaction rates. All the reactions in the code are chemically controlled and therefore the code cannot be used for systems where mixing controlled reactions take place. When one applies currently available chemical kinetic mechanisms, e.g., GRI3.0 or Miller Bowman the detailed chemical reactor model under-predicts the level of CO by at least a factor of 10. This under-prediction is caused by a lack of mixing control in the reaction rates. Therefore, it is important to develop a mechanism that accounts for the mixing control of the reactions. The eddy break-up model is used in FLUENT CFD software and is chosen to determine the rates for mixing controlled reactions for consistency with the CFD computations. In the eddy break-up model, the rate of the reaction is written as:

$$R_{i',k}=\nu_{i',k}\times M_{i'}\times A\times\rho\times(\varepsilon/k)\times(Y_R/\nu_{R,k}\times M_R)\ ,$$

where:
$R_{i'k}$ = reaction rate for species i' in reaction k
$\nu_{i',k}$ = molar stoichiometric coefficient for species i' in reaction k
$M_{i'}$ = molecular weight of species i', kg/kmol
M_R = molecular weight of the limiting reactant, kg/kmol
A = coefficient, here is taken to be equal to 4.0

ρ = density, kg/m^3
ε = turbulent dissipation rate, m^2/s^3
k = turbulent kinetic energy, m^2/s^2
Y_R = mass fraction of reactant R, kg_R/kg_{tot}
$\nu_{R,k}$ = molar stoichiometric coefficient for reactant R in reaction k

For the present case, one needs to calculate the mixing controlled reaction rates for the first two reactions of the global mechanism.

Reaction 1 $CH_4+1.5\times O_2 \rightarrow CO+2H_2O$

Reaction 2 $CO+0.5\times O_2 \rightarrow CO_2$

The rates for these two reactions must be expressed in the form of the global reaction rate so they can be used in the chemical reactor modeling. The global chemical kinetic mechanism reaction rates are written as:

$$R_i=d[X]/dt=10^n\times T^m\times e^{-Ea/RT}\times[X]^x\times[Y]^y,$$

where:
10^n = pre-exponential factor
T = temperature
E = activation energy of the reaction
[X] = concentration of species X
[Y] = concentration of species Y

The eddy break-up rate does not explicitly depend on temperature, on the other hand, that is it depends only on the concentration of the limiting species to the first power. Thus, the global rate of the reaction is simplified as:

$$R_i=d[X]/dt=10^n\times[X]=A\times[X],$$

where:
A = pre-exponential factor
[X] = limiting species concentration

In order, to obtain the pre-exponential term, one needs to analyze the average parameters of the flow field in the specific zone of the combustor: flame front for the reaction 1, and flame brush for the reaction 2. The data (k, epsilon, and the reaction rate) needed for calculating the pre-exponential term can be obtained from CFD solution. The coefficient A does not change significantly in the flame zone. The pre-exponential factor is found to be $A=10^{(3.9-4.1)}$ for reaction 1, and $A=10^{(3.5-3.7)}$ for reaction 2. The species of the limiting (smallest) concentration for reaction 1 is CH_4, and for reaction 2 it is CO. The mixing rates of the reactions are:

$$R_1=10^4\times[CH_4]^1$$

$$R_2=10^{3.65}\times[CO]^1$$

The full chemical kinetic mechanism does not allow implementing mixing rates for hydrocarbon chemistry, however the format of the global mechanism lets one do this. The result of the chemical reactor modeling of the combustor A, using the detailed arrangement of reactor elements can be compared with the results of the CFD simulation. Figure 2.9 shows that NO at the exit of the combustor from the CRM with 5-step global kinetic mechanism of Nicol (1995) with reactions 1 and 2 set by the mixing controlled rates is very close to the CFD result when the same global mechanism is used. The largest discrepancy is for the richest case.

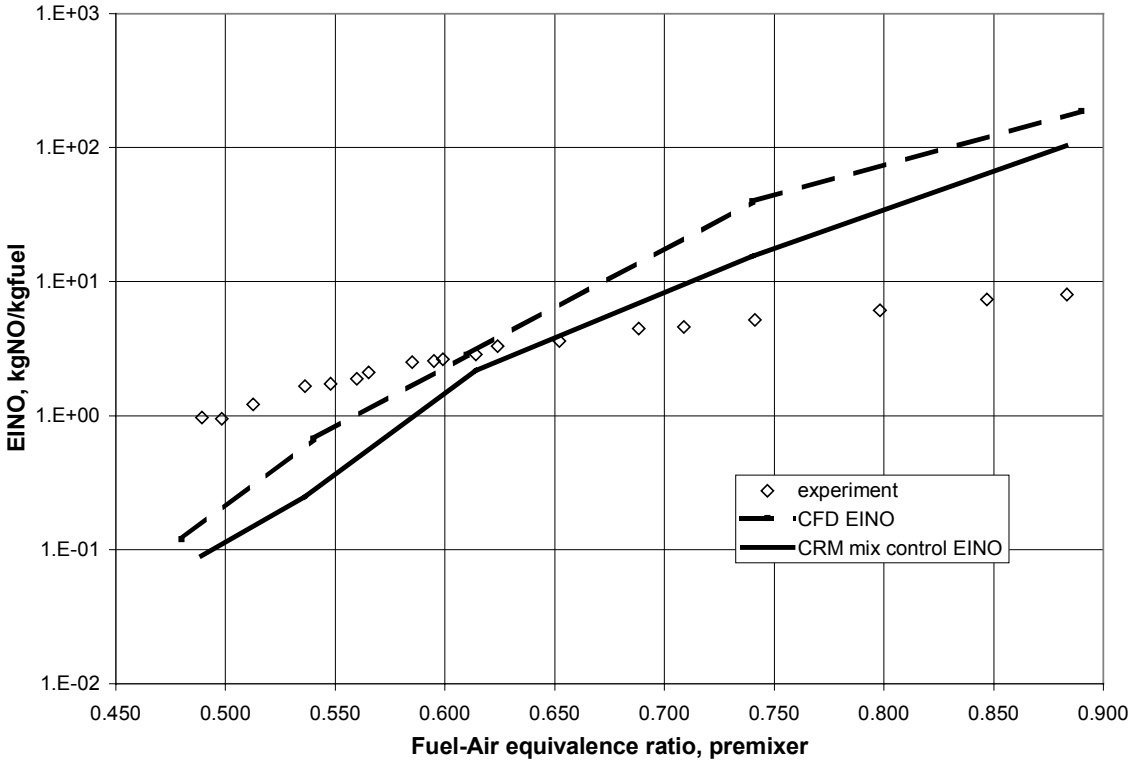

Figure 2.9 Emission index of NO as a function of the fuel-air equivalence ratio for the Combustor A LP Base 1, Operating pressure 9.9 atm. Inlet temperature 646K. Air flow rate = 1.19kg/s

2.5 Comparison to the Experimental Data

The 5-step, 8-atm global mechanism of Nicol (1995) is used in CFD and the CRM calculation of figure 2.9. For the lean cases, both CFD and CMR under-predict NO. This might be explained by unmixedness in the combustor at the lower temperatures, associated with lower fuel equivalence ratio. In the richer cases, NO is over-predicted possibly due to the non-adiabaticity of the actual combustor, which was not modeled, or

because of the limitations of the 5-step global mechanism, which was not developed for high fuel-air equivalence ratios.

The experimental levels of NO show relatively weak dependency on the fuel-air equivalence ratio, which is non-characteristic. In figure 2.10 from Steele (1995), NO levels from different LP combustors are plotted against the flame temperature in the combustor. The experimental data for the combustor A for different flow rates and inlet temperatures show curves that the other combustors do not have. The NO_x levels do not rise with the increase of the flame temperature. This suggests that the combustor A is loosing heat at the higher fuel-air equivalence ratios and the actual temperature in the combustor is lower than predicted. This may explain why the CFD and CRM simulations over-predict NO concentration in the rich cases compared with experimental data.

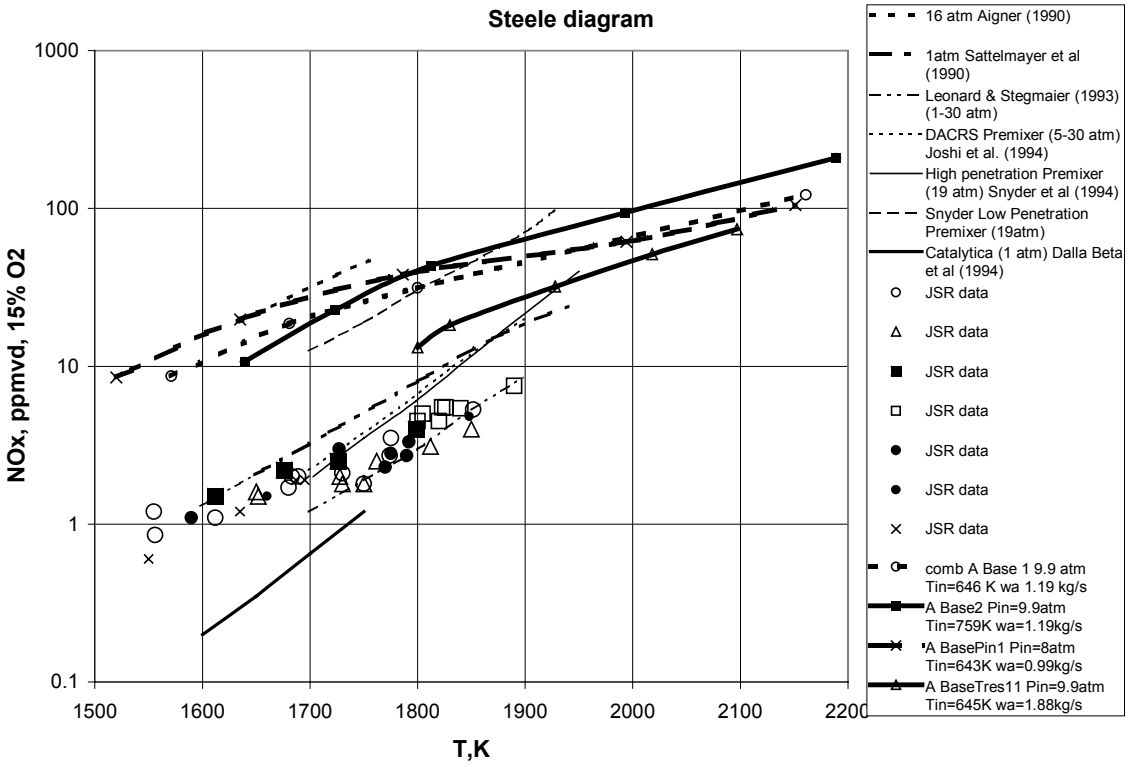

Figure 2.10 Experimental dependency of NOx emissions as a function of peak flame temperature in the combustor

Chapter 3

Development of 8-step global mechanism

3.1 Introduction

In modeling the turbulent combustion by CFD applications, traditionally various three-step or five-step mechanisms of methane oxidation have been used. In three-step mechanisms, the first step is the reaction of methane oxidation to carbon monoxide and water. The second step is the reaction of carbon monoxide oxidation to carbon dioxide and the third step is the carbon dioxide decomposition to carbon monoxide and oxygen. In five-step mechanisms, methane oxidizes to carbon monoxide and diatomic hydrogen. The water-gas shift reaction and the reaction for hydrogen oxidation are added.

There are several global mechanisms developed for methane-air combustion. Most of these global mechanisms are based on their agreement with the experimental data from the particular flame studies. As shown by Nicol (1995), most of the global reaction mechanisms cannot accurately predict CO and CH_4 concentration over wide range of conditions that can exist in the gas turbine combustors. Furthermore, these mechanisms involve only hydrocarbon chemistry and do not predict NO emissions.

In the development of the 5-step global mechanism, Nicol (1995) attempted to capture the mechanisms of NO formation. The first three steps of his mechanism are the reactions that describe the methane oxidation. The two-steps NO formation take into the account different NO pathways in both flame and post-flame zones. In the flame zone, non-thermal NO is the concern. Non-thermal NO is formed via the prompt, NNH, nitrous oxide and Zeldovich mechanisms acted upon by super-equilibrium concentrations of free radicals. These pathways are considered in their total in the first global reaction for NO. In the post-flame zone, thermal NO, that is Zeldovich NO formed in an equilibrium field of free radicals becomes important due to the long residence time and relatively high temperatures. This is taken into account by the second global reaction for NO.

Nitrogen oxide formation in the flame is highly dependent on the concentration of the free radicals, such as CH, OH, O-atom, H-atom. Since carbon monoxide concentration is indicative of free radicals, several of the global rates are based on the concentration of CO.

The 5-step global mechanism of Nicol (1995) was developed by regression analysis of CRM simulations of the combustor using full kinetic mechanisms: Miller and Bowman (1989) and GRI 2.11 (1995) for 1, 8, and 16 atm. In development, a set inlet temperature was used, and the fuel equivalence ration was varied from 0.45 to 0.68. The fuel-equivalence ratio range does not allow using the mechanism for cases with piloted combustion. The fixed pressure mechanisms do not allow the prediction of combustion fields and NO emissions in the intermediate pressure ranges.

The present work considers broader ranges of the fuel-air equivalence ratios and the pressure. The fuel-air equivalence ratio is varied from 0.45 to 0.8 so that modeling the case with piloted combustion is possible. The pressure variation is from 5 to 20 atm. The analysis is based on the GRI 3.0 full kinetic mechanism (1997) that has been shown to model lean-premixed high-intensity combustion process accurately, i.e., see Rutar et al. (2001)

3.2 Methodology

The full chemical kinetic mechanism GRI 3.0 has 53 species, most of them are free radicals, and 325 elementary reactions. The mechanism was specifically developed and optimized for methane-air combustion. This number of species and equations is too large to be incorporated in the modeling of the combustion process that is associated with turbulent modeling. The purpose of this work is to minimize the number of reactions to 5-8 and the number of species to about 7 so that the mechanism can be used conveniently in CDF application.

The rates of the reactions are represented in global form; i.e. for the reaction

$$A+B \rightarrow C+D$$

The expression for the reaction rate of formation of species C and D is

$$R_i = d[C]/dt = d[D]/dt = -d[A]/dt = -d[B]/dt = 10^n \times [A]^a \times [B]^b \times [C]^c \times [D]^d \times \exp(-T_a/T),$$

where:
[A], [B], [C], [D] = species concentrations, $kmol/m^3$
T_a = activation temperature of the reaction, K.

To obtain the global rate, the regression analysis can be performed for the database obtained by CRM simulations of the combustion reactors. The database for the matrix of operating conditions is gathered using the full kinetic mechanism GRI 3.0. The goal of the analysis is to find coefficients “n”, “a”, “b”, “c”, and T_a. To perform the regression analysis, the database should have the information about pressure, temperature, species concentration and the reaction rate; e.g. the net rate of production of species “C”.

The exponential term in the rate expression presents the most difficulty. To simplify the problem, the natural logarithm of the rate expression is taken, then

$$\ln(R_i) = n \times \ln(10) + a \times \ln([A]) + b \times \ln([B]) + c \times \ln([C]) - T_a \times (1/T)$$

Now, one can apply the linear least square fit to the equation above to determine the unknown coefficients. The species concentrations, reaction rate, temperature, and pressure are obtained from the database.

Another important part of this project is to make the reaction rates pressure sensitive. To account for pressure, various adjustments have been investigated. There are:

1. Inserting pressure explicitly into the rate expression:

$$R_i=10^{n}P^{m}[A]^{a}[B]^{b}\exp(-T_a/T)$$

2. Modeling pressure implicitly using surrogate species such as N_2:

$$Ri=10^{n}[N_2]^{m}[A]^{a}[B]^{b}\exp(-T_a/T)$$

3. Determining pressure sensitivity for each species and for the activation temperature in the rate expression:

$$Ri=10^{n0+n1\times P}[A]^{a0+a1\times P}[B]^{b0+b1\times P}\exp(-(T_a+T_{a1}\times P)/T)$$

The later approach appears to be more accurate and has the lowest residuals in the least square fit.

3.3 Development of Three-Step Pressure-Sensitive Global Mechanism for Hydrocarbon Oxidation

The following reactions are chosen for representing the hydrocarbon oxidation:

$$CH_4+1.5\times O_2\rightarrow CO+2\times H_2O$$

$$CO+0.5\times O_2\rightarrow CO_2$$

$$CO_2\rightarrow CO+0.5\times O_2$$

3.3.1 Reaction 1

Determining the reactor arrangement for CMR

Adiabatic PSR

The flame front is a region of large free radical concentrations and rapid oxidation of the fuel. In order to simulate the large free radical concentrations in this region, the PSR model is assumed. In the PSR model, mixing is infinitely fast and the gradients do not exist, except at the inlet of PSR. Practical flames are not mixed sufficient to approach this condition. Nonetheless, the free radical concentrations in the reaction zone of the

practical flame are reasonably well simulated by assuming a PSR of appropriately short residence time. Furthermore, this is the region where CO and free radicals reach their peak concentrations, and thus, where the free radicals have the greatest influence on the reaction chemistry. Thus, the PSR model is used to simulate the flame front

Short PSR followed by PFR

At very lean conditions ($\Phi<0.5$) and for the relatively low operating pressure of 5 atm, not all of the methane is burned in the single PSR with a residence time of two milliseconds or less. These conditions can be met near the flame front as the dome cooling or liner-cooling air is entering into the flame. In this case the unburned methane enters the post-flame zone where it is quickly consumed. A PSR-PFR arrangement is used to model this situation. A PFR is used to simulate the post-flame zone. The residence time in the PSR is short (0.5 ms), and the residence time in the PFR is based on the concentration of methane. The PFR is long enough to reduce the CH_4 concentration to the point where heat release from the reaction 1 can be neglected, i.e., CH_4 mole fraction $\sim 10^{-6}$. Since the temperature in the adiabatic flame near the recirculation zone is high and the methane concentration in this case is low, the methane oxidation in the recirculation zone is not considered. Thus, PSR-PSR reactor arrangement is not used in the Reaction 1 database.

PSR at assigned temperature.

The main reason for incorporating this reactor is to lower the activation temperature of the reaction. It has been observed that if the activation temperature of the reaction is high the CFD code has difficulty of "igniting" the mixture. Broadening the range of operating temperatures reduces the temperature dependency in the reaction rate, which reduces the activation temperature.

Determining the reaction rate expressions.

As mentioned above the rate expressions are developed in global forms and exponent coefficients can be obtained via a linear least square fit. The reaction rate of methane oxidation, $CH_4+1.5\times O_2 \rightarrow CO+2\times H_2O$, is highly dependent on the concentration of free radicals. The simplified way to show the pathway of methane oxidation is:

$$CH_4+OH \rightarrow CH_3+H_2O$$

$$CH_3+O \rightarrow CH_2O+H$$

$$CH_2O+OH \rightarrow HCO+H_2O$$

$$HCO+O \rightarrow CO+OH$$

Accordingly the elementary rates for these reactions may be expressed as:

$$R_i=10^n\times[A]\times[B]\times\exp(-T_a/T)$$

Since many of the species involved are radicals the rate of the Reaction 1 should depend on the concentration of free radicals. The only species that is available in global modeling is CO, which is made in the flame and destroyed, in later combustion. See figures 3.3.1 and 3.3.2 from Glassman (1996). From the figures it is seen that CO rises and falls in the flame and post –flame zone similar to the behavior of the H-atom and OH radical. The above suggests that including the carbon monoxide in the rate expression for Reaction 1 can be beneficial. Besides the CO, the other species to consider for the first rate are methane and diatomic oxygen, since they both appear on the reactant side of the reaction.

The database for fitting the methane oxidation reaction consists of the CRM results using the reactor arrangement described above. GRI 3.0 also predicts some production of methane in the flame due to the recombination of free radicals. In some cases the rate of CH_4 production is about 10% of total rate. To account for this, a net rate of methane destruction is used:

Net Rate of CH_4 Destruction = Rate of CH_4 Destruction – Rate of CH_4 Production

As mentioned above, the activation temperature in the rate expression is a concern, since several investigators have reported that if the activation energy is too high the CFD simulation may not ignite. Non-adiabatic (i.e., assigned temperature) PSR is added to the database to increase the operating temperature range. This seams to lessen the reaction sensitivity to temperature and to lower the activation temperature of the reaction. The following global reaction rate expression gives the best agreement to the CRM database obtained with full kinetics of GRI 3.0.

$$-d[CH_4]/dt=10^{13.354-0.004628\times P}[CH_4]^{1.3-0.01148\times P}\,[O_2]^{0.01426}\,[CO]^{0.1987}\exp\left(-\frac{21932+269.4\times P}{T}\right)$$

Figures 3.3.3-3.3.6 show the comparison of the net rate of methane destruction via global reaction 1 with the full kinetic mechanism for different CRM arrangements, pressures, and equivalence ratios. A 45-degree line on these graphs is a perfect fit.

In the recirculation and post-flame zones the concentration of methane and the rate of its destruction are very low and most likely do not influence the heat release in the reactor. Figures 3.4 and 3.5 show that the global mechanism under-predicts the rate of methane destruction thus will over-predict the CH_4 concentration in the second PSR and in the PFR. This is especially true for the lower end of the pressure range considered here and for the lowest reaction rates.

In the NO modeling discussed in Section 3.4, it is shown that the global rate of prompt NO formation mainly occurs in the flame zone. The over-prediction of CH_4 in the recirculation and in the post-flame zones should have negligible impact on the prompt NO reaction. However, mechanism may under-predict methane (i.e., fuel) burn out.

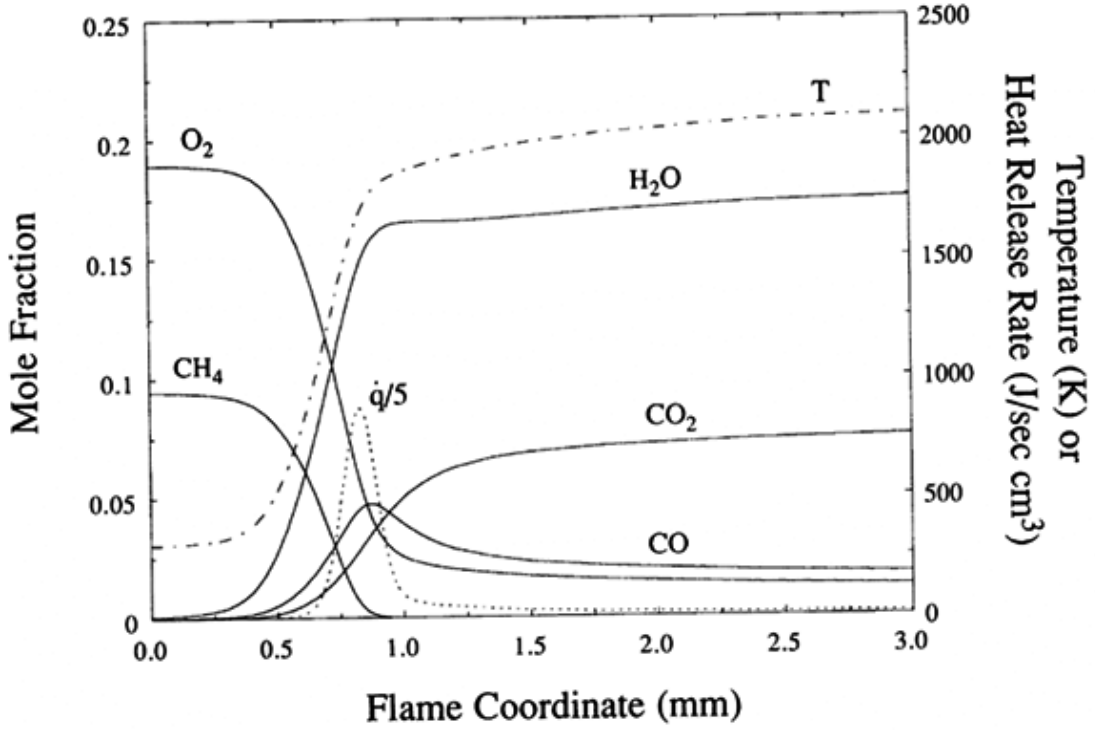

Figure 3.3.1 From Glassman (1996). Composition, temperature, and heat release rate profiles for a stoichiometric methane-air laminar flame at 1 atm and T_0=298 K.

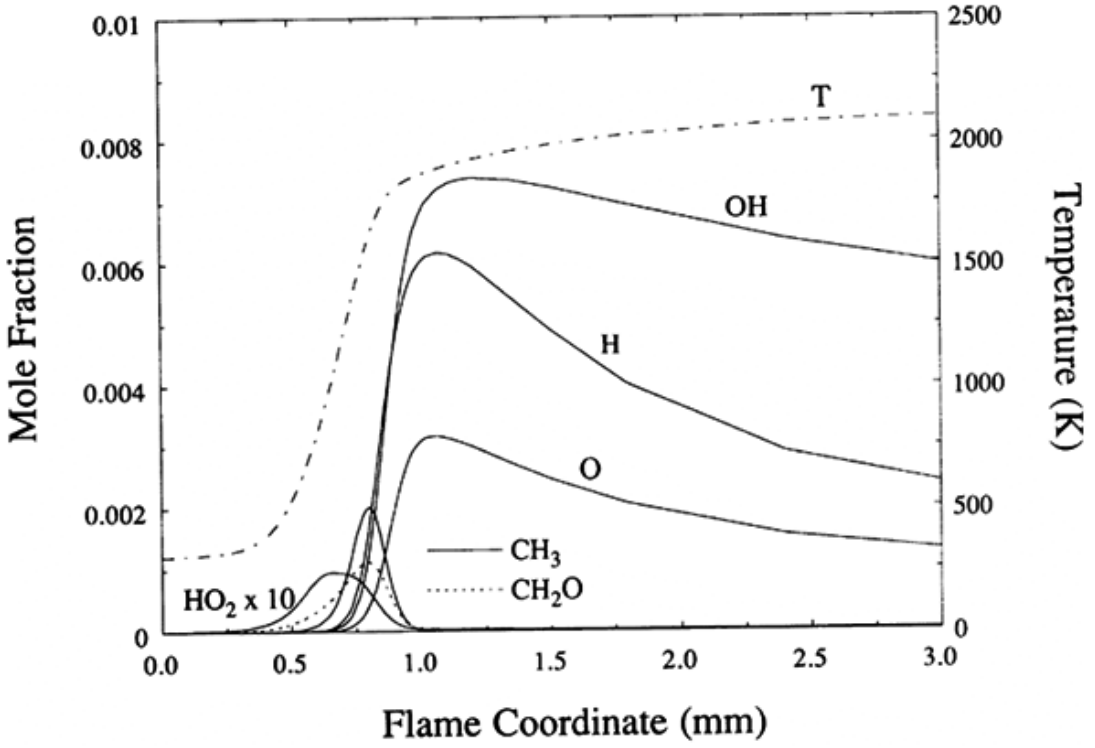

Figure 3.3.2 From Glassman (1996). Radical distribution profiles for Figure 3.3.1

The database for fitting the methane oxidation reaction consists of the CRM results using the reactor arrangement described above. GRI 3.0 also predicts some production of methane in the flame due to the recombination of free radicals. In some cases the rate of CH_4 production is about 10% of total rate. To account for this, a net rate of methane destruction is used:

Net Rate of CH_4 Destruction = Rate of CH_4 Destruction – Rate of CH_4 Production

As mentioned above, the activation temperature in the rate expression is a concern, since several investigators have reported that if the activation energy is too high the CFD simulation may not ignite. Non-adiabatic (i.e., assigned temperature) PSR is added to the database to increase the operating temperature range. This seams to lessen the reaction sensitivity to temperature and to lower the activation temperature of the reaction. The following global reaction rate expression gives the best agreement to the CRM database obtained with full kinetics of GRI 3.0.

$$-d[CH_4]/dt=10^{13.354-0.004628\times P}[CH_4]^{1.3-0.01148\times P}\,[O_2]^{0.01426}\,[CO]^{0.1987}\exp\left(-\frac{21932+269.4\times P}{T}\right)$$

Figures 3.3.3-3.3.6 show the comparison of the net rate of methane destruction via global reaction 1 with the full kinetic mechanism for different CRM arrangements, pressures, and equivalence ratios. A 45-degree line on these graphs is a perfect fit.

In the recirculation and post-flame zones the concentration of methane and the rate of its destruction are very low and most likely do not influence the heat release in the reactor. Figures 3.4 and 3.5 show that the global mechanism under-predicts the rate of methane destruction thus will over-predict the CH_4 concentration in the second PSR and in the PFR. This is especially true for the lower end of the pressure range considered here and for the lowest reaction rates.

In the NO modeling discussed in Section 3.4, it is shown that the global rate of prompt NO formation mainly occurs in the flame zone. The over-prediction of CH_4 in the recirculation and in the post-flame zones should have negligible impact on the prompt NO reaction. However, mechanism may under-predict methane (i.e., fuel) burn out.

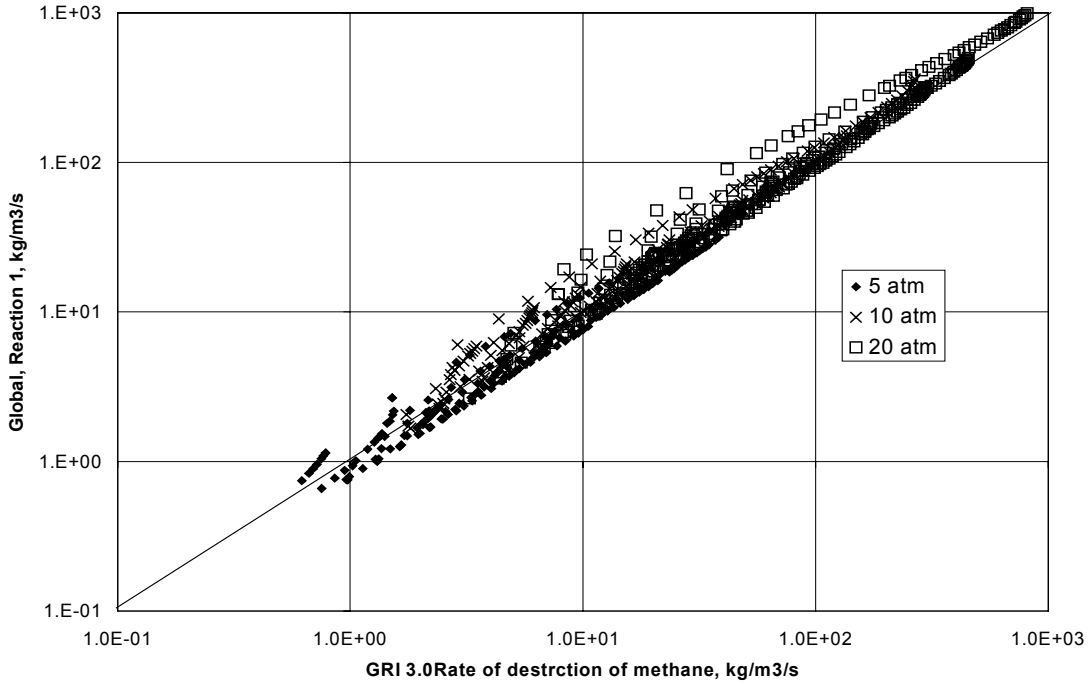

Figure 3.3.3 Net rate of methane destruction in the flame zone modeled as a PSR; inlet temperature: 5 atm – 483 K, 10 atm – 592 K, 20 atm –716 K; residence time varied from blowout to 2 ms; reactor temperatures correspond to adiabatic PSR

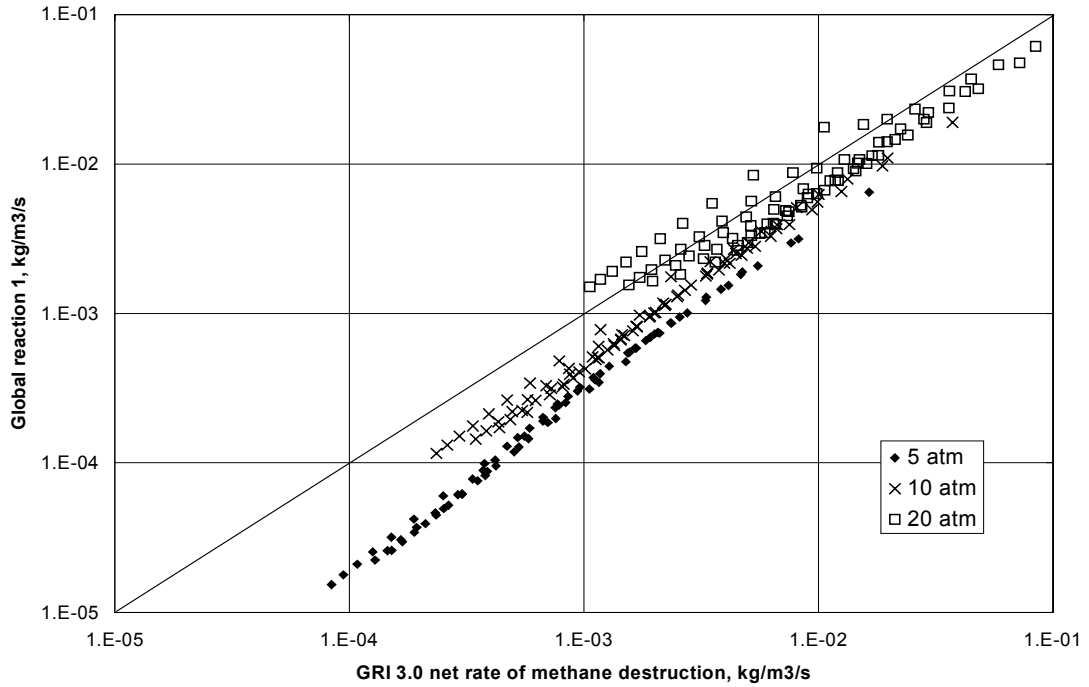

Figure 3.3.4 Net rate of methane destruction in the recirculation zone modeled as adiabatic PSR following a short PSR representing the flame zone. The PSR-PSR reactor arrangement is not included in the data base for the reaction 1. Residence time in the first PSR: 5 atm –1.0 ms, 10 atm – 0.5 ms, 20 atm – 0.25 ms; residence time in the second PSR varied from 2 ms to 15 ms.

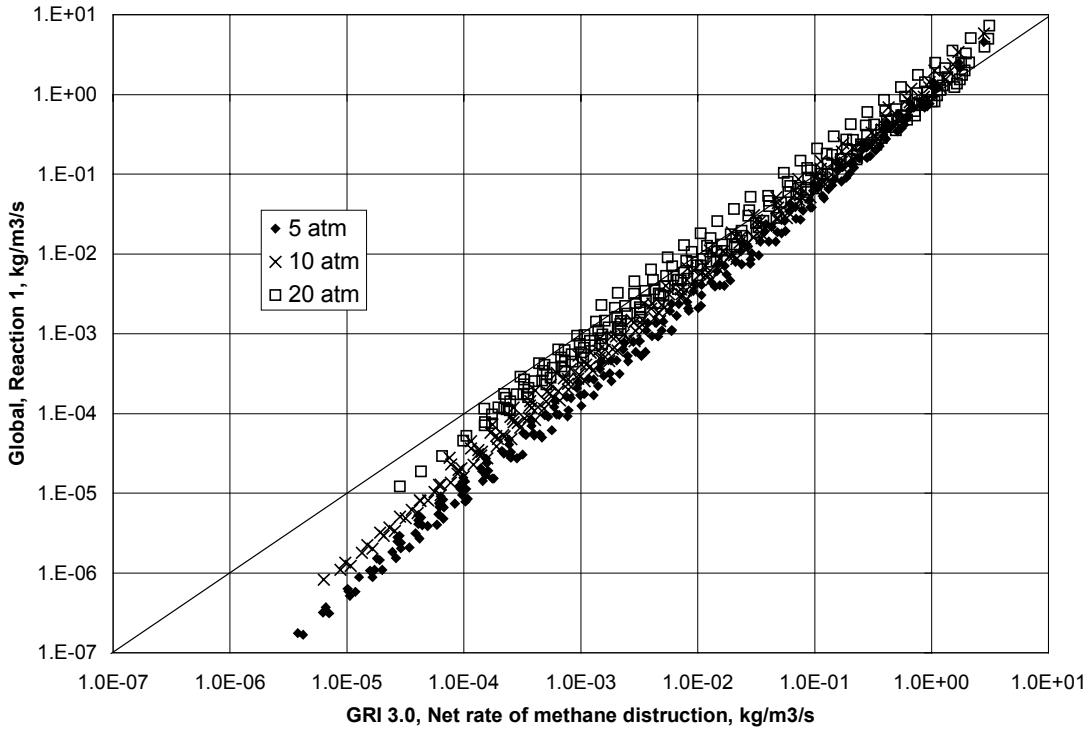

Figure 3.3.5 Net rate of methane destruction in the post-flame zone modeled as adiabatic PFR following short adiabatic PSR representing the flame zone. Residence time in the first PSR: 5 atm – 1.0 ms, 10 atm –0.5 ms, 20 atm – 0.25 ms; residence time in the PFR varied from 0.5 ms to time needed to reduced methane mole fraction to ~ 10^{-6}.

3.3.2 Reactions 2 and 3

The reactions of carbon monoxide oxidation and carbon dioxide decomposition can be viewed as a reverse of one another:

$$CO+0.5\times O2 \leftrightarrow CO2$$

However the importance of each reaction varies in the different parts of the combustion process.

Determining the Reactor Arrangement for CMR

Reaction 2

Oxidation of carbon monoxide is slower than reaction 1; thus the lifetime of CO is longer than CH_4. This explains the presence of CO in the flame zone, the recirculation zone and the post-flame zone. Since carbon monoxide is responsible for some of the heat release in the combustion process, it is important to accurately predict carbon monoxide concentration throughout the combustor.

Single PSR

Similar to the methane, carbon monoxide releases energy when it is oxidized. Destruction of carbon monoxide determines the flame temperature and the concentration of CO is indicative of the concentration of flame free radicals. Since the CO concentrations are observed in the flame, the single PSR is an important regime to study. Based on the CFD simulations of the Combustor A, the residence time in the PSR that represents the flame zone is up to 1.5 ms.

PSR followed by PFR

The post flame zone is where most of the carbon monoxide is converted to CO_2. Thus, it is imperative to include the PSR-PFR arrangement in the database for the second reaction. The residence time in the PSR varies with pressure and can be from 0.5 ms for 20 atm to 1.5 ms for 1.5 atm. In the LP combustor, two post-flame conditions can be found:

1. When cooling air mixes with hot products of reaction. In this case, the combustion happens with fuel-air equivalence ratios less than the premixer Φ.

2. In the case with piloted combustion and on the centerline of the burner, the post-flame zone does not have any cooling air added to the reactants. In this case, shorter adiabatic post-flame zone is used.

The residence time for each type of post-flame zone are estimated from the CFD simulations. To model the first condition, a PFR with additional air and residence times up to 20 ms is used. In the second regime, an adiabatic PFR with a residence time up to 8 ms is used.

Two PSRs in series

Since carbon monoxide leaves the flame zone unreacted, it is present in the recirculation zone of the reactor. The residence time in the first PSR in this case is similar to the PSR-PFR arrangement. Based on the results of the CFD compitation, the residence time in the second PSR is up to 15 ms.

Reaction 3

At long residence times, carbon dioxide and carbon monoxide come to equilibrium. In the present work, the rate of CO_2 dissociation is fitted only as the combustion field approaches equilibrium. Thus, a PSR_PFR arrangement is used. One should be aware that in the flame zone, some of the carbon dioxide is converted back to the CO. For given residence times in the PSR, the maximum amount of CO_2 decomposition is about 10%. Interestingly, about the same amount of carbon dioxide is made directly from hydrocarbon material in the flame zone. Both of these flame-zone effects are neglected, however they are in the same order of magnitude and act in the opposite directions, therefore, they tend to offset each other.

Determining the rate expression

Reactions 2 and 3 describe the relation between the same species and can be viewed as a reverse of one another. However, reaction 2 is most important in the flame zone where the heat release takes place and reaction 3 is not that important until the CO concentration is rather small and CO_2 is high. From the detailed kinetic analysis of the CO_2 formation in the flame zone, one notes that from 5 to 10 percent of CO_2 made bypasses the CO and is formed directly from hydrocarbon radicals. The rate of formation of carbon dioxide is not exactly equal to the rate of destruction of carbon monoxide. The rate of CO destruction is used in this analysis. Thus reaction 2 under-predicts the rate of CO_2 formation. Since the reaction 3 under-predicts the rate of CO_2 dissociation in the flame zone, under-predicting the rate of CO_2 formation in reaction 2 should give the better agreement with the full chemical kinetic mechanism in the flame zone.

The simplified pathway for oxidation of CO in the moist air can be described using the following elementary reactions:

$$CO + OH \rightarrow CO_2 + H$$

$$H + O_2 \rightarrow OH + O$$

$$O + H_2O \rightarrow OH + OH$$

$$OH + H + M \rightarrow H_2O + M$$

This simplified mechanism is largely driven by the hydroxyl radical. One may try to model the behavior of the OH radical based on equilibrium chemistry.

$$H_2O + 0.5 \times O_2 \leftrightarrow 2 \times OH$$

Based on the above, the reactions 2 and 3 yield to the best agreement with the full kinetic mechanism if the following expressions are used:

$$R_2 = 10^{14.338+0.1091\times P}[CO]^{1.359-0.0109\times P}[H_2O]^{0.0912+0.0909\times P}[O_2]^{0.891+0.0127\times P}\exp(-(22398+75.1\times P)/T)$$

$$R_3 = 10^{15.8144-0.07163\times P}[CO_2] \times \exp(-(64925.8-334.31\times P)/T)$$

Figures 3.3.6-3.3.9 compare the global rates with the GRI 3.0 mechanism results for different reactor arrangements, pressures, and equivalence ratios. Figures 3.3.10 and 3.3.11 show the rates of CO and CO2 destruction in the PFR approaching equilibrium.

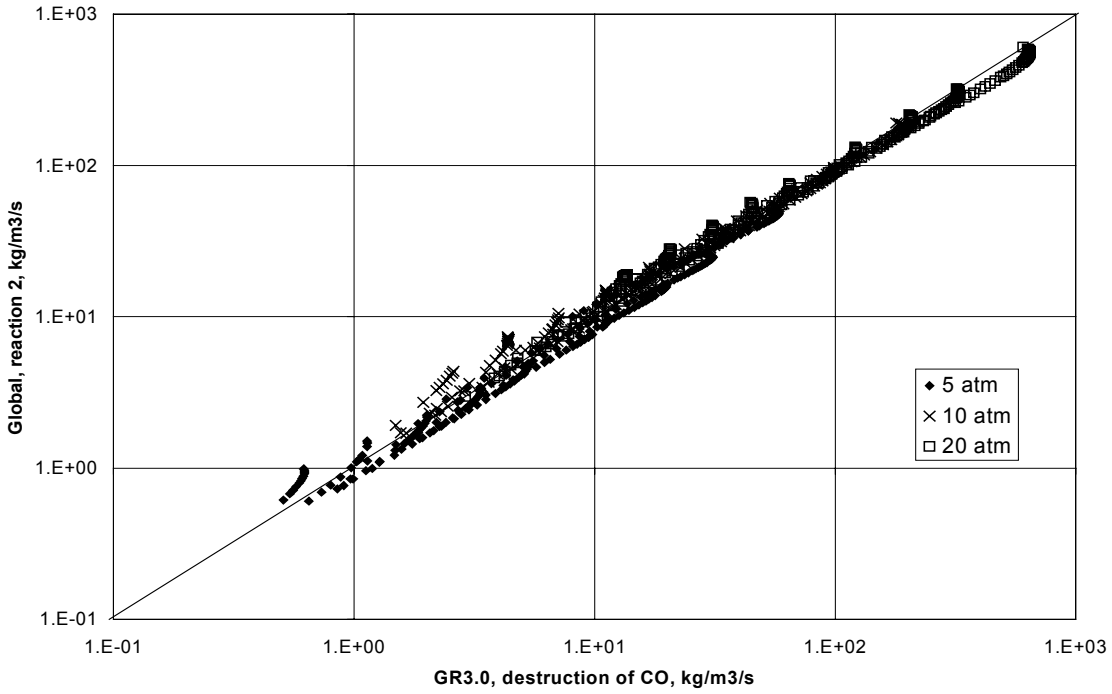

Figure 3.3.6 Rate of carbon monoxide destruction in the PSR; inlet temperature: 5 atm – 483K, 10 atm –592 K, 20 atm – 716 K, residence time varied from blowout to 2 ms; reactor temperature corresponds to adiabatic temperature in PSR.

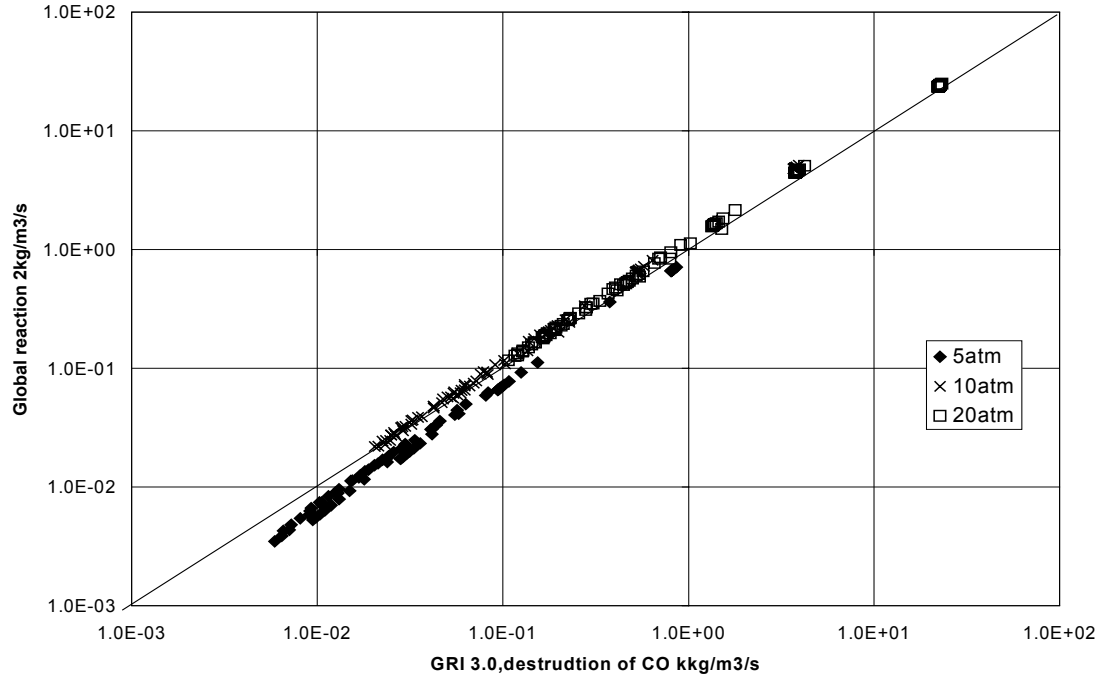

Figure 3.3.7 Rate of carbon monoxide destruction in the second PSR. Inlet temperature: 5 atm – 483K, 10 atm –592 K, 20 atm – 716 K; first PSR residence time: 5 atm – 2 ms, 10 atm –1.0 ms, 20 atm – 0.5 ms; second PSR residence time varied from 2 to 15 ms; reactor temperature corresponds to adiabatic PSR.

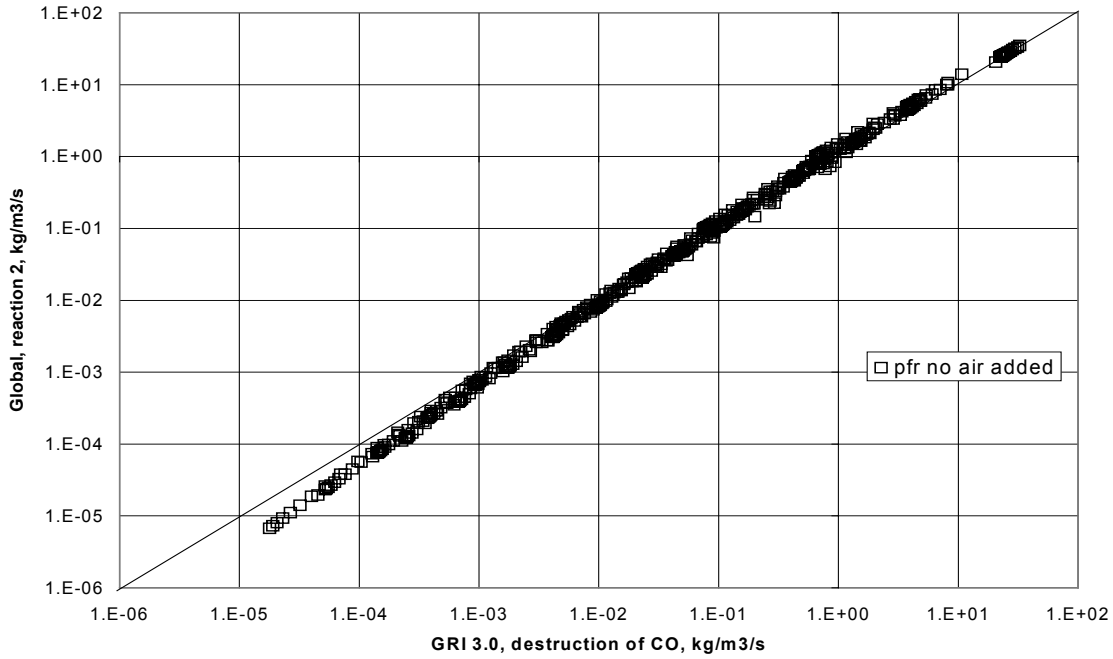

Figure 3.3.8 Rate of carbon monoxide destruction in the adiabatic PFR. Inlet temperature: 5 atm – 483K, 10 atm –592 K, 20 atm – 716 K; PSR residence time: 5 atm – 2 ms, 10 atm –1.0 ms, 20 atm – 0.5 ms; PFR residence time varied from 0.5 to 10 ms.

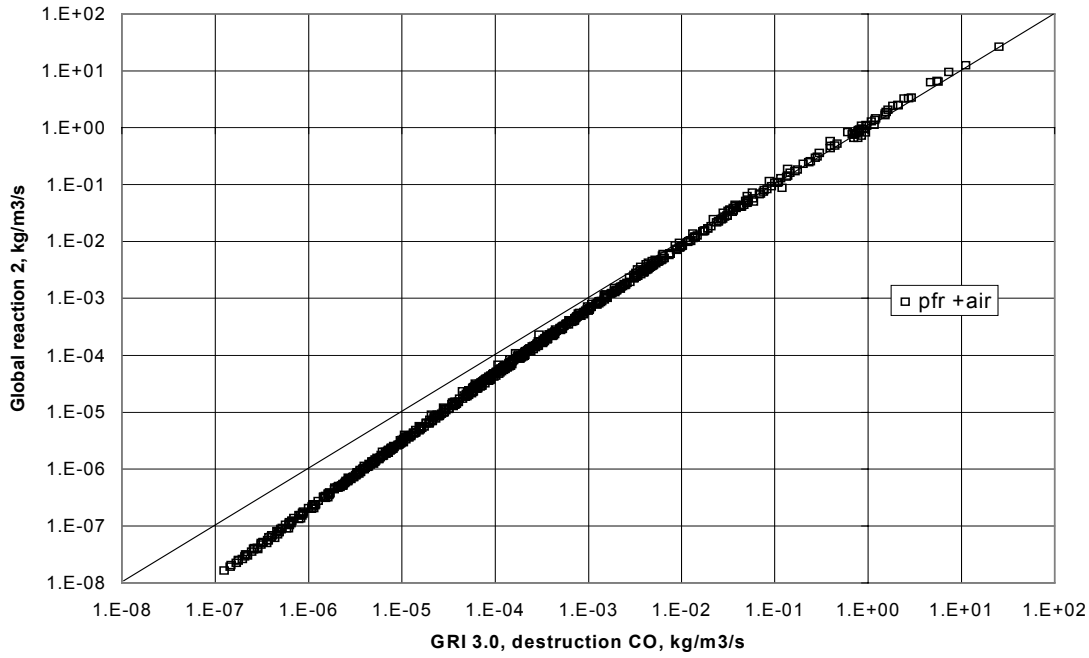

Figure 3.3.9 Rate of carbon monoxide destruction in the PFR with cooling air added. Inlet temperature: 5 atm – 483K, 10 atm –592 K, 20 atm – 716 K; PSR residence time: 5 atm – 2 ms, 10 atm –1.0 ms, 20 atm – 0.5 ms; PFR residence time varied from 2 to 20 ms.

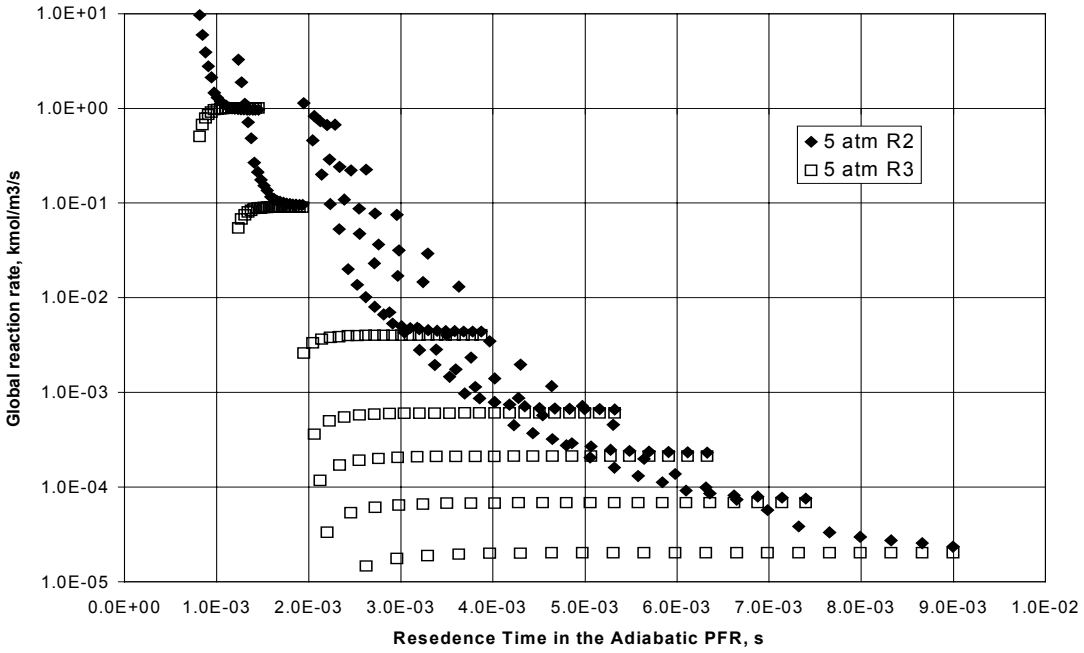

Figure 3.3.10 rates of CO and CO2 destruction in the adiabatic PFR approaching equilibrium for 5 atm. Inlet temperature 483 K; residence time in PRS varies from 0.75 ms to 2.5 ms (higher residence time corresponds to the lower Φ).

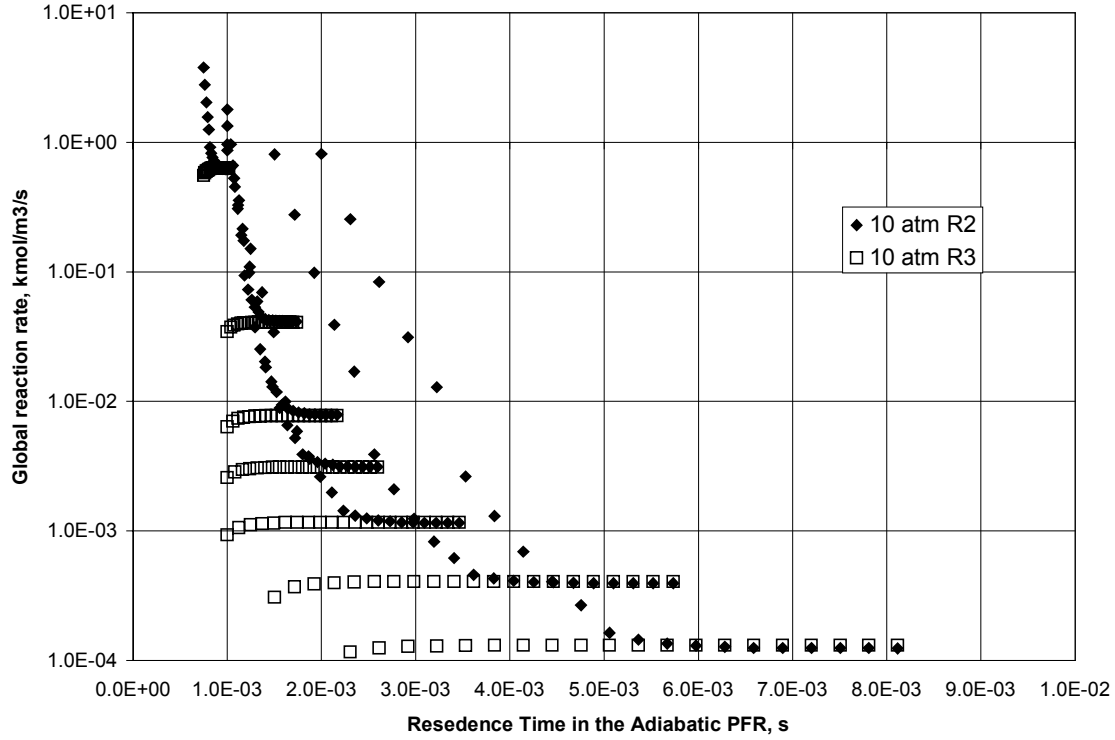

Figure 3.3.11 rates of CO and CO2 destruction in the adiabatic PFR approaching equilibrium for 10 atm. Inlet temperature 592 K; residence time in PRS varies from 0.75 ms to 2.5 ms (higher residence time corresponds to the lower Φ).

3.4 Development of the global mechanism for the formation of nitrogen oxide

3.4.1 Introduction

The formation of oxides of nitrogen in GT combustors is a complex process that depends on many parameters. The flame structure plays a significant role in determining the total amount of NO produced. The factors that determine the NO rate of formation are the local equivalence ratio, temperature, and various species concentrations.

There are four major mechanisms of NO formation considered in this analysis:

1. Zeldovich mechanism

2. Nitrous oxide mechanism

3. Prompt NO mechanism

4. NNH mechanism

Each pathway of NO formation contributes to the overall NO, but the amount of each contribution varies with location in the combustor. It is important to model the mechanisms separately. Figures 3.4.1 through 3.4.6 show the relative contribution of each mechanism in the flame zone, modeled as a single PSR. The fuel-air equivalence ratio and residence time are varied. The data are normalized by the total rate of NO production in the flame zone for each condition, such the sum of the contributions of all mechanisms is equal to unity.

Form the graphs one can note that with an increase of the residence time in the PSR, the relative contributions from the prompt and NNH mechanisms to NO formation becomes small, while the Zeldovich and N_2O mechanisms become significant. This gives an idea what combustion zones should be considered for modeling these mechanisms.

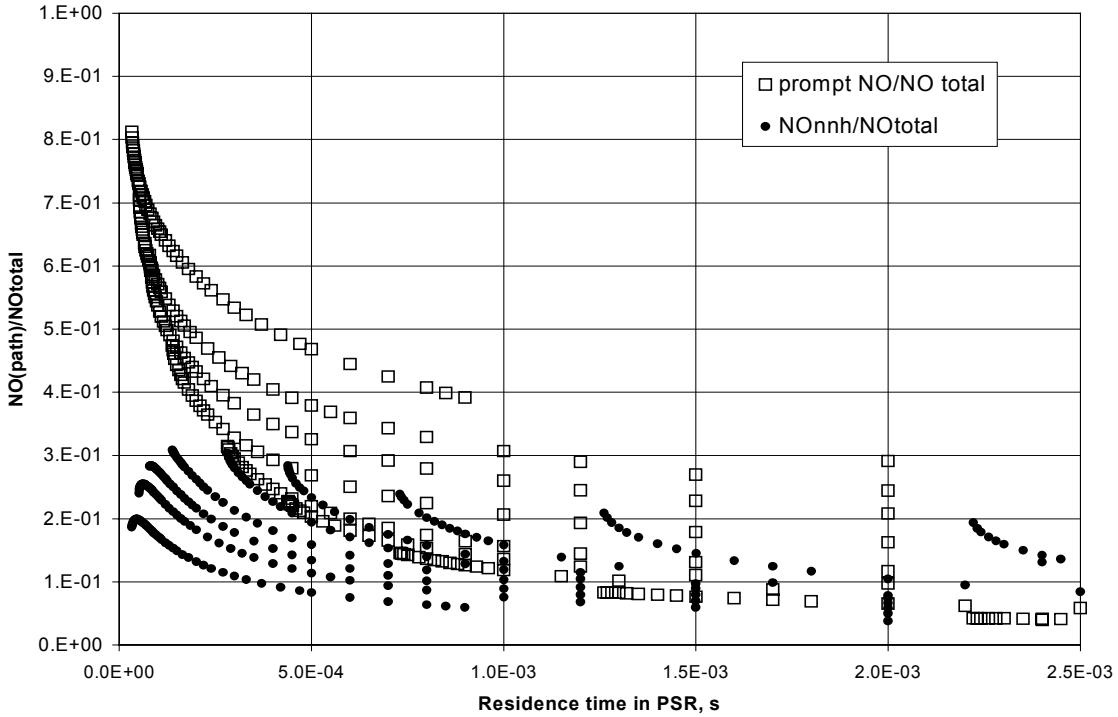

Figure 3.4.1 Prompt and NNH pathways of NO formation in PSR at 5 atm. Inlet temperature 483 K; residence time in the PSR varied from blowout to 2.5 ms; temperature in the PSR corresponds to the adiabatic temperature for given residence time

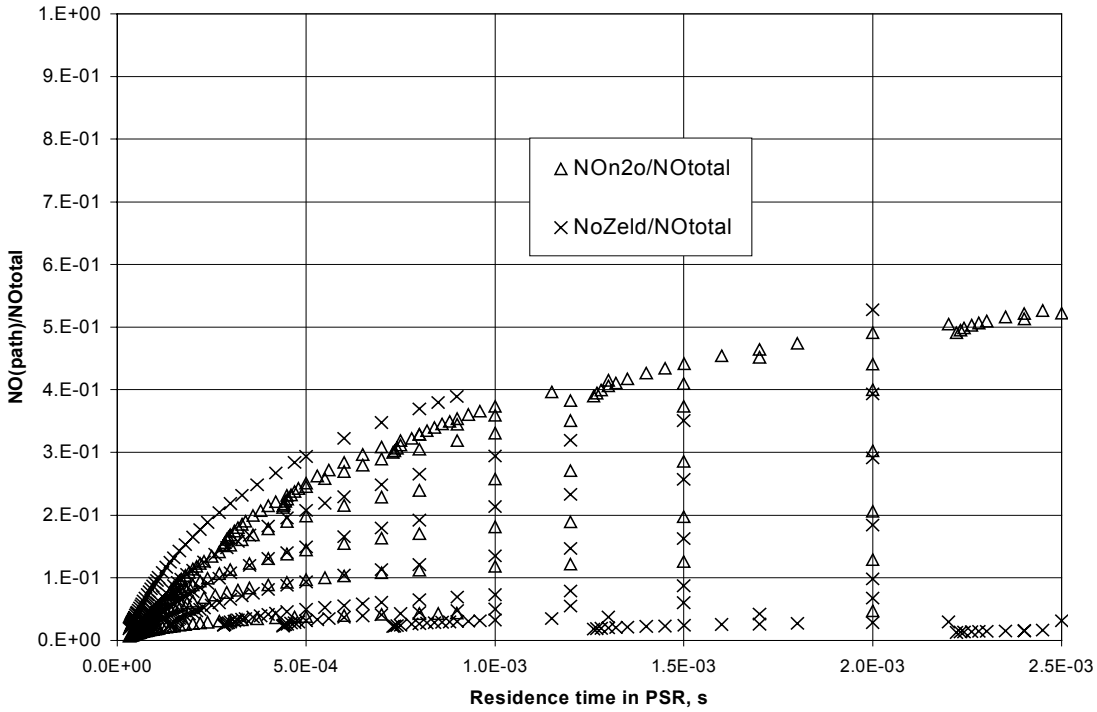

Figure 3.4.2 N_2O and Zeldovich pathways of NO formation in PSR at 5 atm. Inlet temperature 483 K; residence time in the PSR varied from blowout to 2.5 ms; temperature in the PSR corresponds to the adiabatic temperature for given residence time.

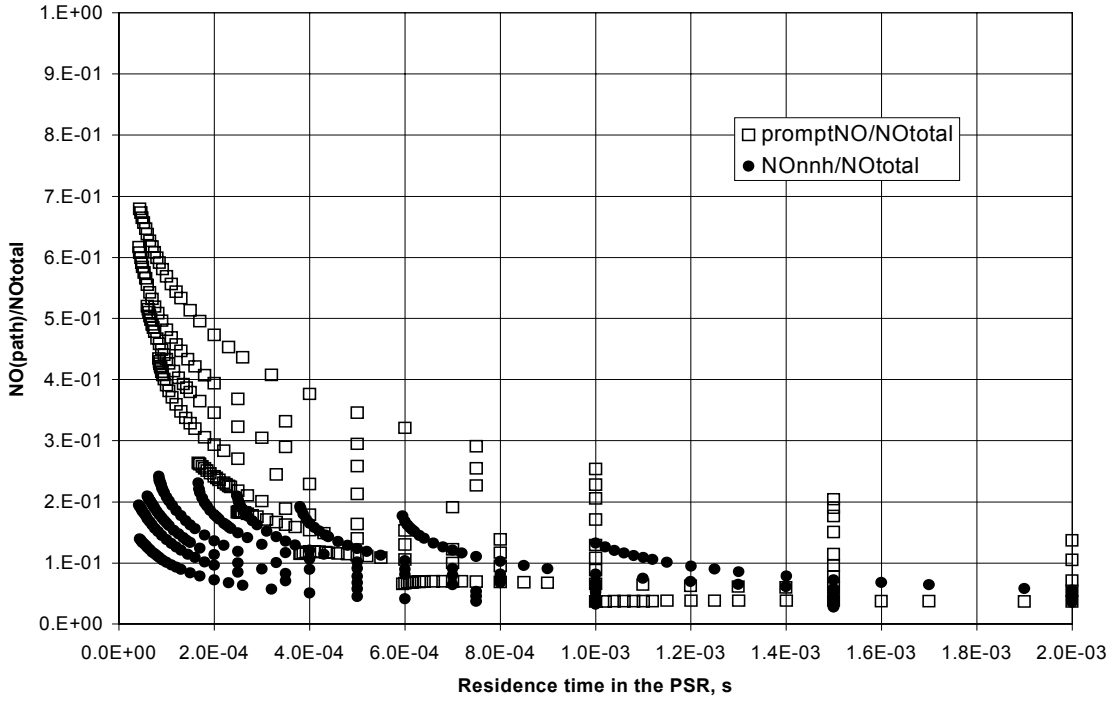

Figure 3.4.3 Prompt and NNH pathways of NO formation in PSR at 10 atm. Inlet temperature 592 K; residence time in the PSR varied from blowout to 2 ms; temperature in the PSR corresponds to the adiabatic temperature for given residence time.

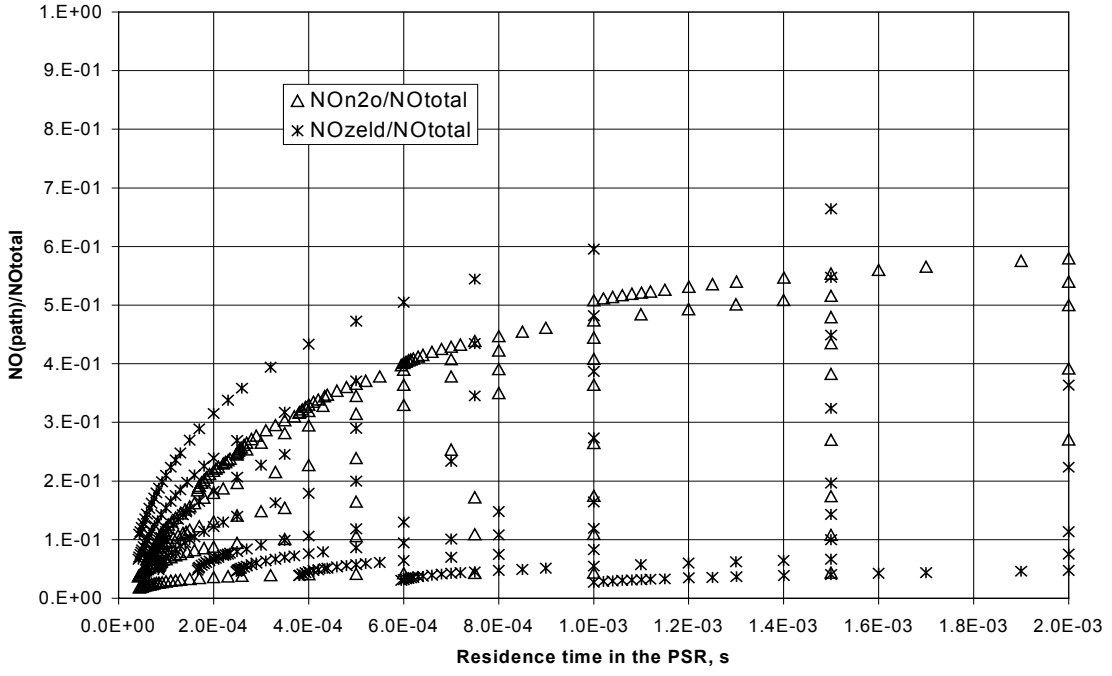

Figure 3.4.4 N_2O and Zeldovich pathways of NO formation in PSR at 10 atm. Inlet temperature 592 K; residence time in the PSR varied from blowout to 2 ms; temperature in the PSR corresponds to the adiabatic temperature for given residence time.

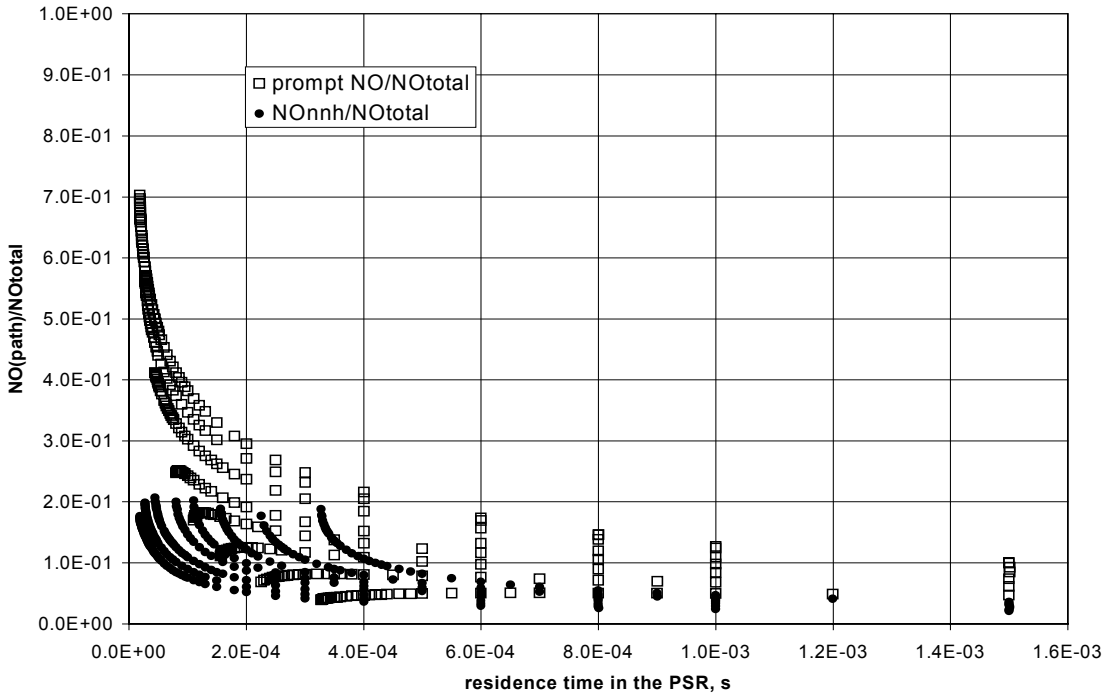

Figure 3.4.5 Prompt and NNH pathways of NO formation in PSR at 20 atm. Inlet temperature 716 K; residence time in the PSR varied from blowout to 1.5 ms; temperature in the PSR corresponds to the adiabatic temperature for given residence time.

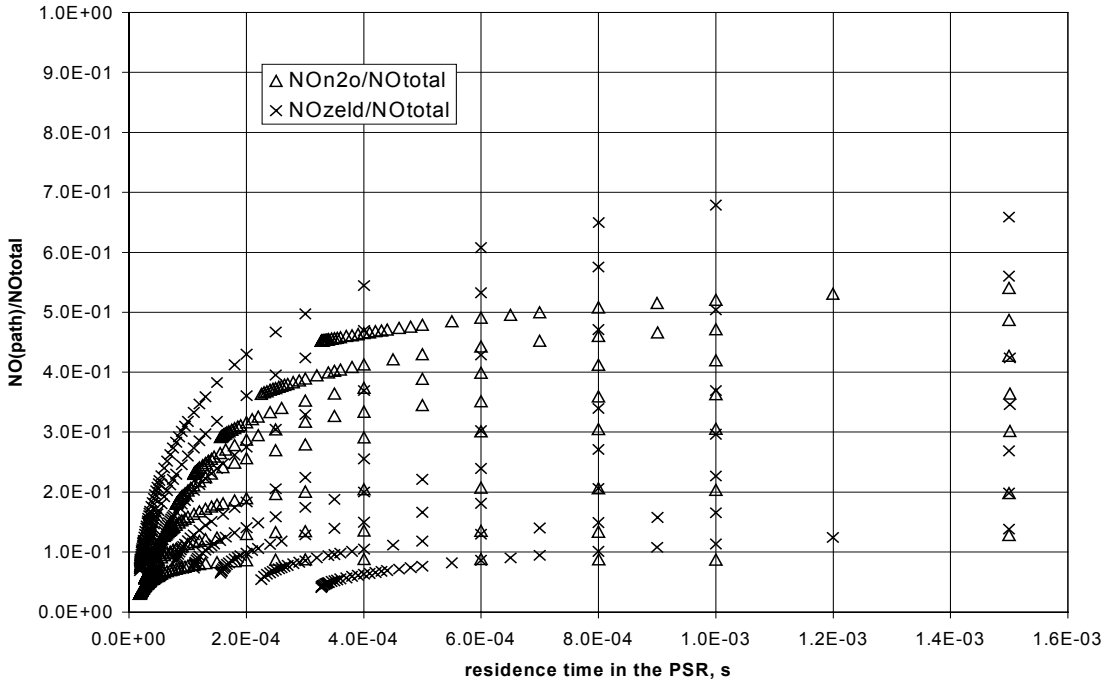

Figure 3.4.6 N_2O and Zeldovich pathways of NO formation in PSR at 20 atm. Inlet temperature 716 K; residence time in the PSR varied from blowout to 1.5 ms; temperature in the PSR corresponds to the adiabatic temperature for given residence time.

3.4.2 Zeldovich Mechanism

At the high temperatures in the flame, O-atoms from the H_2-O_2 system can start the Zeldovich chain reaction by attacking diatomic nitrogen. This reaction is enhanced in the flame zone due to the super-equilibrium concentrations of O-atom:

1. $O+N_2 \rightarrow NO+N$

2. $N+O_2 \rightarrow NO+O$

Often the third reaction is added to the to the mechanism:

3. $N+OH \rightarrow NO+H$

In lean-premixed combustion, the concentration of NO is small thus the backward rates can be neglected. Then the rate of formation of NO can be written as

$$dNO/dt = k_{f1}[N_2][O] + k_{f2}[N][O_2] + k_{f3}[N][OH],$$

where the rate constants of the reactions are:

$$k_{f1} = 2 \times 10^{14} \exp(-315/R_u T)$$

$$k_{f2} = 6.4 \times 10^{9} \exp(-26/R_u T)$$

$$k_{f3} = 3.8 \times 10^{13}$$

The activation energy has the units of kJ/gmol.

Since reactions 2 and 3 rapidly destroy N-atom, one can make a steady-state assumption for the N-atom.

$$d[N]/dt = 0 = k_{f1}[N_2][O] - k_{f2}[N][O_2] - k_{f3}[N][OH]$$

$$[N] = k_{f1}[N2][O] / (k_{f2}[O2] + k_{f3}[OH])$$

and

$$dNO/dt = 2 \times k_{f1}[N_2][O]$$

In the post-flame zone it may be valid to assume that O-atom is equilibrium with O_2.

$$0.5 \times O_2 \leftrightarrow O$$

The equilibrium constant for this expression is:

$$Kp = \exp(-(g_O - 0.5 \times g_{O2})/(R_u T))$$

Then, with the assumption of O-atom equilibrium the rate of formation of Zeldovich NO can be written as:

$$dNO/dt \text{ (thermal Zeldovich)} = 10^{14.967}[N_2][O_2]^{0.5} \times T^{-0.5}\exp(-68899/T)$$

This expression is called the thermal Zeldovich NO formation rate. It is a R8 in the eight-step global mechanism.

3.4.3 Nitrous oxide mechanism of NO formation

In the nitrous oxide mechanism, NO is formed via the intermediate species N_2O that is produced in the flame by the following reaction:

$$O + N_2 + M \leftrightarrow N_2O + M$$

Bowman (1992) states that this reaction is important in fuel-lean combustion at low temperatures and high pressures. Both conditions are observed in LP combustors for gas turbines. For the combustion process where temperature is greater than 1500K, the average lifetime of N_2O is calculated to be less than 10 ms. This suggests that N_2O should not be significantly found in the combustor exhaust.

The major steps of the N_2O mechanism are:

$$N_2O + H \rightarrow N_2 + OH$$

$$N_2O + O \rightarrow N_2 + O_2$$

$$N_2O + O \rightarrow NO + NO$$

$$N_2O + H \leftrightarrow NH + NO$$

$$O + H_2 + M \leftrightarrow H_2O + M$$

Two of these reactions form NO. Detailed chemical kinetic modeling using GRI 3.0 predicts that at some conditions the N_2O mechanism can contribute up to 80% of total amount of nitrogen oxide produced. Figures 3.4.2, 3.4.4, and 3.4.6 show that the relative amount of NO produced by both Zeldovich and nitrous oxide mechanisms increases with the residence time of the mixture in the PSR.

Global modeling of the nitrous oxide mechanism of formation in the combustor presents some difficulties. While one global reaction rate for the nitrous oxide and Zeldovich mechanism in the flame zone works fine, with representation of the super-equilibrium concentration of O and H atoms by CO, the same rate fails to predict NO formation in the post-flame and recirculation zones. The problem is that CO goes to equilibrium faster

than NO. This led to developing a separate post-flame nitrous oxide mechanism in the procedure similar to the thermal Zeldovich mechanism.

From the results of GRI 3.0 one can determine that the dominant reactions of the N_2O mechanism in the post-flame zone are:

$$N_2O+O \rightarrow NO+NO$$

$$N_2O+H \rightarrow NH+NO$$

The NH reacts to NO by:

$$NH+O_2 \rightarrow NO+OH$$

$$NH+O \rightarrow NO+H$$

Thus, assuming that any NH formed oxidizes to NO, the rate of NO formation via the nitrous oxide mechanism is:

$$d[NO]/dt = 2\times k_{f1}[N_2O][O] + 2\times k_{f2}[N_2O][H]$$

The concentrations of the species of interest can be found from equilibrium calculations, assume the following equilibrium expressions:

$$N_2O \leftrightarrow N_2+0.5\times O_2$$

$$0.5\times O_2 \leftrightarrow O$$

$$0.5\times H_2O \leftrightarrow H+0.25\times O_2$$

The equilibrium constants for these expressions are:

$$K_p = \exp(-(g_{N2}+0.5\times g_{O2}-g_{N2O}) / (R_uT))$$

$$K_p = \exp(-(g_{O}-0.5\times g_{O2}) / (R_uT))$$

$$K_p = \exp(-(g_{H}+0.25\times g_{O2}-0.5\times g_{H2O}) / (R_uT))$$

Plugging in the computed equilibrium constants to the rate expressions one obtains the rate of NO formation where the equilibrium assumptions for O-atom, H-atom, and N_2O are made. By analogy with thermal Zeldovich NO, this is called thermal nitrous oxide NO.

$$dNO/dt(\text{thermal } N_2O) = 10^{14.592}[N_2][H_2O]^{0.5}[O_2]^{0.25} \times T^{-0.7}\exp(-69158/T) + 10^{10.317}[N_2][O_2] \times \exp(-52861/T)$$

Figures 3.4.7 and 3.4.8 show the rate of NO formation in the PFR via thermal nitrous oxide NO and the total rate of NO formation via N_2O mechanism. The thermal nitrous oxide NO steps are reactions 6 and 7 in the 8-step global mechanism.

$$R_6 = 10^{14.592}[N_2][H_2O]^{0.5}[O_2]^{0.25} \times T^{-0.7}\exp(-69158/T)$$

$$R_7 = 10^{10.317}[N_2][O_2] \times \exp(-52861/T)$$

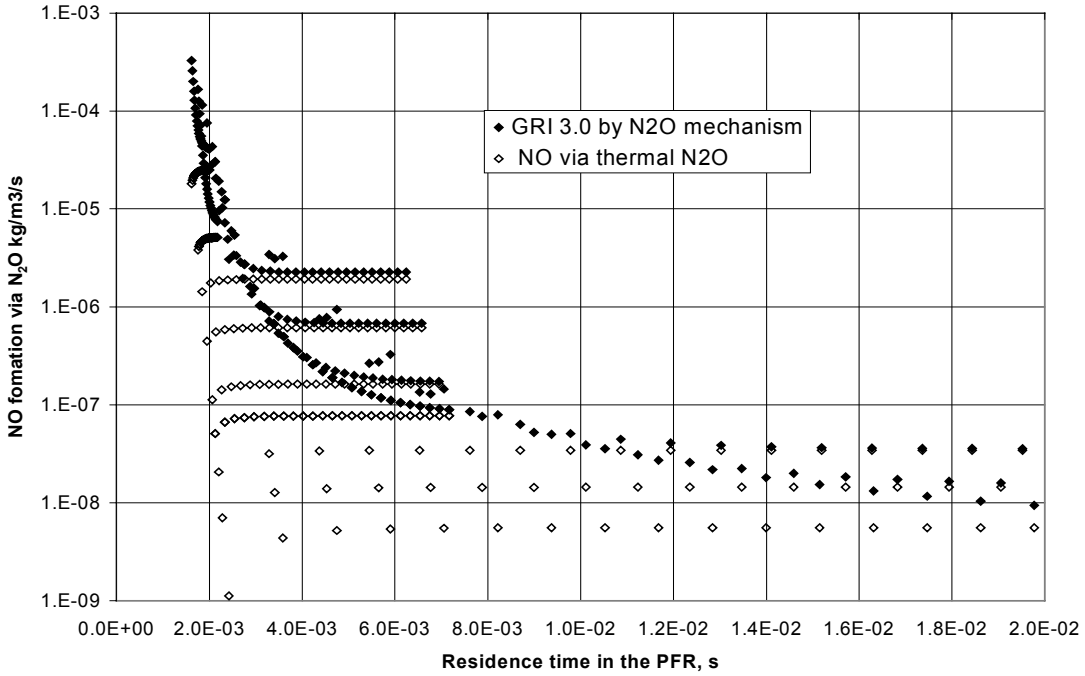

Figure 3.4.7 Formation of NO via N_2O and thermal N_2O mechanisms in adiabatic PFR at 5 atm. Inlet temperature 483 K; residence time in PSR 2 ms.

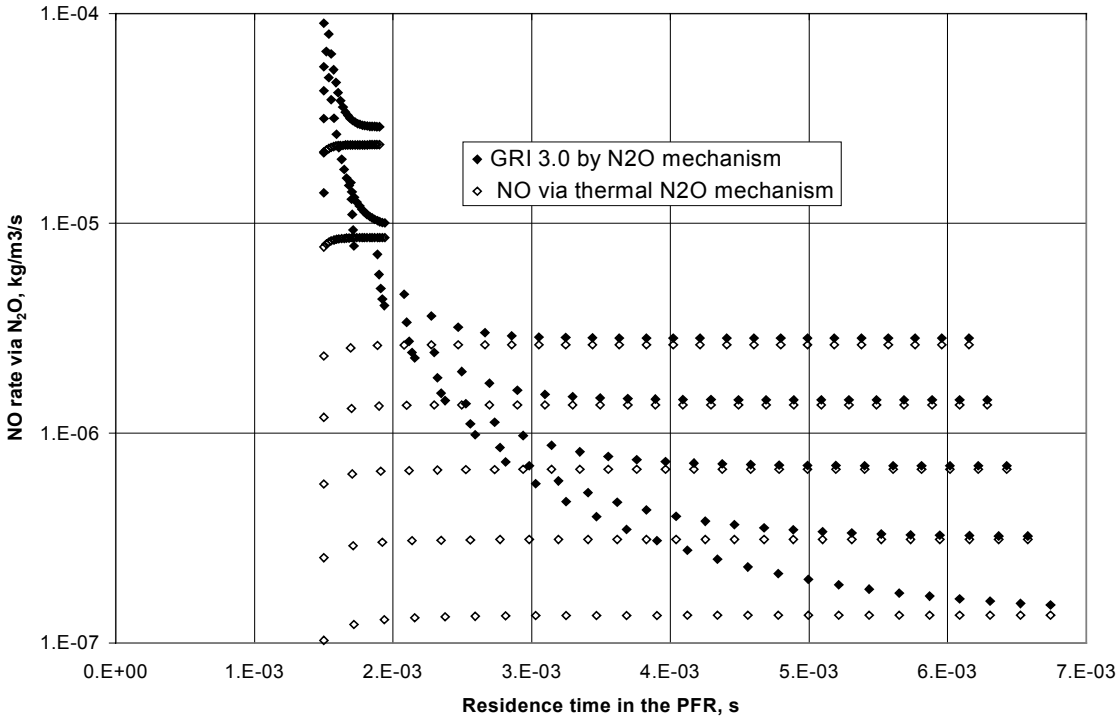

Figure 3.4.8 Formation of NO via N_2O and thermal N_2O mechanisms in adiabatic PFR at 10 atm. Inlet temperature 592 K; residence time in PSR 1.5 ms.

3.4.4 Reaction 4

Reaction 4 of the 8-step global mechanism consists of flame zone NO formation via the nitrous oxide and Zeldovich mechanisms combined. In this case, NO forms in the field of super-equilibrium O, H, and OH radical concentrations. The rate does not include the Zeldovich thermal and N_2O thermal effects. The rate of NO formation for this mechanism can be written as:

$$R4 = dNO/dt = dNO/dt(\text{Zeldovich}) + dNO/dt(N_2O) \\ -dNO/dt(\text{Zeldovich thermal}) - dNO/dt(N_2O \text{ thermal}),$$

where

$$dNO/dt(\text{Zeldovich}) = 2\times k_{f1(\text{Zeldovich})}[N_2][O]$$

$$dNO/dt(N_2O) = 2\times k_{f1(N2O)}[N_2O][O] + 2\times k_{f2(N2O)}[N_2O][H]$$

$$dNO/dt(\text{Zeldovich thermal}) = 10^{14.967}[N_2][O_2]^{0.5}\times T^{-0.5}\exp(-68899/T)$$

$$dNO/dt(N_2O \text{ thermal}) = 10^{14.893}[N_2][H_2O]^{0.5}[O_2]^{0.25}\times T^{-0.7}\exp(-69158/T) \\ +10^{10.618}[N_2][O_2]\times\exp(-52861/T)$$

The forward rate constants of the reactions are obtained from the GRI 3.0:

$$k_{f1(\text{Zeldovich})} = k_{f1} = 2\times 10^{14}\, T^{-0.5}\exp(-37888/T))$$

$$k_{f1(N2O)} = 10^{10.462}\exp(-11658/T)$$

$$k_{f2(N2O)} = 10^{13.793}T^{-0.45}\exp(-16262.4/T)$$

The above coefficients allow the determination of the rate of non-equilibrium NO from the GRI 3.0 mechanism The least square fit for reaction 4 of the global mechanism is based on the species: CO, N_2, O_2. The chemical reactors used for determining of reaction 4 include the flame zone (PSR), the recirculation zone (PSR2), and the post-flame zone without any air added (PFR adiabatic). The lowest residuals of the least square fit are obtained with the following rate expression:

$$R_4 = 10^{14.122+0.0376\times P}[CO]^{0.8888-0.0006\times P}[O_2]^{1.1805+0.0344\times P}\exp(-(46748+126.6\times P)/T)$$

Figures 3.4.9, 3.4.10, and 3.4.11 show the agreement of the fit for reaction 4 with data obtained from GRI 3.0 for the different chemical reactors. The comparisons show good agreement for NO formation via reaction 4 reactive to GRI 3.0. However, reaction 4 somewhat under-predicts the NO level in the flame zone for 5 atm and for low fuel-air

equivalence ratios (0.45-0.55). Also the reaction 4 somewhat over-predicts the NO production in the recirculation zone.

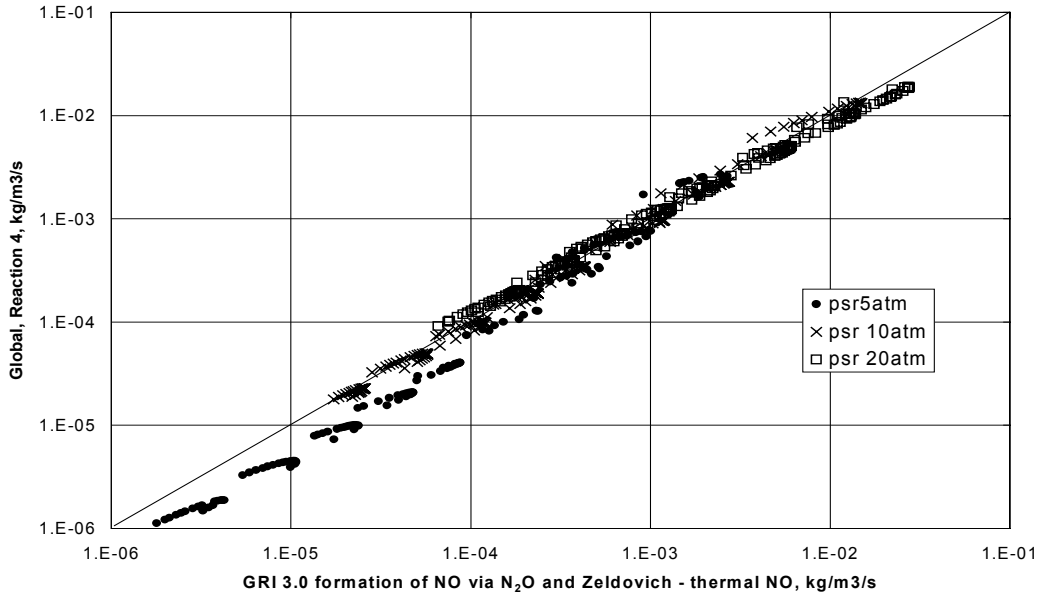

Figure 3.4.9 Formation of NO in the flame (modeled as PSR) via N_2O and Zeldovich mechanisms without thermal NO versus global reaction 4. Inlet temperature: 5 atm –483 K, 10 atm – 592 K, 20 atm – 716 K; temperature in the PSR corresponds to the adiabatic flame temperature. Residence time in the PSR varies from the blowout to 2.5 ms.

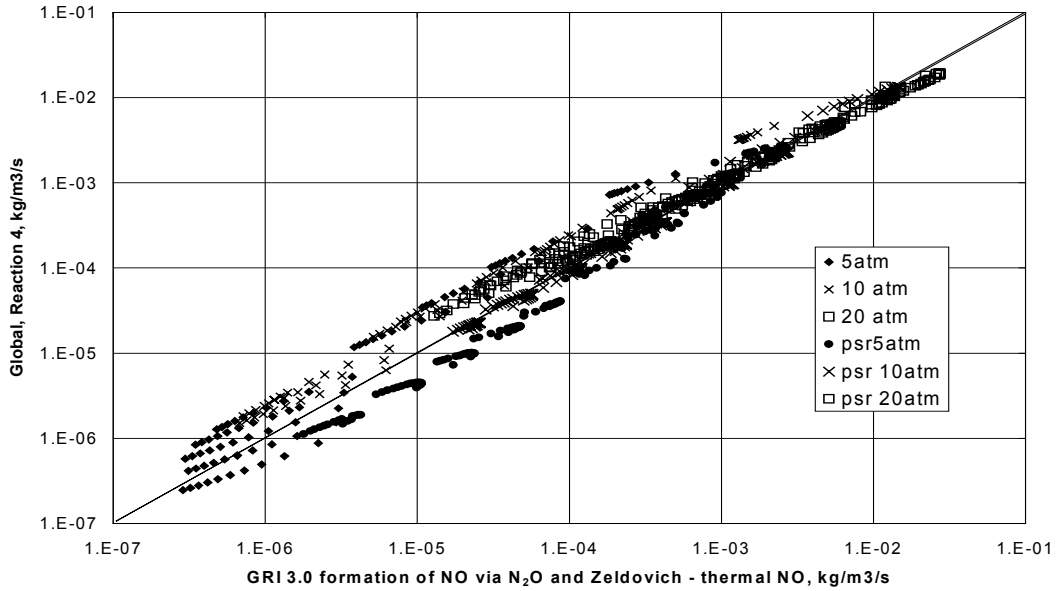

Figure 3.4.10 Formation of NO in the recirculation zone (modeled as PSR2) via N_2O and Zeldovich mechanisms without thermal NO versus global reaction 4. Inlet temperature: 5 atm –483 K, 10 atm – 592 K, 20 atm – 716 K; temperature in the PSR corresponds to the adiabatic flame temperature. Residence time in the adiabatic PSR2 varied from 2 ms to 20ms.

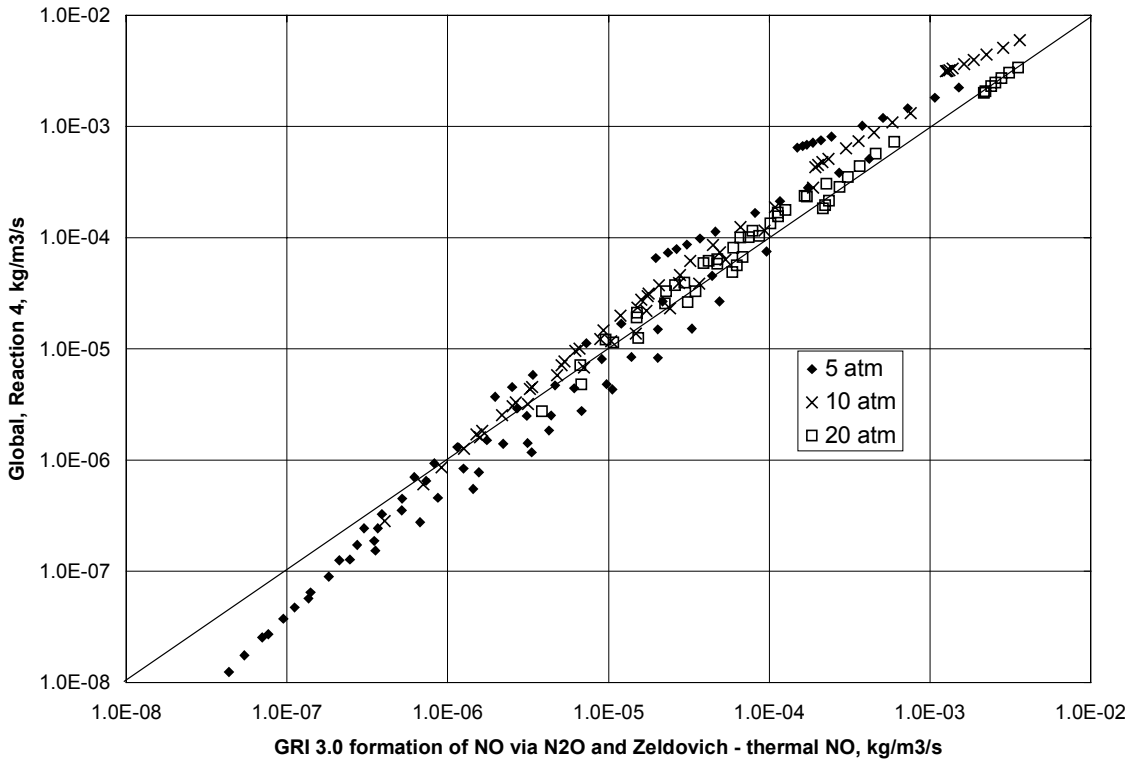

Figure 3.4.11 Formation of NO in the post-flame zone (modeled as adiabatic PFR) via N_2O and Zeldovich mechanism without thermal NO versus global reaction 4. Inlet temperature: 5 atm –483 K, 10 atm – 592 K, 20 atm – 716 K; temperature in the PSR corresponds to the adiabatic flame temperature. Residence time in the adiabatic PFR varies from 2 ms to 20ms.

3.4.5 NNH mechanism of NO formation

Bozzelli and Dean (1995) proposed a mechanism of NO formation in flames via the reaction

$$NNH+O \rightarrow NH+NO$$

Under the lean premixed condition in the GT combustor, NH is oxidized to nitrogen oxide as follows:

$$NH+O_2 \rightarrow NO+OH$$

$$NH+O \rightarrow NO+H$$

Harrington et al. (1996) tested the NNH mechanism in a low-pressure flame to minimize the amount of NO made by other known mechanisms. In their research, though the agreement was imperfect, the NNH mechanism provided the explanation for NO formation at the tested conditions. Therefore, one needs to include this pathway in the combustion model.

3.4.6 Prompt NO

A number of investigators have tried to capture the mechanism on NO formation in the flame zone. The concentration of free radicals in the flame zone is several magnitudes greater than in the post-flame. Fenimore (1971) showed that in the flame zone a mechanism other than Zeldovich contributes to NO formation. He called the mechanism "prompt NO". This pathway of NO formation is not found in non-hydrocarbon flames. Fenimore concluded that NO is formed by the reaction of hydrocarbon radicals and diatomic nitrogen. He suggested that the following reactions could form NO in the hydrocarbon flame.

$$CH+N_2 \rightarrow HCN+N$$

$$C_2+N_2 \rightarrow 2\times CN$$

All three products of these reactions tend to form NO when attacked by other free radicals. The second reaction should not be a strong contributor in methane air combustion since, C_2 species is unlikely to significantly appear in the methane break down. On the other hand, CH is known to be present in the methane-air flame.

The N-atom, when colliding with diatomic oxygen follows the Zeldovich pathway:

$$N+OH \rightarrow NO+H$$

$$N+O_2 \rightarrow NO+O$$

Nitrogen oxide can be formed from HCN via the following reactions:

$$HCN+O \rightarrow NCO+H$$

$$NCO+H \rightarrow NH+CO$$

$$NH+(H, OH) \rightarrow N+(H_2, H_2O)$$

$$N+OH \rightarrow NO+H$$

$$N+O_2 \rightarrow NO+O$$

$$NH+O_2 \rightarrow NO+OH$$

$$NH+O \rightarrow NO+H$$

Detailed analysis of the pathways of NO formation in the typical LP combustor shows that prompt NO can contribute up to 80% of total nitrogen oxide formed in the flame zone. The biggest contribution from the prompt mechanism comes at lower pressure (5 atm) and higher fuel-air equivalence ratio (Φ greater than 0.7). Figures 3.3, 3.4, and 3.5 show the normalized rates of NO formation versus residence times in the perfectly stirred reactor.

In the modeling of the Fenimore mechanism, only reaction CH+N2→HCN+N is considered with the assumption that all of the products of the reaction eventually end up as NO. Since the global mechanism does not explicitly include any hydrocarbon radicals, a surrogate species must be found to represent the CH radical. The only species that is present in the flame zone, similar to the hydrocarbon radicals and available for modeling, is CH_4.

Before the prompt reaction occurs, the concentration of methane is high, but there are no radicals present. The concentration of hydrocarbon radicals is rising in the flame zone very rapidly similar to carbon monoxide. Attempts to insert CO into the global reaction for prompt NO were not successful, however, probably due to the longevity of carbon monoxide in the flame.

The rate of formation of nitrogen oxide via the prompt pathway can be simplified to the following expression

$$dNO/dt = k_f \times [CH][N_2]\exp(-E_a / (R_u T))$$

The values for k_f and E_a are obtained from GRI 3.0. The concentrations of CH and N_2; and temperature are specific to a particular case.

3.4.7 Reaction 5

Figures 3.4.1, 3.4.3, and 3.4.5 show the normalized rate of NO formation by the NNH mechanism for different operating pressures of the combustor. It is decaying rapidly with the amount of time that the mixture spends in the flame. From the global point of view, the rate exhibits very similar behavior to the prompt mechanism, thus in modeling of the global reaction mechanism we combine the NNH and prompt mechanisms together.

The database for the least square fit for the NNH and the prompt NO mechanisms is obtained using a single PSR. The reactor is adiabatic for most cases, however some cases are assigned a temperature less than the adiabatic temperature. Since the prompt mechanism is most important at the rich fuel-air equivalence ratios and low pressures, more weight is given to these conditions. The conditions where the prompt mechanism contributes less than 5% of the total NO are not considered in this analysis, with a purpose of tuning the mechanism in the region of its greatest importance.

Performing the least square fit gives the following form:

$$R_5=10^{n0+n1\times P}[CH_4]^{a0+a1\times P}[O_2]^{b0+b1\times P}\exp(-(T_a+T_{a1}\times P)/T)$$

The diatomic nitrogen does not change its concentration sufficiently to influence the reaction rate, thus it is not explicitly included in the reaction. However the pre-exponential factor carries the pressure dependency in it, which is an implicit reference to N_2. The least residuals for the reaction rate are given by the formula:

$$R_5=10^{14.2466+0.10779\times P}[CH_4]^{2.0886-0.03193\times P}[O_2]^{-1.6674+0.04122\times P}\exp(-(48772.3+789.05\times P)/T)$$

Figure 3.4.12 shows the agreement between the full kinetic mechanism and the global rate of NO formation via the prompt and NNH pathways.

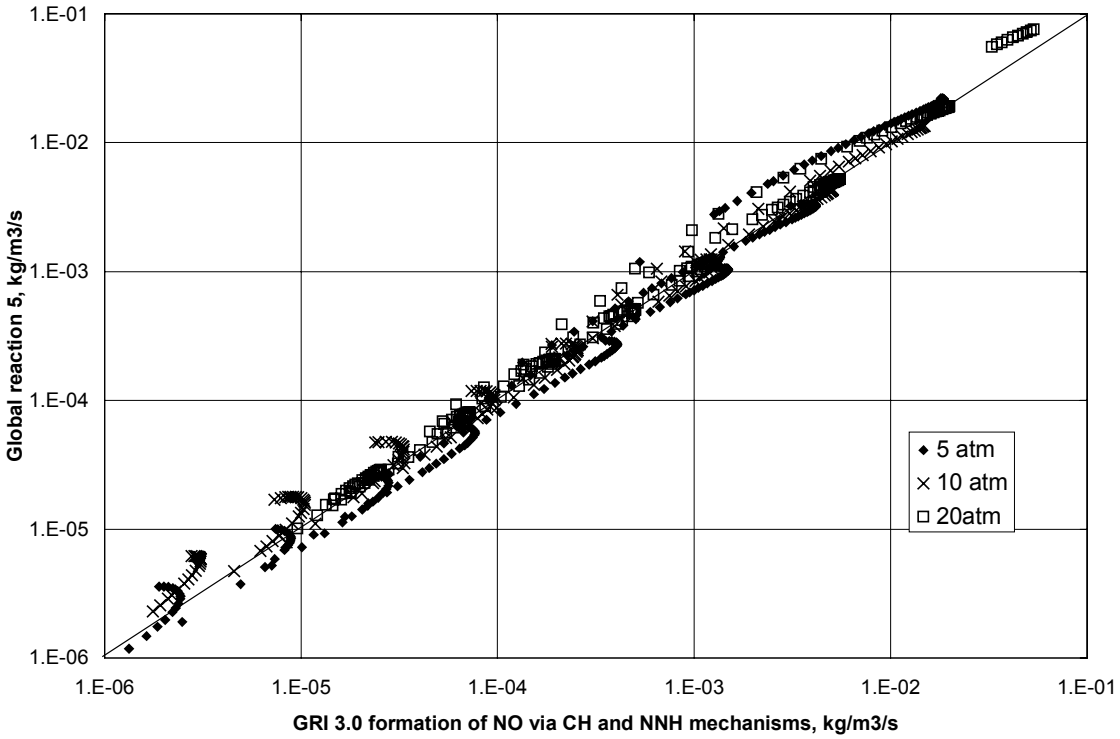

Figure 3.4.12 Formation of NO in the flame (modeled as PSR) via NNH and prompt mechanisms versus global reaction 5. Inlet temperature: 5 atm –483 K, 10 atm – 592 K, 20 atm – 716 K; temperature in the PSR corresponds to the adiabatic flame temperature. Residence time in the PSR varies from the blowout to 2.5 ms.

3.5 Summary of the eight-step global mechanism

The global mechanism consists of eight reactions in the global format and includes seven species. There are three reactions for methane oxidation and five reactions for formation of nitrogen oxide. The reactions are:

Reaction 1 $CH_4+1.5\times O_2 \rightarrow CO+2\times H_2O$

Reaction 2 $CO+0.5\times O_2 \rightarrow CO_2$

Reaction 3 $CO_2 \rightarrow CO+0.5\times O_2$

Reaction 4 $N_2+O_2 \rightarrow 2\times NO$ (via non-thermal N_2O and Zeldovich mechanisms)

Reaction 5 $N_2+O_2 \rightarrow 2\times NO$ (via NNH and prompt mechanisms)

Reaction 6 $N_2+O_2 \rightarrow 2\times NO$ (via thermal N_2O + H)

Reaction 7 $N_2+O_2 \rightarrow 2\times NO$ (via thermal N_2O + O)

Reaction 8 $N_2+O_2 \rightarrow 2\times NO$ (via thermal Zeldovich)

The rates of the reaction are found by the best agreement with the detailed chemical mechanism GRI 3.0. The rates of the reactions are:

$$R_1=10^{13.354-0.004628\times P}[CH_4]^{1.3-0.01148\times P}\,[O_2]^{0.01426}\,[CO]^{0.1987}\exp\left(-(21932+269.4\times P)/T\right)$$

$$R_2=10^{14.338+0.1091\times P}[CO]^{1.359-0.0109\times P}[H_2O]^{0.0912+0.0909\times P}[O_2]^{0.891+0.0127\times P}\exp\left(-(22398+75.1\times P)/T\right)$$

$$R_3=10^{15.8144-0.07163\times P}\,[CO_2]\times\exp\left(-(64925.8-334.31\times P)/T\right)$$

$$R_4=10^{14.122+0.0376\times P}[CO]^{0.8888-0.0006\times P}[O_2]^{1.1805+0.0344\times P}\exp\left(-(46748+126.6\times P)/T\right)$$

$$R_5=10^{14.2466+0.10779\times P}[CH_4]^{2.0886-0.03193\times P}[O_2]^{-1.6674+0.04122\times P}\exp\left(-(48772.3+789.05\times P)/T\right)$$

$$R_6=10^{14.592}[N_2][H_2O]^{0.5}[O_2]^{0.25}\times T^{-0.7}\exp\left(-69158/T\right)$$

$$R_7=10^{10.317}[N_2][O_2]\times\exp\left(-52861/T\right)$$

$$R_8=10^{14.967}\,[N_2][O_2]^{0.5}\,T^{-0.5}\times\exp\left(-68899/T\right)$$

The units used in the rate expressions are: activation energy = K, concentrations = $kmol/m^3$, reaction rates = $kmol/(m^3\times s)$.

Figures 3.5.1 through 3.5.3 show the agreement of the 8 step global mechanism with detailed chemical kinetic mechanism GRI 3.0 in terms of NO production for different zones of the combustor.

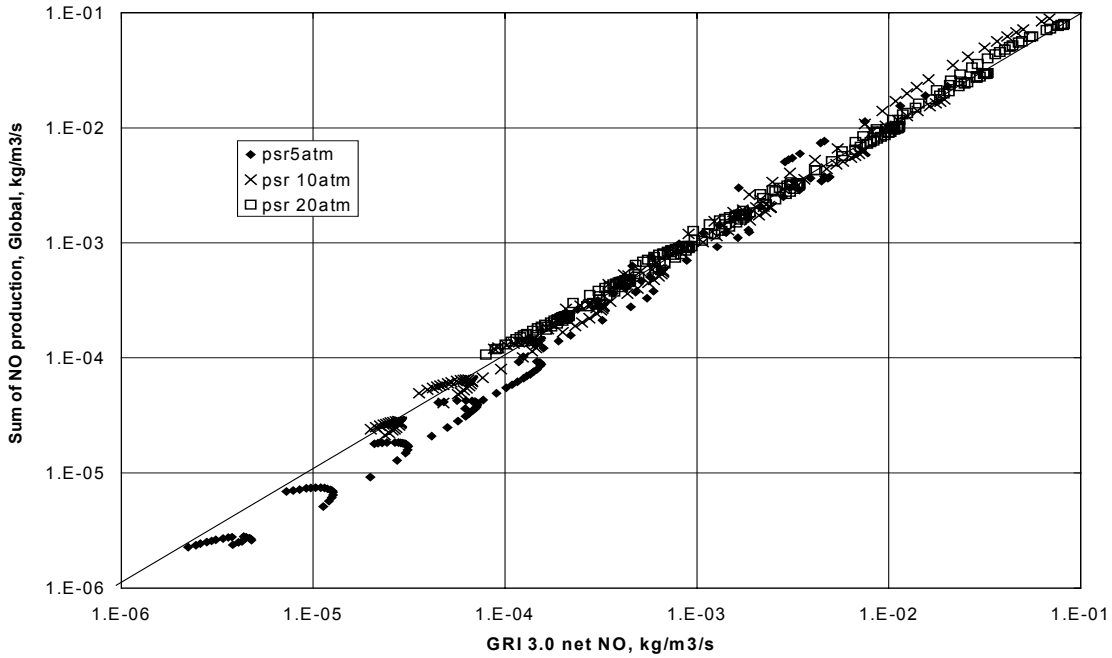

Figure 3.5.1 Formation of NO by the global mechanism versus total rate of NO production by GRI 3.0 in the flame (modeled as PSR). Inlet temperature: 5 atm –483 K, 10 atm – 592 K, 20 atm – 716 K; temperature in the PSR corresponds to the adiabatic flame temperature. Residence time in the PSR varies from the blowout to 2.5 ms.

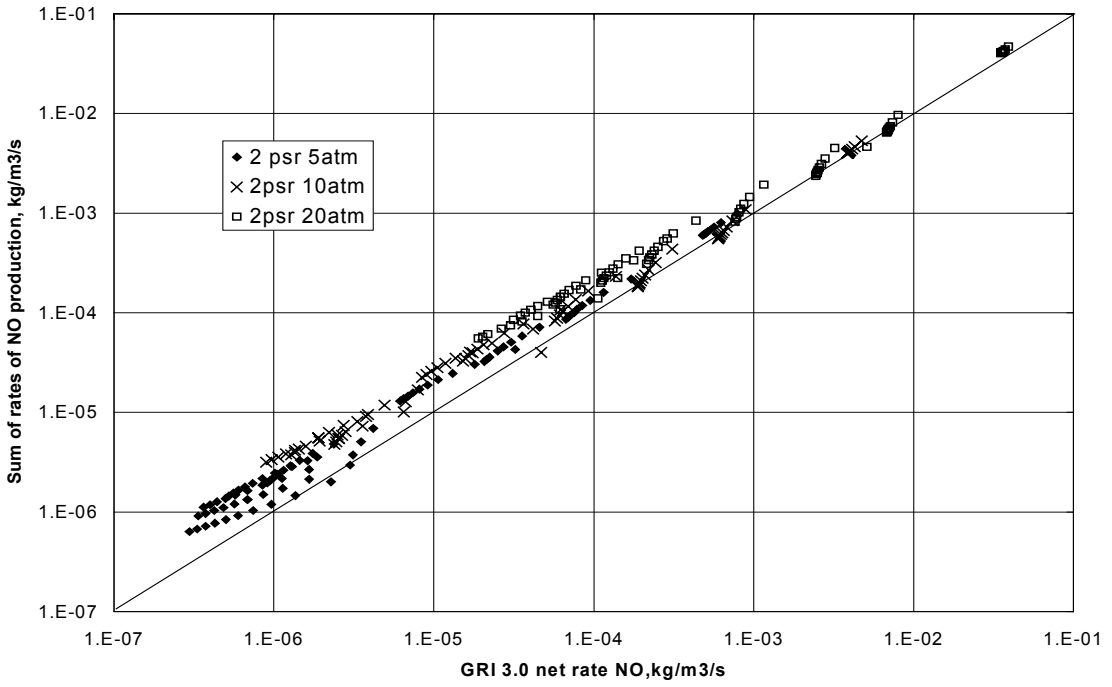

Figure 3.5.2 Formation of NO by global mechanism versus total rate of NO production by GRI 3.0 in the recirculation zone (modeled as PSR2). Inlet temperature: 5 atm –483 K, 10 atm – 592 K, 20 atm – 716 K; temperature in the PSR corresponds to the adiabatic flame temperature. Residence time in the adiabatic PSR2 varies from 2 ms to 20ms.

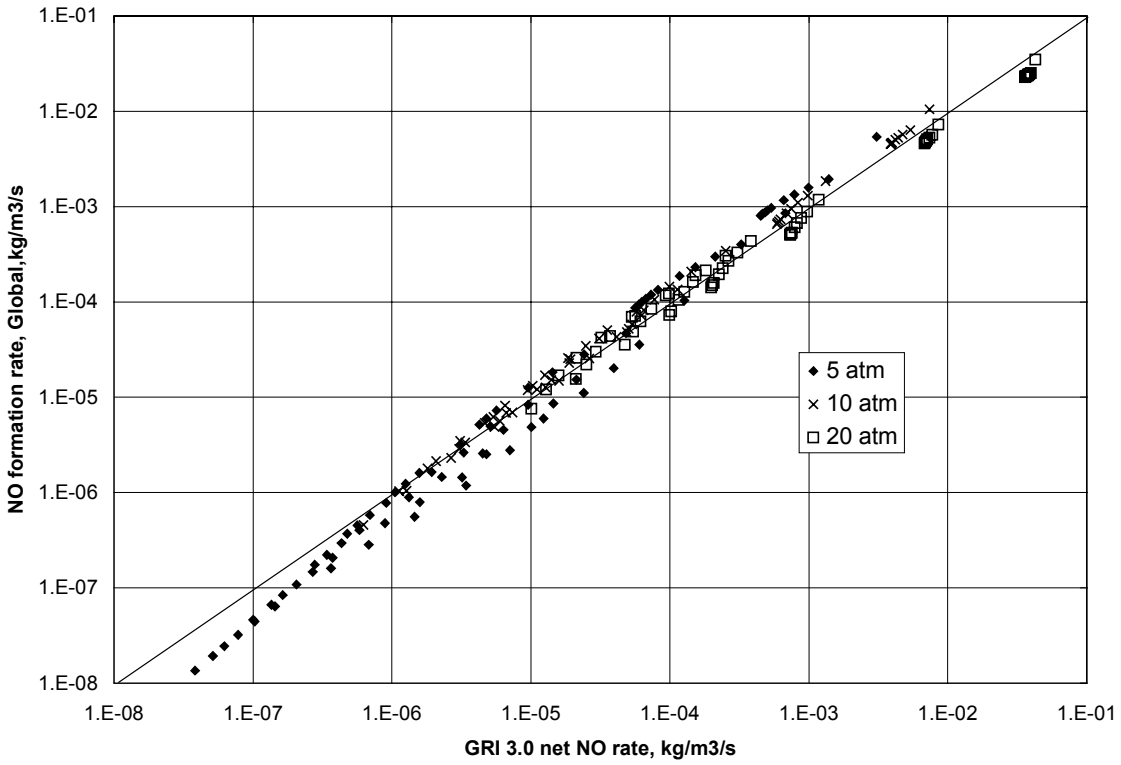

Figure 3.5.3 Formation of NO by global mechanism versus net rate of NO production by GRI 3.0 in the post-flame zone (modeled as adiabatic PFR followed by a PSR). Inlet temperature: 5 atm –483 K, 10 atm – 592 K, 20 atm – 716 K; temperature in the PSR corresponds to the adiabatic flame temperature. Residence time in the adiabatic PFR varies from 2 ms to 20ms.

Chapter 4

Validation of 8-step Global Mechanism

4.1 Introduction

The discussion in this chapter is focused on validation of the new 8-step global mechanism. This is done by using the 8-step mechanism in PSR, PSR-PSR, and a PSR-PFR simulation of high-pressure jet-stirred reactor (HP- JSR) database for NO_x and CO. Two databases are considered in this analysis: one of Karin U.M. Bengtsson (1998) and the other one of Teodora Rutar (2000).

The multi-jet HP-JSR used by Bengtsson was operated at pressures up to 20 bars, residence times of 1.0, 1.5, and 2.0 ms, a fuel-air equivalence ratio of 0.55, and temperatures of 1783 and 1823 K. The concentrations of species were measured at the reactor outlet within a sampling tube. The volume of the sampling tube up to the sampling point is about 16% of the total volume of the reactor. The experimental data show the negative dependency of the measured NOx emission on pressure and slightly positive on residence time in the reactor.

The HP-JSR of Rutar is a single jet reactor. It was operated at pressures of 3.0, 4.7 and 6.5 atm, for residence times between 0.5 and 4.0 ms. Data were gathered for preheated and unheated inlet conditions. Within the reactor the temperature was measured by a thermocouple placed in the recirculation zone and it was corrected by two independent methods (heat balance for the thermocouple and heat transfer by the JSR wall). The measurements of the species concentrations were taken in the recirculation zone. The data show some NOx decrease with the increase of pressure. The modeling of the Rutar HP-JSR depends on the residence time in the reactor. At the short residence times the JSR can be modeled successfully by a single PSR. At high residence times, associated with the low flow rates, the reactor is modeled by two consecutive PSRs. For the later case the turbulent flame zone occupies only a small part of the JSR and is represented by the first PSR. The post-flame zone is modeled by the second PSR. The basis for choosing the type of the chemical reactor can be found by analyzing the regimes of turbulent combustion.

There are three regimes of turbulent premixed combustion as described in Turns (2000):

1. Wrinkled laminar flames, in which case the laminar flame thickness (δ_L) is smaller than the smallest eddy (l_K, Kolmogorov scale)

2. Flamelets-in-eddies regime, in which case the flame thickness is larger than the Kolmogorov scale but smaller than the integral turbulent scale.

3. Distributed reaction, in which case the flame thickness is larger than the integral scale.

The division between the regimes is rather arbitrary, and can be described by non-dimensional numbers: Damkohler and turbulent Reynolds numbers. The Damkohler number (Da) = mixing time/chemical time, and the turbulent Reynolds number (Re) = $u'd_0/\nu$, with u' = the turbulent component of velocity, here taken to be 10% of inlet jet velocity, d_0 = the integral turbulent scale (equals the inlet jet diameter) and ν = the kinematic viscosity.

In Rutar et al. (2001) the authors show that both the Bengtsson and Rutar HP-JSR have Da less than unity, and can be classified as having the fast mixing and slow chemistry. This supports the assumption of PSR for modeling of the JSRs.

4.2 Modeling and Discussion of the Results for the Bengtsson's Reactor

The jet-stirred reactor of Bengtsson has a volume of 19.6 cm^3, and has 20 inlet nozzles of d_0=0.6 mm. Premixed methane and air enter the JSR at 12^o radial angle and create highly swirling flow. With the Da of about 0.01 the reactor can be modeled as a PSR. The best agreement of Chemical Reactor Modeling to the experimental data for NO_x and CO is obtained by representing the system as a PSR with a volume of 88% of the total JSR volume. A PFR volume of 12% plus an additional 16% of total volume, which represents the sampling tube, follows the PSR. This modeling of the reactor is presented in the article of Rutar et al. (2001). Rutar et al. indicate that the 12% of the volume that is located near the exit and represented by the PFR might not be as well-stirred as most of the JSR. This PSR-PFR arrangement is different than that originally used by Bengtsson (1998), where a PSR-PSR-PFR arrangement was used. The temperature at the exit of PFR is matched to the temperature measured by the thermocouple (1828 K). In this modeling, it is assumed that this temperature was corrected to accommodate the radiation effect of the thermocouple and the walls. The inlet temperature is set to match the desired measured temperature, assuming adiabatic reaction throughout the reactor.

The reactor is modeled with both the full GRI 3.0 mechanism and the new 8-step global mechanism. The concentration of CO is modeled closely by the PSR-PFR arrangement of Rutar et al. The size of the PFR zone determines the amount of CO at the exit. Most of the NO in the Bengtsson reactor is formed in the PSR via the N_2O and Zeldovich pathways. In the global mechanism the rate of NO formation by the nitrous oxide mechanism depends of CO concentration, thus, carbon monoxide should be modeled correctly by global mechanism in order to match the experimental NO_x. Figure 4.1 show the levels of CO concentration in the PSR zone. Figures 4.2 and 4.3 show the NO formation pathway contributions in the PSR zone of the modeled reactor. Nitrous oxide and Zeldovich mechanisms contribute the most in NO formation. The cases at 5 atm have the largest discrepancy between GRI 3.0 and the 8-step global mechanism, this is consistent with the comparison of two mechanisms in the previous chapter. Global under-predicts the rate of reaction 4 at the low pressures.

Table 4.1 shows the amount of NO that is made via the different mechanisms in GRI 3.0 modeling and the amount that is made via different reactions in the global mechanism. The table also shows the mole fraction of species that contribute to NO formation in both the GRI 3.0 and 8-step global mechanisms.

Figure 4.4 and 4.5 compare the total amount of NOx and CO made in the reactor as function of pressure for cases of 1 and 2 ms. Both GRI 3.0 and the global mechanism show good agreement with the experimental data. The poorest agreement for CO at the exit is observed for the cases with the short residence time (1 ms). In this cases the residence time in the PFR is shorter than needed for reaching the CO-CO_2 equilibrium condition for which reaction 3 is tuned. The rate of reaction 3 is smaller than the rate of decomposition of carbon dioxide to CO in GRI 3.0. While in the PSR (see figure 4.1) this effect is not obvious; however, in the short PFR the global mechanism reaches the equilibrium point faster than GRI 3.0. At the longer residence time (2 ms), GRI 3.0 and the global mechanism have better agreement in modeling the CO concentration.

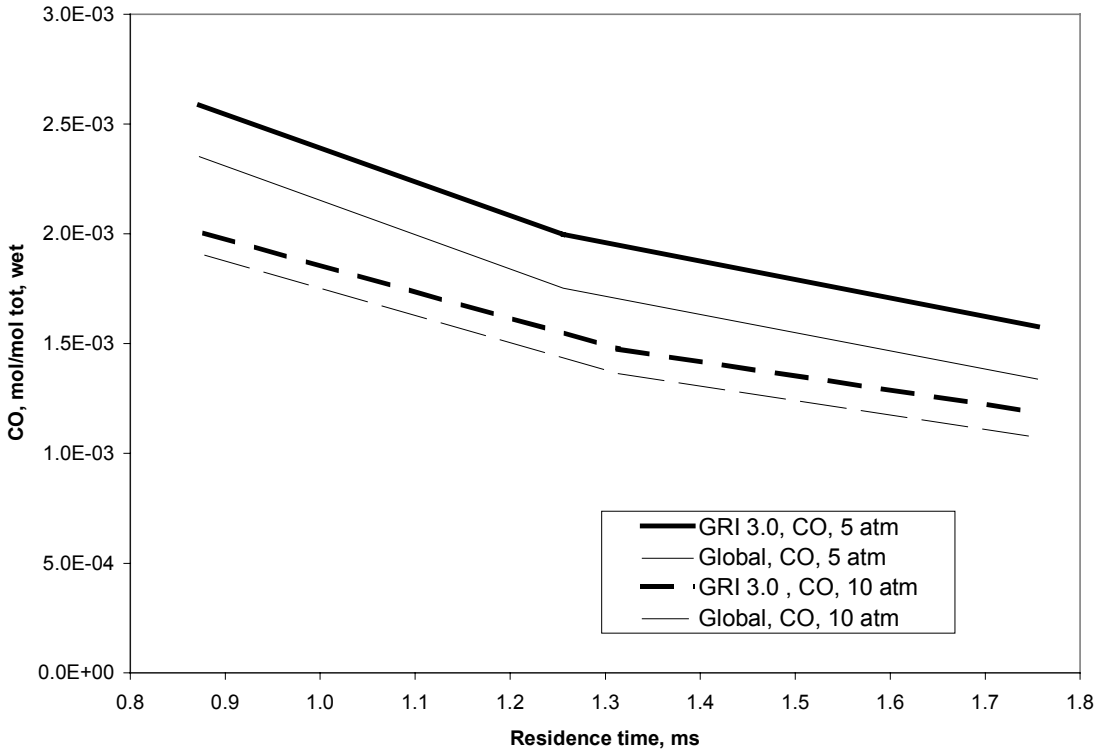

Figure 4.1 Mole fraction of CO in the PSR of the modeled Bengtsson reactor

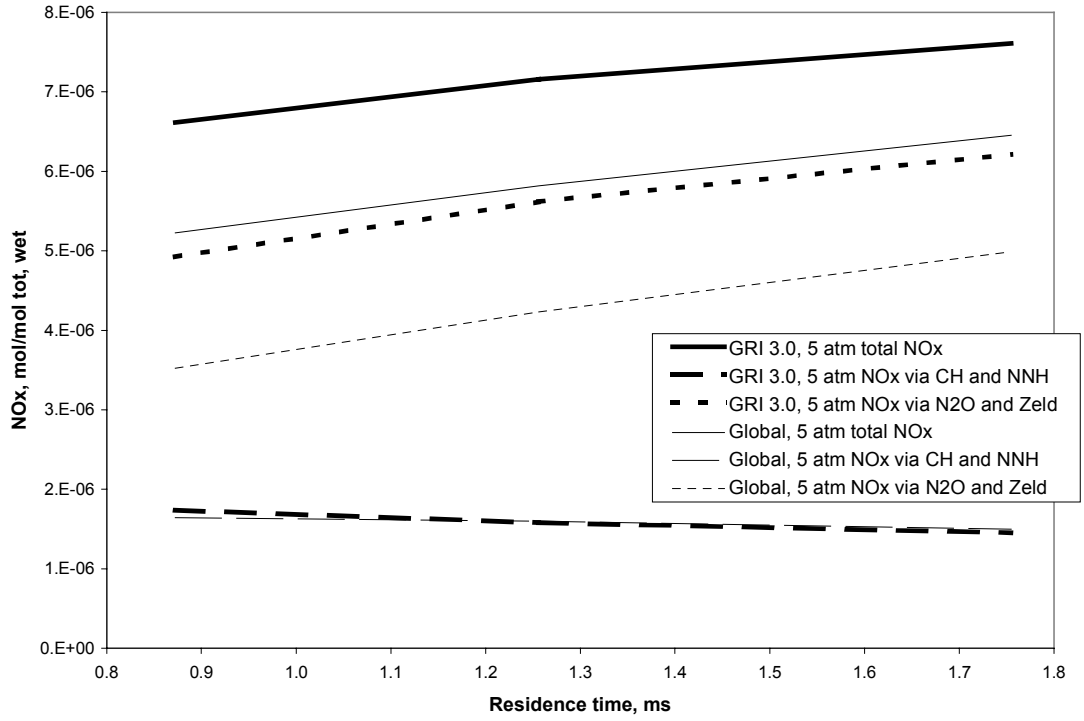

Figure 4.2 Mole fraction of NO formed by different pathways for the 5 bar cases in the PSR of the modeled Bengtsson reactor

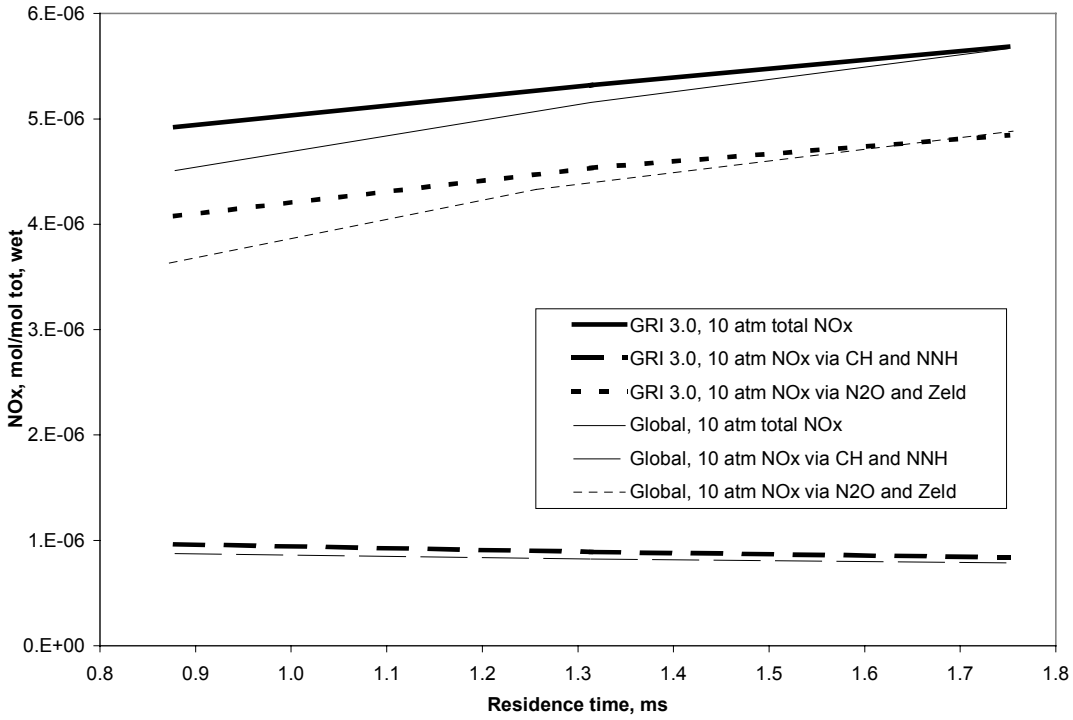

Figure 4.3 Mole fraction of NO formed by different pathways for the 10 bar cases in the PSR of the modeled Bengtsson reactor

Pressure		5 atm						10atm						15atm		20atm	
res. time, ms		1		1.5		2		1		1.5		2		2		2	
element type		PSR	PFR	PSR	PFR	PSR	PFR	PSR	PFR	PSR	PFR	PSR	PFR	PSR	PFR	PSR	PFR
res. time, ms		0.87	0.27	1.32	0.42	1.76	0.58	0.88	0.28	1.31	0.42	1.75	0.56	1.75	0.55	1.75	0.55
T PSR		1797	1828	1803	1828	1808	1828	1806	1828	1811	1828	1814	1828	1817	1828	1818	1828
Inlet T K		619		617		616.5		616.5		617		617		617		616.5	
PHI		0.55		0.55		0.55		0.55		0.55		0.55		0.55		0.55	
units		mol/mol		mol/mol		mol/mol		mol/mol		mol/mol		mol/mol		mol/mol		mol/mol	
Measured NO		6.5E-06		6.7E-06		7.0E-06		5.3E-06		5.8E-06		5.8E-06		5.0E-06		4.7E-06	
GRI 3.0 NO		7.2E-06		7.7E-06		8.1E-06		5.3E-06		5.7E-06		6.0E-06		4.9E-06		4.2E-06	
Global NO		5.6E-06		6.2E-06		6.8E-06		4.8E-06		5.4E-06		5.9E-06		5.0E-06		4.0E-06	
GRI 3.0 flame zone spicies	CH	3.04E-09		1.96E-09		1.31E-09		9.03E-10		5.69E-10		4.07E-10		2.01E-10		1.21E-10	
	CH4	1.73E-04		1.11E-04		8.79E-05		1.33E-04		9.84E-05		7.97E-05		7.49E-05		7.14E-05	
	CO	2.59E-03		2.00E-03		1.58E-03		2.00E-03		1.48E-03		1.19E-03		1.03E-03		9.30E-04	
	CO2	5.17E-02		5.24E-02		5.28E-02		5.23E-02		5.29E-02		5.32E-01		5.34E-02		5.35E-02	
	H	6.26E-05		4.53E-05		3.36E-05		1.90E-05		1.33E-05		1.04E-05		5.45E-06		3.52E-06	
	NNH	4.77E-10		3.47E-10		2.59E-10		2.91E-10		2.06E-10		1.60E-10		1.27E-10		1.09E-10	
	NO	6.62E-06		7.16E-06		7.61E-06		4.92E-06		5.32E-06		5.57E-06		4.49E-06		3.86E-06	
	N2	7.45E-01		7.46E-01		7.46E-01		7.46E-01		7.46E-01		7.46E-01		7.46E-01		7.46E-01	
	N2O	2.15E-06		2.11E-06		2.03E-06		2.55E-06		2.35E-06		2.17E-06		2.08E-06		1.99E-06	
	O	3.32E-04		2.71E-04		2.24E-04		1.23E-04		1.00E-04		8.61E-05		4.94E-05		3.35E-05	
	O2	9.04E-02		9.01E-02		8.98E-02		9.04E-02		9.00E-02		8.99E-02		8.98E-02		8.98E-02	
	NO: NNH	6.55E-07		5.58E-07		4.79E-07		2.98E-07		2.55E-07		2.27E-07		1.54E-07		1.20E-07	
	NO: CH	1.09E-06		1.03E-06		9.76E-07		6.68E-07		6.39E-07		6.15E-07		4.59E-07		3.69E-07	
	NO: N2O	3.86E-06		4.28E-06		4.58E-06		3.20E-06		3.41E-06		3.49E-06		2.80E-06		2.38E-06	
	NO: Zeld	1.07E-06		1.35E-06		1.65E-06		8.86E-07		1.14E-06		1.35E-06		1.20E-06		1.10E-06	
	NO:N2O,Zel	4.93E-06		5.63E-06		6.23E-06		4.09E-06		4.55E-06		4.84E-06		4.00E-06		3.48E-06	
	NO:NNH,CH	1.75E-06		1.59E-06		1.46E-06		9.65E-07		8.94E-07		8.42E-07		6.13E-07		4.89E-07	
	NO: PSR	6.68E-06		7.21E-06		7.68E-06		5.05E-06		5.44E-06		5.68E-06		4.61E-06		3.97E-06	
Global flame zone spicies	CH4	1.50E-04		1.16E-04		9.01E-05		1.29E-04		9.45E-05		7.58E-05		7.30E-05		7.65E-05	
	CO	2.35E-03		1.75E-03		1.34E-03		1.90E-03		1.36E-03		1.08E-03		9.70E-04		8.71E-04	
	CO2	5.17E-02		5.29E-02		5.23E-02		5.25E-02		5.31E-02		5.34E-02		5.35E-02		5.36E-02	
	H2O	1.09E-01		1.09E-01		1.09E-01		1.09E-01		1.09E-01		1.09E-01		1.09E-01		1.09E-01	
	NO	5.23E-06		5.82E-06		6.46E-06		4.51E-06		5.16E-06		5.67E-06		4.76E-06		3.81E-06	
	N2	7.46E-01		7.46E-01		7.46E-01		7.46E-01		7.46E-01		7.47E-01		7.47E-01		7.47E-01	
	O2	9.09E-02		9.04E-02		9.02E-02		9.05E-02		9.02E-02		9.00E-02		9.00E-02		8.99E-02	
	NO:N2O,Zel	3.52E-06		4.21E-06		4.99E-06		3.63E-06		4.33E-06		4.88E-06		4.14E-06		3.21E-06	
	NO:NNH,CH	1.65E-06		1.60E-06		1.50E-06		8.77E-07		8.25E-07		7.86E-07		6.28E-07		6.04E-07	
	NO: PSR	5.17E-06		5.81E-06		6.49E-06		4.51E-06		5.16E-06		5.67E-06		4.77E-06		3.81E-06	

Table 4.1 Results of the PSR-PFR modeling for the Bengtsson reactor. The species mole fractions are taken in the PSR, the inlet temperature is varied to obtain the measured temperature at the exit tube of the reactor. The first PSR is 88% of the total JSR volume. The PFR is 12 % plus 16% of the JSR volume for the exit tube.

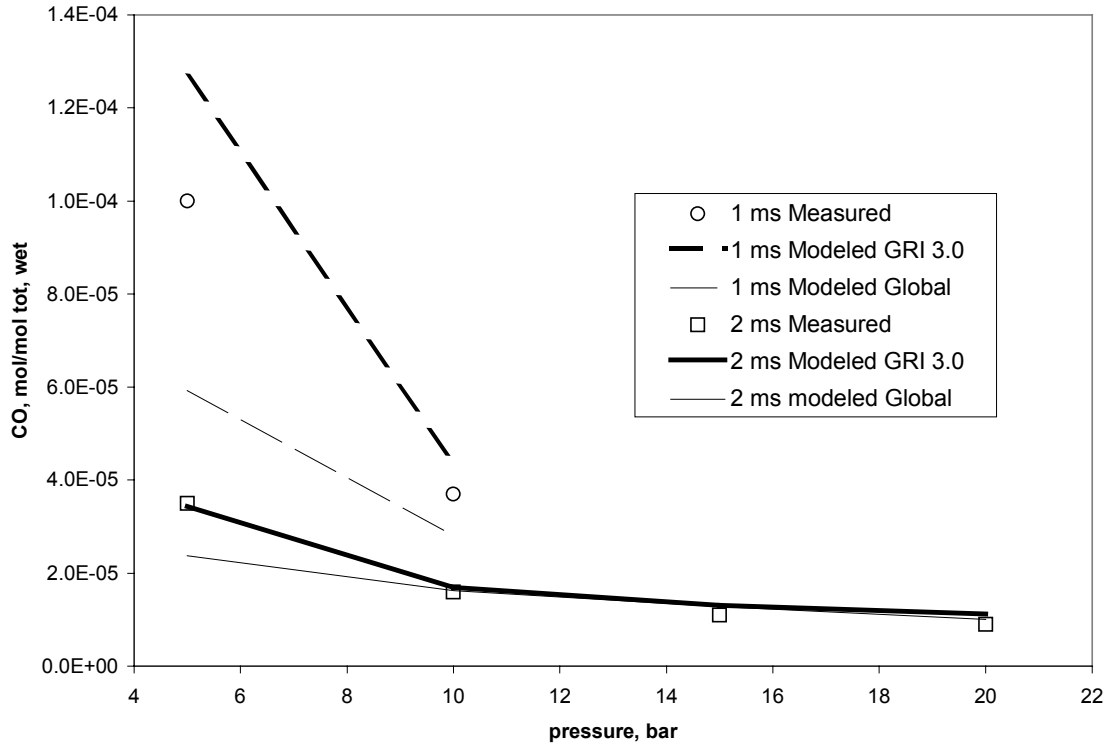

Figure 4.4 CO mole fractions at the exit of Bengtsson reactor as a function of pressure

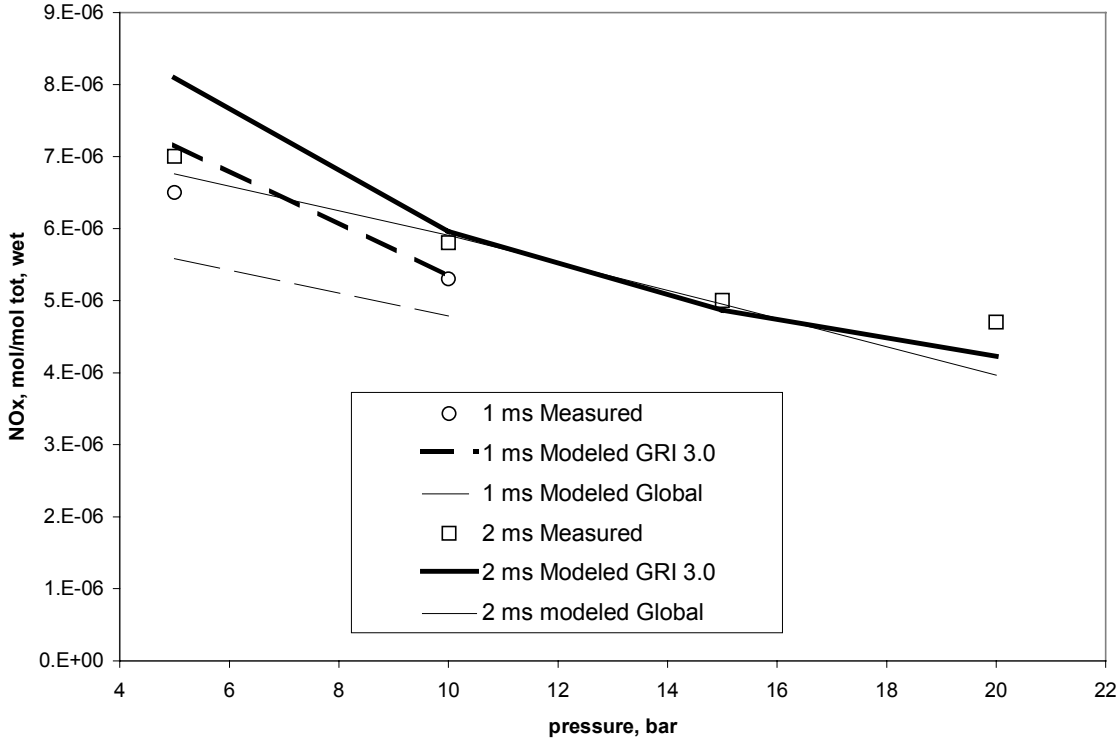

Figure 4.5 NO_x mole fractions at the exit of Bengtsson reactor as a function of pressure

4.3 Modeling and Discussion of the Results for Rutar's Reactor

The JSR of Rutar has a volume of 1.5 cm^3. The fuel-air mixture enters the reactor through the single inlet jet of d_0=1.4 mm, located on the axis of symmetry of the reactor. The jet impinges on the top of the reactor and creates the recirculating flow. In the reactor, the Da varies with the flow rate. Cases with higher flow rates and low residence time, when Da is less than 0.15, are modeled as a single PSR. At Da=0.15 the transition occurs and the length of the flame is equal to the height of the reactor. The length of the flame can be calculated as $h=5d_0u'/S_T$, where S_T is a turbulent burning velocity (Rutar, 2000). For cases with Da greater than 0.15the reactor is modeled as two PSRs in series. The PSR1 and PSR2 represent the flame front and the post-flame zone, respectively.

The first reactor is modeled as adiabatic in GRI 3.0 because the chemical energy release rate is much higher than the rate of heat transfer from the flame. The residence time in the first reactor is adjustable and it was chosen to find the best agreement between the measured and modeled NO_x and CO concentrations. For the cases with the longest residence times, the conditions in the PSR1 are very close to blowout, this is the flame zone is quite small. The 8-step global mechanism has different blowout residence time than GRI 3.0 due to the lack of hydrocarbon radicals and the endothermic reactions that are associated with them. Thus, for adequate comparison of the global mechanism with GRI 3.0, PSR1 with an assigned temperature is used. That is, for the global modeling PSR1 is assigned the temperature found in the adiabatic GRI 3.0 modeling. The second PSR is always assigned the measured temperature, because of the heat loss through the wall of the JSR.

Table 4.2 shows that for the cases that are modeled by a single PSR most of the NO is formed by nitrous oxide mechanism. Since the rate of NO formation via the nitrous oxide pathway in the global mechanism is tied to the carbon monoxide concentration, the accurate global mechanism of CO formation and destruction is imperative to predict NO formation rates by the global model. Figures 4.6, 4.7, and 4.8 show that global mechanism predicts carbon monoxide concentration well, especially in cases with the heated inlet. In the development of the global mechanism the preheated air assumption was made and the database was collected for the preheated inlet. In the cases with two PSR zones, the formation of NO is more complex. The flame zone NO is formed primary by prompt and NNH mechanisms. This is more pronounced in cases of short PSR1 and high fuel-air equivalence ratio. Table 4.3 shows the species mole fractions in each element, which represent the flame zone and the recirculation zone for the cases that are modeled as 2 PSR in series. Figures 4.9, 4.10, and 4.11 show the NO formation pathways in the flame zone of Rutar's reactor. As expected the modeling of the preheated cases gives the best agreement between GRI 3.0 and the 8-step global mechanism.

Figures 4.12, 4.13, and 4.14 show the modeled CO mole fractions for the recirculation zone of the JSR, which may be regarded as the exit of the JSR. The difference between the 8-step global and GRI 3.0 for all cases is within 15% (relative). The global mechanism slightly under-predicts CO concentration in the second PSR, which can be explained by the slow CO_2 dissociation in the global mechanism. Figures 4.15, 4.16 and

4.17 show the NO_x mole fractions in the recirculation zone of Rutar's reactor. The plots show both single PSR and PSR-PSR arrangements. The best agreement for NO_x is obtained for the cases with the preheated inlet. As expected global under-predicts NO_x for the cases with an unheated inlet.

		6.5 atm unheated			6.5 atm preheated		4.7 atm unheated	
Res. t PSR, ms		0.54	0.89	1.34	0.75	1.56	0.79	1.40
pressure, atm		6.5	6.5	6.5	6.5	6.5	4.7	4.7
Inlet T, K		338	343	348	570	573	353	360
T PSR		1820	1825	1830	1805	1825	1819	1829
PHI		0.75	0.71	0.67	0.57	0.59	0.72	0.694
units		mol/mol	mol/mol	mol/mol	mol/mol	mol/mol	mol/mol	mol/mol
Exp.	CO	4.11E-03	2.77E-03	1.24E-03	1.94E-03	7.90E-04	2.81E-03	2.30E-03
	NO	1.20E-05	9.10E-06	9.60E-06	6.10E-06	7.20E-06	1.03E-05	8.80E-06
GRI 3.0 Flame species, mole fraction, wet	CH	1.37E-08	6.77E-09	3.15E-09	2.81E-09	1.38E-09	1.44E-08	6.08E-09
	CH4	2.19E-04	1.48E-04	1.07E-04	1.54E-04	9.01E-05	1.67E-04	1.10E-04
	CO	4.45E-03	2.90E-03	2.03E-03	2.65E-03	1.58E-03	3.72E-03	2.41E-03
	CO2	6.76E-02	6.60E-02	6.37E-02	5.38E-02	5.65E-02	6.57E-02	6.52E-02
	H	1.30E-04	7.18E-05	4.37E-05	4.92E-05	2.77E-05	1.43E-04	7.98E-05
	H2O	1.43E-01	1.37E-01	1.31E-01	1.12E-01	1.15E-01	1.37E-01	1.34E-01
	NNH	1.29E-09	7.19E-10	4.41E-10	4.89E-10	2.80E-10	1.03E-09	5.81E-10
	NO	1.10E-05	1.00E-05	9.55E-06	6.36E-06	7.97E-06	1.17E-05	1.17E-05
	N2	7.30E-01	7.34E-01	7.37E-01	7.44E-01	7.43E-01	7.33E-01	7.35E-01
	N2O	1.64E-06	1.83E-06	1.89E-06	2.33E-06	2.07E-06	1.52E-06	1.61E-06
	O	3.05E-04	2.34E-04	1.89E-04	2.52E-04	1.73E-04	3.93E-04	2.89E-04
	O2	5.19E-02	5.83E-02	1.96E-01	8.58E-02	8.18E-02	5.73E-02	6.09E-02
	NO: NNH	1.28E-06	9.14E-07	6.76E-07	5.71E-07	4.60E-07	1.40E-06	1.03E-06
	NO: CH	4.10E-06	3.45E-06	2.44E-06	1.15E-06	1.24E-06	4.63E-06	3.56E-06
	NO: N2O	3.89E-06	4.52E-06	4.85E-06	3.73E-06	4.56E-06	4.43E-06	5.29E-06
	NO: Zeld	9.94E-07	1.35E-06	1.73E-06	9.98E-07	1.77E-06	1.36E-06	1.98E-06
	NO: N2O,Z	4.88E-06	5.87E-06	6.58E-06	4.73E-06	6.33E-06	5.79E-06	7.27E-06
	NO: NNH,CH	5.38E-06	4.36E-06	3.12E-06	1.72E-06	1.70E-06	6.03E-06	4.59E-06
	NO: total	1.03E-05	1.02E-05	9.70E-06	6.45E-06	8.03E-06	1.18E-05	1.19E-05
Global flame species	CH4	2.12E-04	1.42E-04	1.02E-04	1.58E-04	8.76E-05	1.71E-04	1.09E-04
	CO	5.57E-03	2.78E-03	1.83E-03	2.46E-03	1.36E-03	3.54E-03	2.11E-03
	CO2	6.77E-02	6.63E-02	6.40E-02	5.41E-02	5.68E-02	6.61E-02	6.56E-02
	H2O	1.45E-01	1.38E-01	1.32E-01	1.13E-01	1.16E-01	1.39E-01	1.36E-01
	NO	7.77E-06	7.23E-06	7.36E-06	5.10E-06	6.94E-06	8.93E-06	9.05E-06
	N2	7.31E-01	7.34E-01	7.37E-01	7.44E-01	7.43E-01	7.33E-01	7.35E-01
	O2	5.21E-02	5.85E-02	6.51E-02	8.60E-02	8.20E-02	5.76E-02	6.11E-02
	NO: N2O,Z	2.65E-06	3.59E-06	4.65E-06	3.55E-06	5.38E-06	3.31E-06	4.63E-06
	NO: NNH,CH	5.06E-06	3.76E-06	2.76E-06	1.58E-06	1.62E-06	5.62E-06	4.47E-06
	NO: total	7.71E-06	7.35E-06	7.41E-06	5.13E-06	7.00E-06	8.93E-06	9.10E-06

Table 4.2 Results of the PSR modeling for Rutar's JSR.

		6.5 atm unheated				6.5 atm preheated				4.7 atm unheated			
Total res time		2. ms		4 ms		2 ms		4 ms		2 ms		3.6 ms	
zone		PSR1	PSR2	PSR1	PSR2	PSR1	PSR2	PSR1	PSR2	PSR1	PSR2	PSR1	PSR2
Elem.res time,ms		0.126	1.897	0.070	3.833	0.169	1.910	0.046	3.888	0.126	1.840	0.070	3.214
T PSR, K		1757	1836	1751	1880	1804	1840	1774	1884	1704	1836	1739	1879
PHI		0.7		0.73		0.61		0.66		0.68		0.72	
Inlet Tem K		360		373		576		573		373		393	
units		mol/mol tot		mol/mol tot		mol/mol tot		mol/mol tot		mol/mol tot		mol/mol tot	
NO measured tot		7.50E-06		1.03E-05		6.20E-06		1.00E-05		7.10E-06		1.09E-05	
NO GRI 3.0 total		7.19E-06		9.72E-06		7.31E-06		9.74E-06		6.41E-06		1.12E-05	
NO Global total		6.04E-06		9.41E-06		6.53E-06		1.07E-05		5.92E-06		1.12E-05	
GRI3.0	CH	5.4E-08	2.6E-11	1.2E-07	2.8E-11	2.3E-08	6.7E-12	1.4E-07	1.9E-11	6.9E-08	4.3E-11	2.1E-07	4.9E-11
	CH4	7.7E-04	2.1E-06	1.4E-03	1.5E-06	4.3E-04	1.1E-06	1.5E-03	1.5E-06	9.5E-04	2.4E-06	1.3E-03	1.7E-06
	CO	1.2E-02	6.0E-04	1.9E-02	4.6E-04	7.5E-03	3.5E-04	2.0E-02	4.3E-04	1.4E-02	7.2E-04	2.0E-02	6.3E-04
	CO2	5.4E-02	6.8E-02	4.9E-02	7.1E-02	5.1E-02	5.9E-02	4.2E-02	6.5E-02	5.0E-02	6.6E-02	4.8E-02	7.0E-02
	H	3.0E-04	6.6E-06	4.8E-04	6.0E-06	2.0E-04	3.3E-06	5.5E-04	5.3E-06	4.2E-04	1.1E-05	7.8E-04	1.2E-05
	NNH	2.8E-09	6.7E-11	4.4E-09	6.3E-11	2.0E-09	3.3E-11	5.3E-09	5.6E-11	2.7E-09	8.2E-11	5.2E-09	8.9E-11
	NO	5.5E-06	7.2E-06	5.5E-06	9.7E-06	5.9E-06	7.3E-06	4.9E-06	9.7E-06	4.3E-06	6.4E-06	6.8E-06	1.1E-05
	N2	7.3E-01	7.4E-01	7.2E-01	7.3E-01	7.4E-01	7.4E-01	7.3E-01	7.4E-01	7.3E-01	7.4E-01	7.2E-01	7.3E-01
	N2O	1.3E-06	1.1E-06	9.6E-07	7.7E-07	1.9E-06	9.8E-07	1.1E-06	8.6E-07	1.0E-06	1.1E-06	8.0E-07	8.5E-07
	O	5.2E-04	5.8E-05	5.8E-04	5.3E-05	5.8E-04	4.8E-05	8.1E-04	5.9E-05	6.8E-04	9.1E-05	9.5E-04	8.7E-05
	O2	6.7E-02	5.9E-02	6.6E-02	5.3E-02	8.2E-02	7.8E-02	7.9E-02	6.6E-02	7.2E-02	6.3E-02	6.7E-02	5.4E-02
	NO: NNH	1.2E-06	4.4E-08	1.1E-06	7.5E-08	5.7E-07	1.9E-08	1.2E-06	7.6E-08	1.1E-06	6.0E-08	1.6E-06	1.1E-07
	NO: CH	3.1E-06	2.9E-08	3.9E-06	7.2E-08	1.2E-06	7.7E-09	3.1E-06	5.2E-08	2.4E-06	3.4E-08	4.7E-06	7.6E-08
	NO N2O	1.2E-06	8.5E-07	7.1E-07	1.3E-06	3.7E-06	5.6E-07	6.8E-07	1.5E-06	7.5E-07	9.9E-07	6.7E-07	1.6E-06
	NO: Zeld	1.9E-07	8.1E-07	1.1E-07	2.3E-06	1.0E-06	7.1E-07	1.3E-07	2.8E-06	9.7E-08	8.9E-07	1.2E-07	2.3E-06
	NO: N2O,Z	1.4E-06	1.7E-06	8.2E-07	3.7E-06	4.7E-06	1.3E-06	8.1E-07	4.3E-06	8.5E-07	1.9E-06	7.8E-07	3.9E-06
	NO: NNH,CH	4.3E-06	7.4E-08	5.0E-06	1.5E-07	1.7E-06	2.6E-08	4.3E-06	1.3E-07	3.6E-06	9.4E-08	6.3E-06	1.8E-07
	NO: element	5.7E-06	1.7E-06	5.8E-06	3.8E-06	6.4E-06	1.3E-06	5.1E-06	4.5E-06	4.4E-06	2.0E-06	7.0E-06	4.0E-06
8-step Global	CH4	7.9E-04	2.8E-06	1.3E-03	1.7E-06	4.6E-04	1.8E-06	1.4E-03	1.9E-06	1.1E-03	3.7E-06	1.4E-03	2.4E-06
	CO	1.4E-02	5.0E-04	2.1E-02	3.4E-04	7.6E-03	2.5E-04	2.1E-02	2.9E-04	1.7E-02	6.0E-04	2.2E-02	4.7E-04
	CO2	5.3E-02	6.8E-02	4.9E-02	7.1E-02	5.1E-02	5.9E-02	4.2E-02	6.5E-02	4.8E-02	6.6E-02	4.6E-02	7.0E-02
	NO	4.3E-06	6.0E-06	5.0E-06	9.4E-06	4.8E-06	6.5E-06	4.9E-06	1.1E-05	3.6E-06	5.9E-06	6.5E-06	1.1E-05
	N2	7.3E-01	7.4E-01	7.3E-04	7.3E-01	7.4E-01	7.4E-01	7.3E-01	7.4E-01	7.3E-01	7.4E-01	7.3E-01	7.3E-01
	O2	6.7E-02	6.0E-02	6.5E-02	5.3E-02	8.3E-02	7.9E-02	7.9E-02	6.6E-02	7.4E-02	6.4E-02	6.7E-02	5.4E-02
	NO: N2O,Z	9.4E-07	2.1E-06	6.6E-07	4.8E-06	2.0E-06	1.8E-06	8.0E-07	6.1E-06	5.4E-07	2.3E-06	5.9E-07	4.8E-06
	NO: NNH,CH	3.3E-06	5.8E-09	4.3E-06	1.1E-08	2.8E-06	1.7E-09	4.1E-06	1.0E-08	3.0E-06	8.8E-09	5.9E-06	1.7E-08
	NO: element	4.3E-06	2.1E-06	4.9E-06	4.8E-06	4.8E-06	1.8E-06	4.9E-06	6.1E-06	3.6E-06	2.3E-06	6.5E-06	4.8E-06

Table 4.3 Modeling results for the two PSR arrangement of Rutar's JSR. The exit and sampling location of the reactor is presented by PSR2.

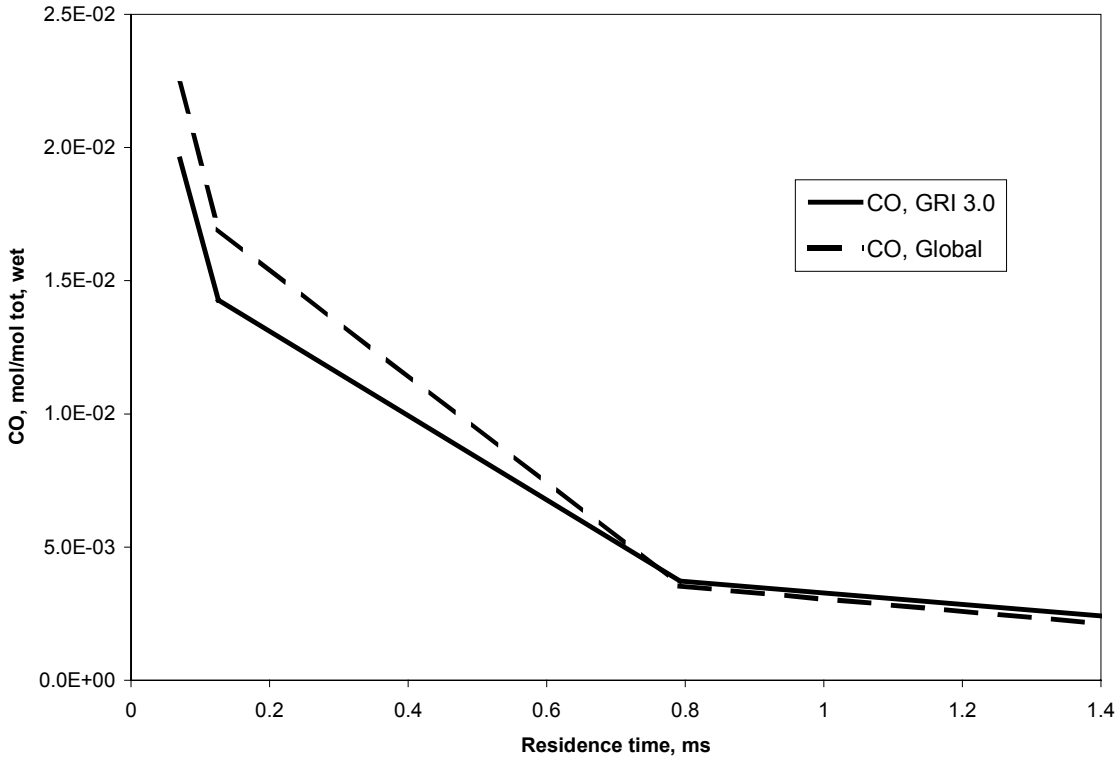

Figure 4.6 CO formation in the PSR for the unheated inlet, 4.7 atm

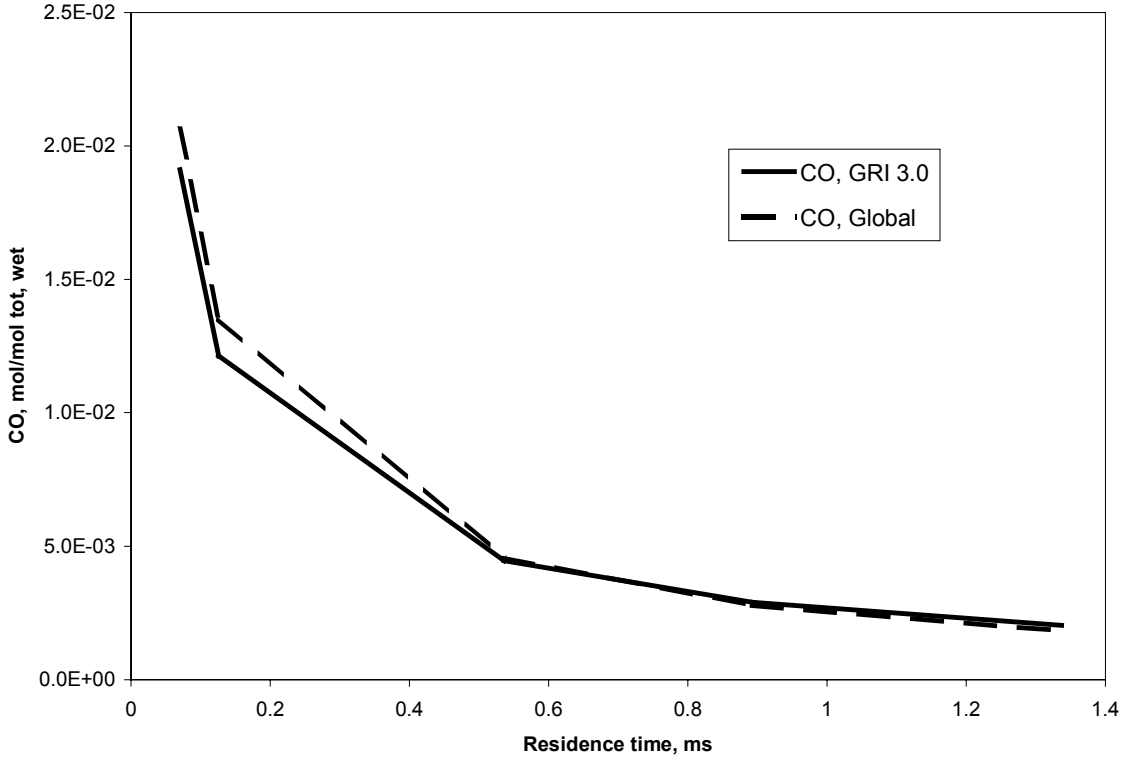

Figure 4.7 CO formation in the PSR for the unheated inlet, 6.5 atm

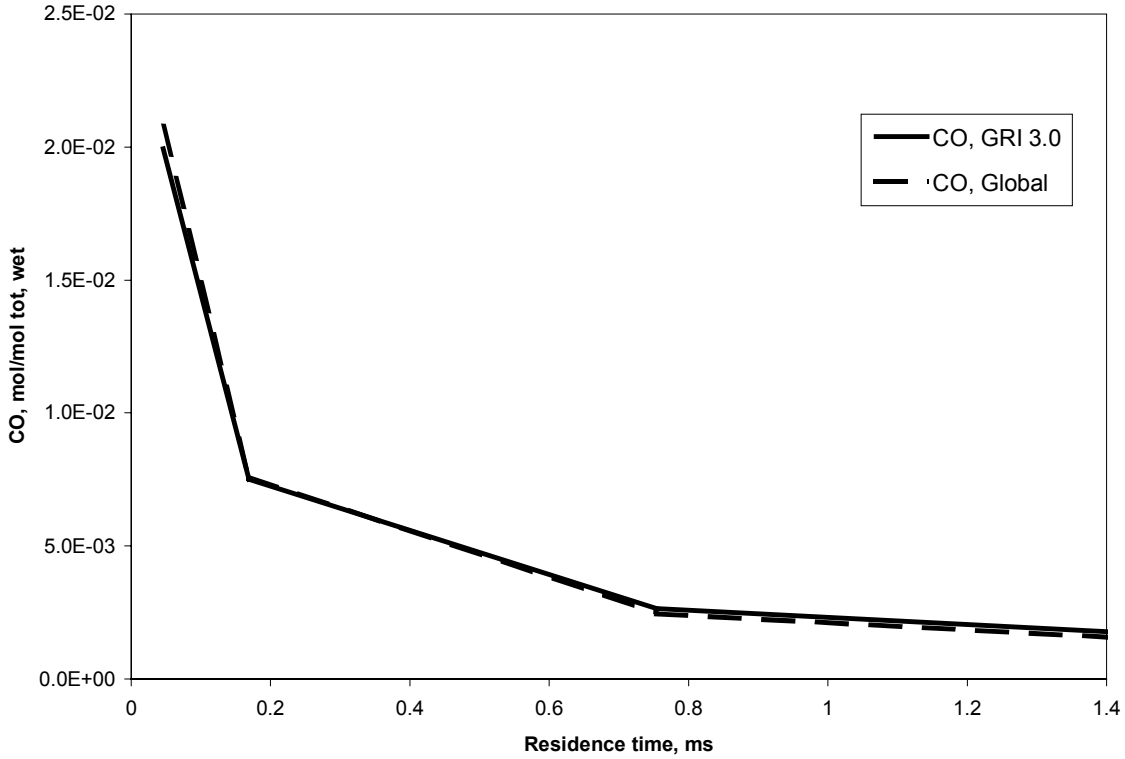

Figure 4.8 CO formation in the PSR for the heated inlet, 6.5 atm

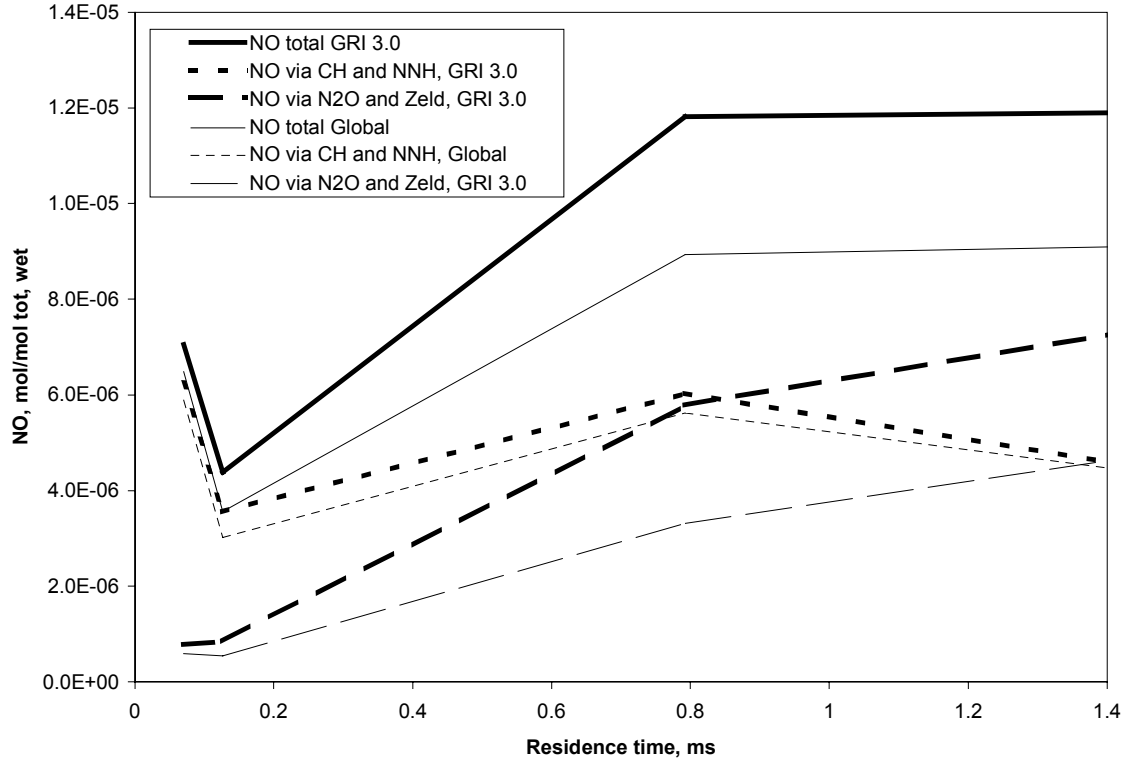

Figure 4.9 NO formation in the PSR for the unheated inlet, 4.7 atm

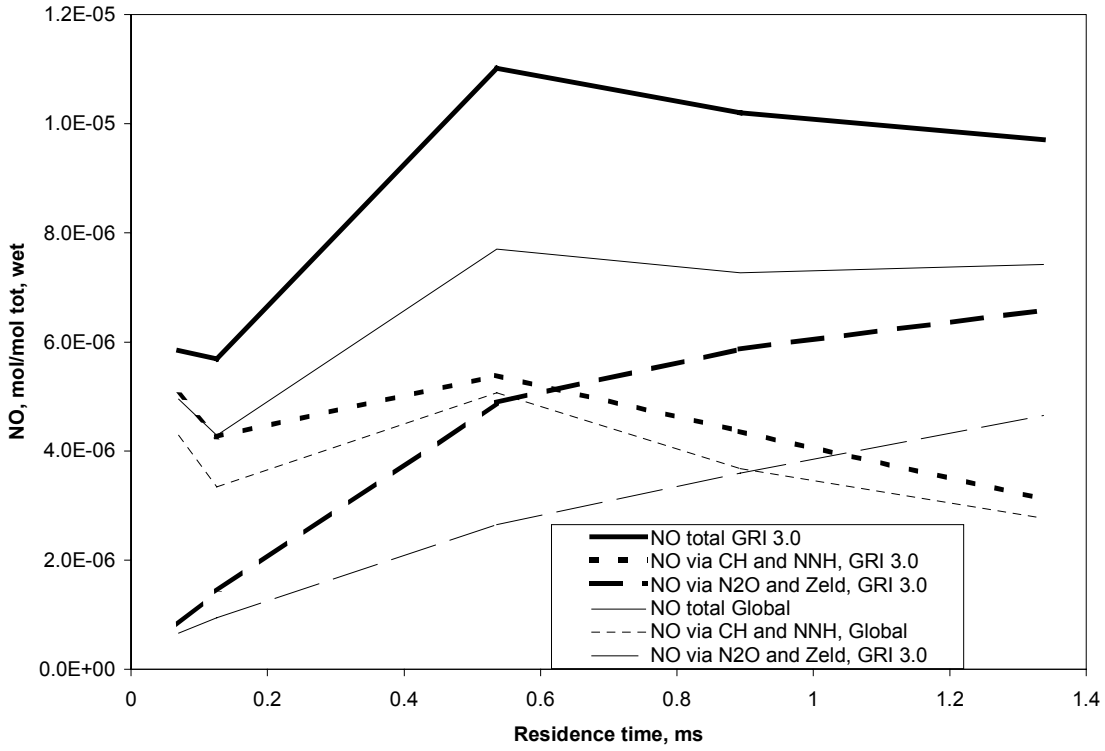

Figure 4.10 NO formation in the PSR for the unheated inlet, 6.5 atm

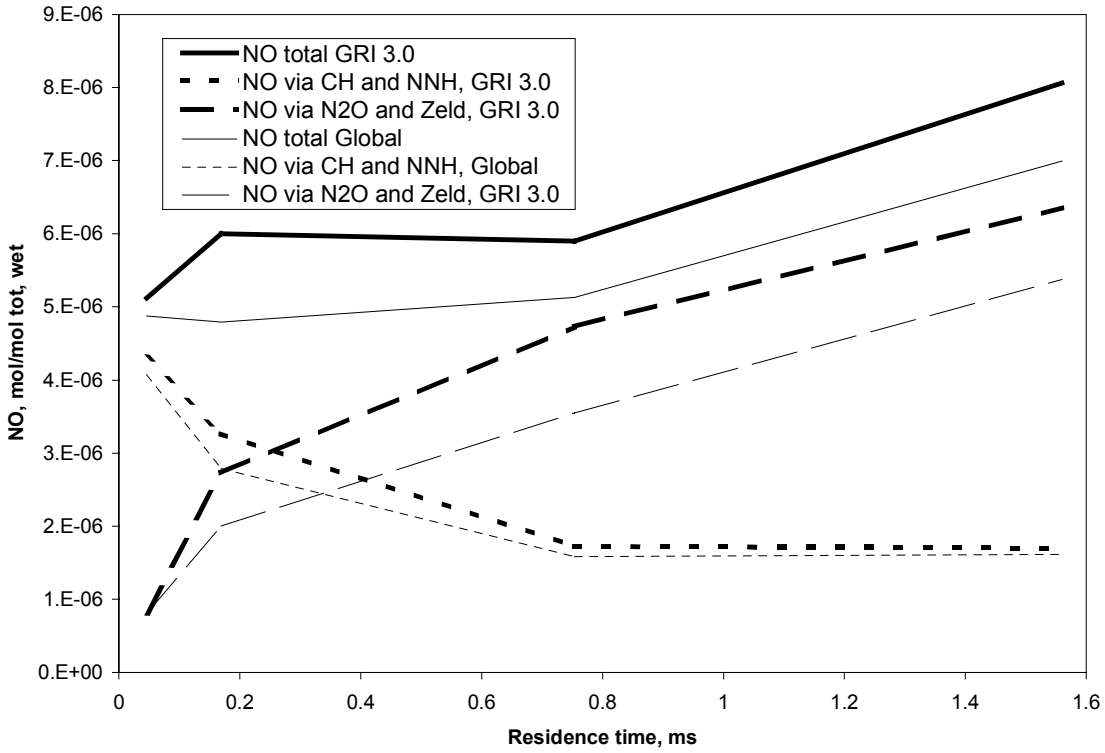

Figure 4.11 NO formation in the PSR for the heated inlet, 6.5 atm

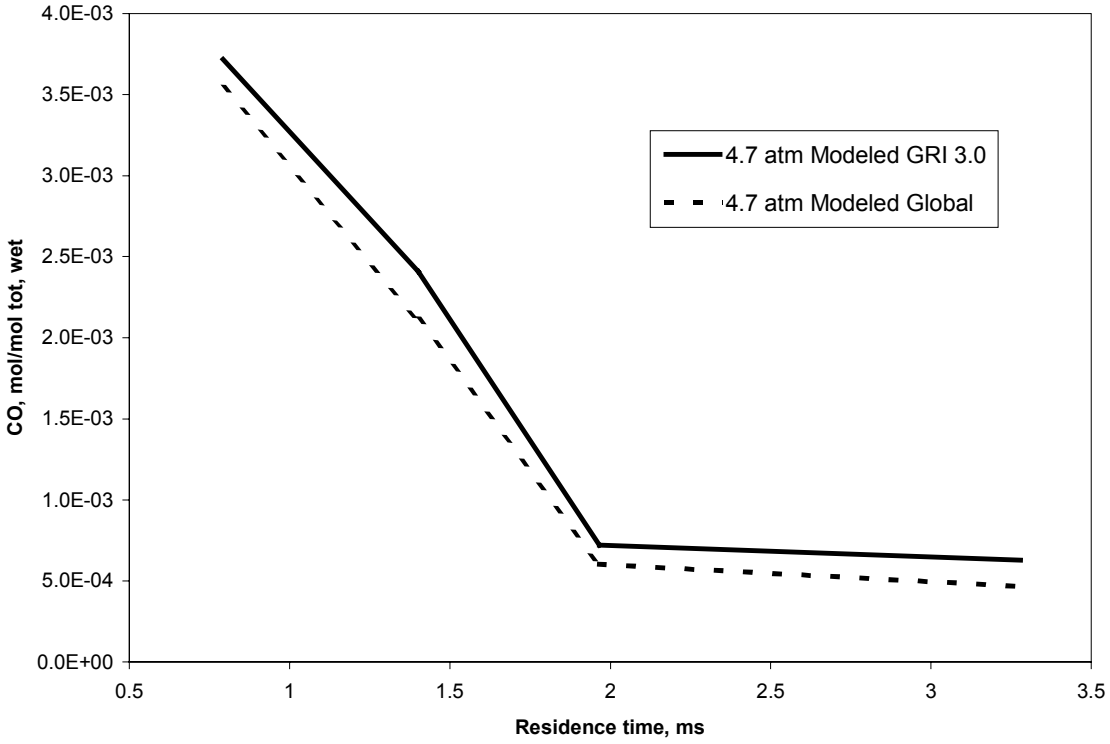

Figure 4.12 CO mole fraction in the recirculation zone of Rutar's JSR for unheated inlet, 4.7 atm

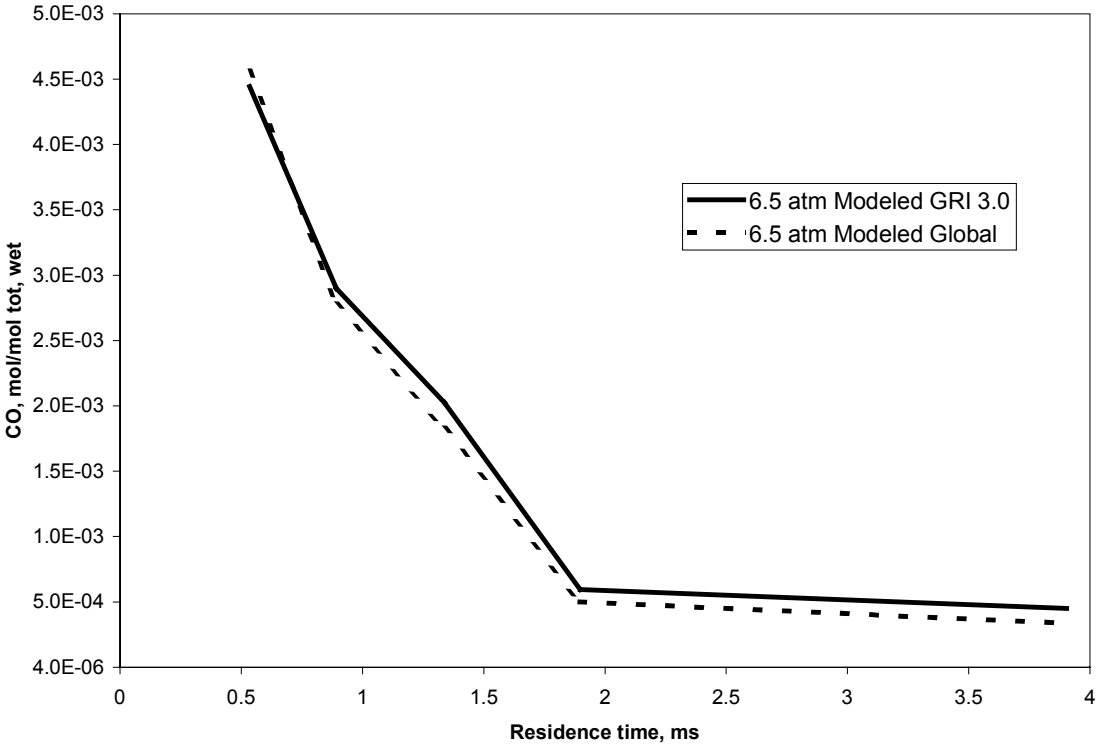

Figure 4.13 CO mole fraction in the recirculation zone of Rutar's JSR for unheated inlet, 6.5 atm

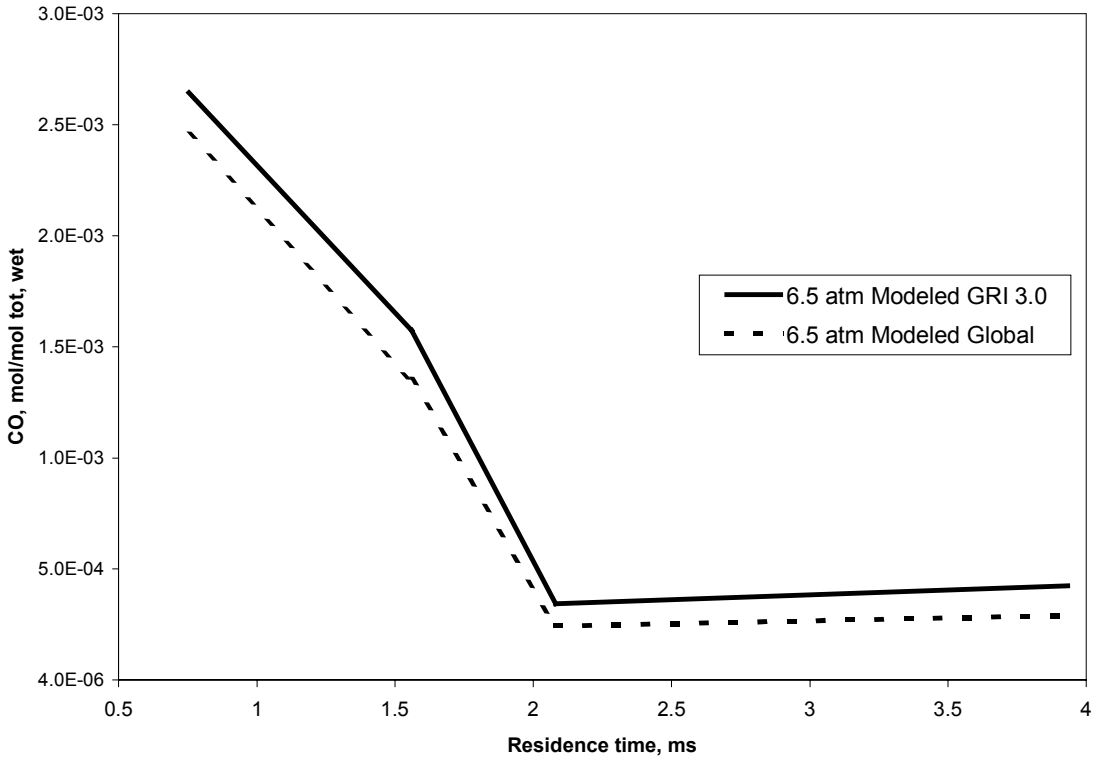

Figure 4.14 CO mole fraction in the recirculation zone of Rutar's JSR for heated inlet, 6.5 atm

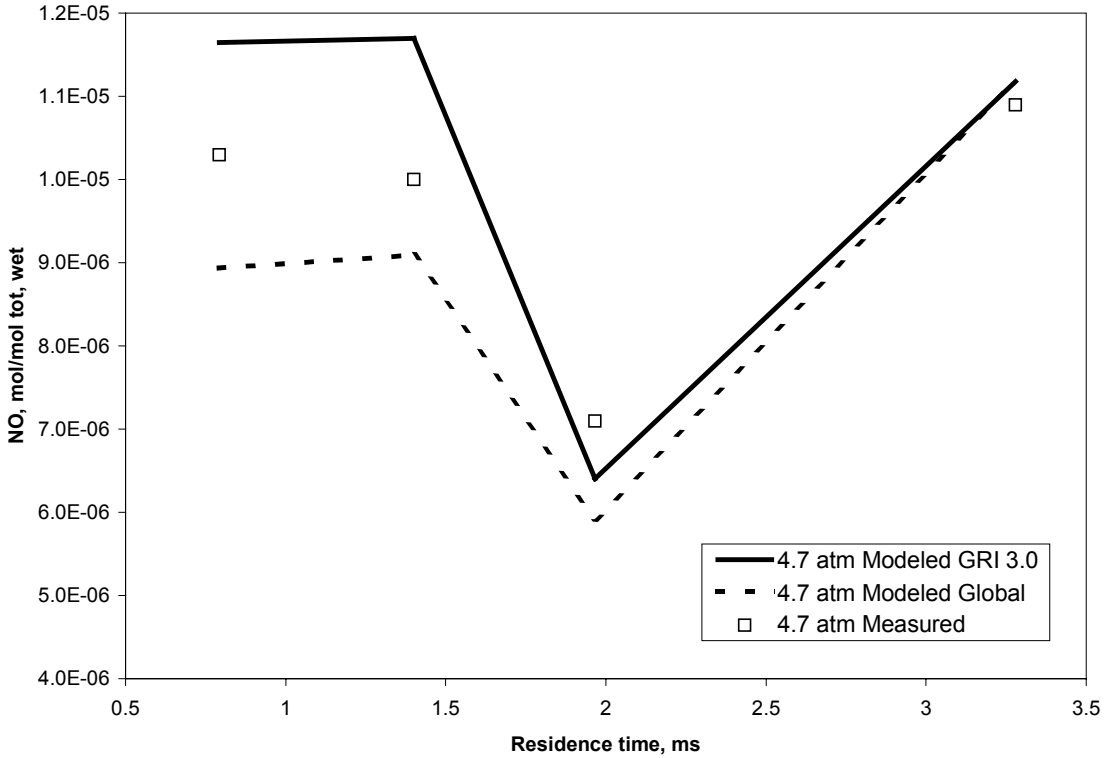

Figure 4.15 NO mole fraction for the recirculation zone of Rutar's JSR for unheated inlet, 4.7 atm

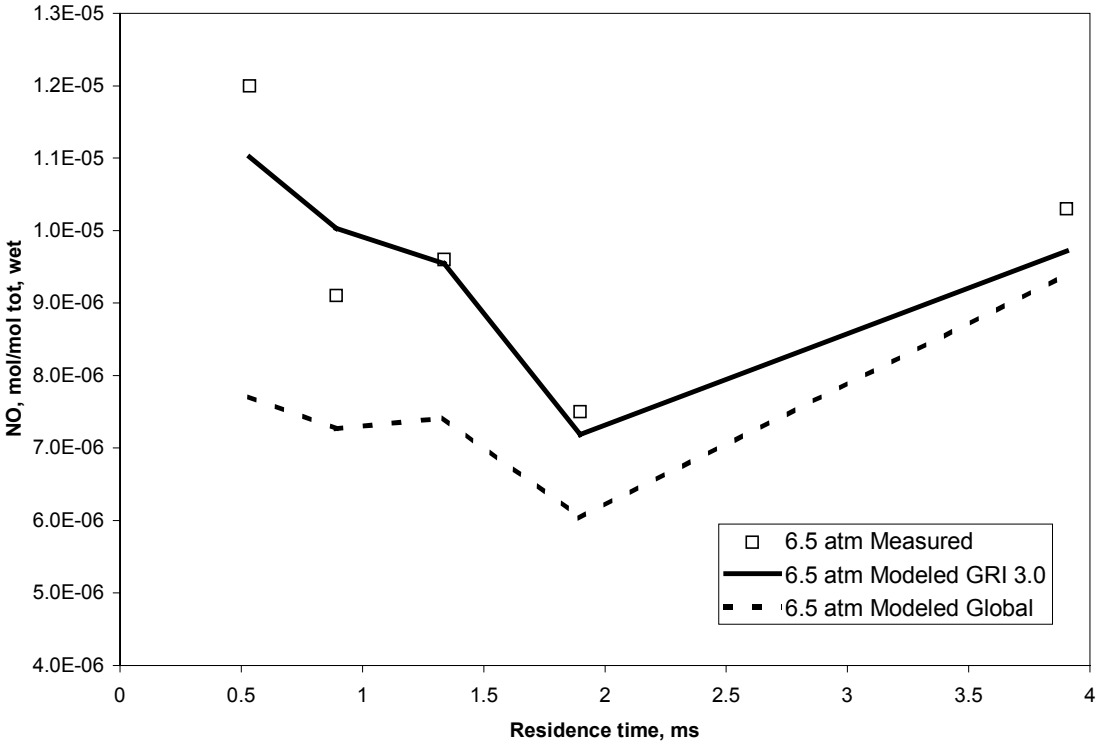

Figure 4.16 NO mole fraction for the recirculation zone of Rutar's JSR for unheated inlet, 6.5 atm

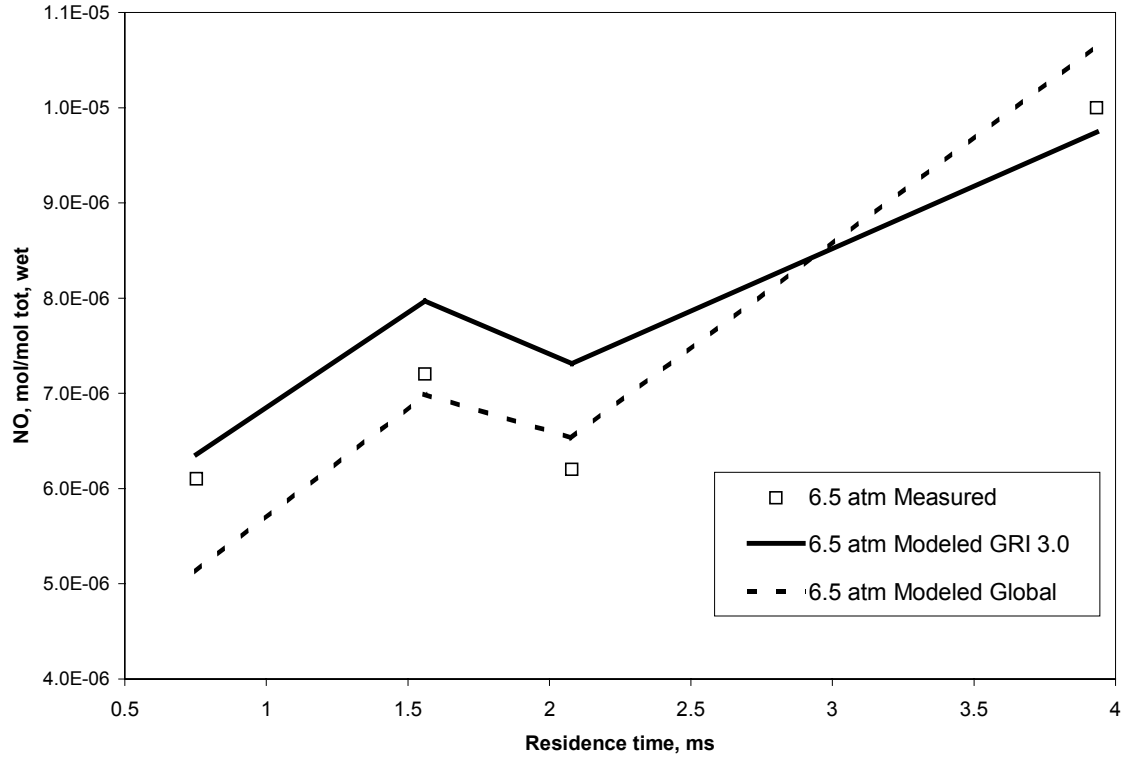

Figure 4.17 NO mole fraction for the recirculation zone of Rutar's JSR for heated inlet, 6.5 atm

4.4 Validation of the Eight-Step Global Mechanism via CFD of Combustor A

The eight-step global kinetic mechanism is also validated against the experimental data for Combustor A obtained by Mellor et al. (1996). This validation is performed using FLUENT 5 CFD code to model the lean-premixed gas turbine combustor as a two-dimensional axi-symmetric flow. The boundary conditions include: the swirling uniformly premixed fuel-air mixture at the entrance of the combustor (with the tangential velocity component equal to the axial velocity component), pilot air without any fuel entering through the pilot inlet, dome and liner cooling air entering the combustor as film cooling streams. The outlet of the combustor is modeled as pressure outlet at the defined operating condition. The heat transfer through liner is not modeled. Reynolds averaged Navier-Stokes equations with the standard k-ε momentum equations closure model are solved by the code. Although the k-ε is not accurate for flows with adverse pressure gradient (Wilcox, 1993), and the Reynolds Stress Model would be more appropriate in this modeling, Malte et al. (2000) compare the results of different momentum equations closure models and show that the k-ε model gives similar flow fields to RSM in Combustor A. In present work, the simulation with the RSM closure model did not converge, probably due to the grid non-uniformity. Thus, the standard k-ε momentum closure model is used for the present CFD simulations.

The rates of the volumetric reaction of methane oxidation and nitric oxide formation are determined as a limiting rate between the eddy break-up model (Magnussen and Hjertager model, 1976) and the chemical kinetic rate of the global mechanism. The smallest of the rates is chosen in the calculation. In reaction 1 of the global mechanism, the reactants are premixed and the rate of the reaction 1 depends on the mixing between the fresh mix and hot recirculation products and not on the rate of mixing between the fuel and air.

When in the Eddy break-up model, the code automatically chooses the slower rate of two following expressions. The rate of the reaction for diffusion flame is written as, where Y_R denotes fuel or oxygen mass fraction:

$$R_{i',k}=\nu_{i',k}\times M_{i'}\times A\times\rho\times(\varepsilon/k)\times(Y_R/\nu_{R,k}\times M_R)\ ,$$

The rate of the diffusion controlled reaction for the premixed flame is expressed as, where Y_P denotes the mass fraction of the product species for the particular reaction:

$$R_{i',k}=\nu_{i',k}\times M_{i'}\times A\times B\times\rho\times(\varepsilon/k)\times(\Sigma_P Y_P/\Sigma^N_{j'}\nu_{j',k}\times M_{j'})\ .$$

Additional terms in the equations are defined as follows:
$R_{i'k}$ = reaction rate for species i' in reaction k
$\nu_{i',k}$ = molar stoichiometric coefficient for species i' in reaction k
$M_{i'}$ = molecular weight of species i', kg/kmol
M_R = molecular weight of the limiting reactant, kg/kmol

$M_{j'}$ = molecular weight of the species j', kg/kmol
A = empirical coefficient
B = empirical coefficient
ρ = density, kg/m^3
ε = turbulent dissipation rate, m^2/s^3
k = turbulent kinetic energy, m^2/s^2
$\nu_{R,k}$ = molar stoichiometric coefficient for reactant R in reaction k
$\nu_{j',k}$ = molar stoichiometric coefficient for product j' in reaction k

The empirical coefficients in the eddy break-up model by default are A= 4 and B= 0.5. In order for the rate to be controlled by the second expression, the coefficients are adjusted to increase the first rate but keep the second rate unchanged, such as: A_1=1000 and B_1=0.002. This adjustment is only applicable for the Reaction 1 of the global mechanism, where the presence of hot recirculation gas is required to ignite the methane-air mixture. After the mixture is ignited and carbon monoxide is present in the flame, the rate of the reaction 2 does not depend on the eddy break-up because both O_2 and CO are present at the same location. Thus, reaction 2 is taken to be controlled by chemical kinetic rate at all times by setting the coefficient $A = 10^5$. The other reactions in the global mechanism appear to be slow enough to be in chemical kinetic mode.

As mentioned above, the k-ε closure model under-predicts the turbulence effects in the cases with high swirling flows and the Reynolds stress model (as well as the renormalized group model) did not converge in simulation using the current grid. The reaction rates that are based on the turbulent parameters are also under-predicted if the k-ε model is used, thus the empirical coefficient A and B in the eddy dissipation model should be adjusted to match turbulent parameters k and ε. The other reason for the adjustment of the A and B coefficients in the code is that the empirical coefficients were not developed to accommodate the highly swirling flow, which increases the mixing rate between the fresh air-fuel mixture and the hot recirculation gas that ignites it. Peters (2000) notes that when eddy break-up model is used in CFD simulation, the constants A and B must be "tuned" within the wide range to obtain reasonable results for any particular problem. Different values of the A and B coefficients for reaction 1 were tested against the experimental data over the range of fuel-air equivalence ratios between 0.48 and 0.75. The closest agreement with the experimental data is obtained if $A \times B=10$ for reaction 1. Figures 4.18 and 4.19 show the comparison of the CFD results for NO and CO for five-step global and eight-step global mechanism using default and "tuned" coefficients.

Combustor A operates under the nominal operating conditions: pressure of 10 atm, inlet temperature on 650 K, and flow rates of 0.6 kg/s for the premixer air and 1.098 kg/s for the total air. Three premixer fuel-air equivalence ratios are used for the validation of the eight step global mechanism (0.48, 0.61, and 0.74). The results of the CFD simulation with the eight-step global mechanism are compared to the experimental data and the results of Malte and Nicol (2000) five-step mechanism. Figures 4.18 and 4.19 show CO and NO exit plane emissions of the Combustor A for different CFD simulations and for

the experimental data of Mellor (1996). Over the complete range of the premixer ϕ, the 8-step mechanism with $A \times B=10$ for reaction 1 and reaction 2 in kinetic control shows the best agreement with the experimental CO. Nitric oxide is also reasonably well predicted by this setup, except for the leanest ϕ, when poor NO agreement is obtained. Further characterization of the agreement is discussed in Table 4.4.

Figures 4.20 to 4.30 depict the flow fields and species mole fraction for the eight-step global mechanism. When compared with five-step global mechanism of Nicol (1995), the CFD simulations using the eight-step global mechanism predict different flow fields and species mole fraction in the combustor and at the exit plane. Generally, the hydrocarbon oxidation is slower in the eight-step global mechanism. This results in the slightly higher local concentration of CO in the combustor and lower maximum temperatures. This effect can be seen the most in the lean case (ϕ=0.48) when the CO is quenched near the outer wall of the combustor by the excess air of the liner cooling. The five-step global mechanism does not show the CO quenching for this equivalence ratio. See figures 4.29 and 4.30. As a result of this effect the CO mole fraction at the exit plane is much higher for the ϕ=0.48 ratio than in the case with five-step global mechanism. This is consistent with the experimental data of Mellor (1996). See figure 4.18.

The other major difference in using the new global chemistry is the presence of the prompt NO reaction in the eight-step global mechanism (reaction 5). Since the rate of this reaction depends on the concentration of the methane, the reaction contributes the most to the NO formation in the richest case. The presence of the prompt NO mechanism allows fairly good agreement with experimental data for the cases with the fuel-air equivalence ratio above about 0.6.

Reaction 5 (the prompt NO reaction) is also very sensitive to the methane diffusion into the area where the hot temperatures are present. This is especially true for the CFD code used, when gas diffuses into the recirculation zone and spends a long time in it (more than 1 sec) before leaving. The gas velocities and thus the diffusion reaction rate of the reaction 1 are slower than in the jet and the methane does not quickly, this can lead to the unrealistically large NO concentrations. In this case, the recirculation zone acts as an energy sink producing the large quantities of NO via endothermic reaction. The 8 step global mechanism was tested against the detailed kinetic mechanism GRI 3.0 in CRM for cases with long residence time. At the residence time of 10 sec the 8-step mechanism performed well up to ϕ=0.6, and at the residence time of 1 sec the global mechanism matched the GRI 3.0 results up to ϕ=0.75. At longer residence times, or large ϕ's (and thus, for the larger flame temperature), the eight-step global mechanism over-predicts NO concentration since it does not consider a reverse reaction of NO reduction. These residence times are not applicable to the real combustor (the mean residence time of the combustor A is about 30 ms), however they can be achieved in the numerical simulation using present CFD code, which predicts a maximum residence time of more than 6 sec).

For the higher equivalence ratios the temperatures are high enough (about 2200 K) that the adiabatic assumption might not hold, and where the experimental combustor would

lose heat, the model assumes the adiabatic boundary conditions and produces excessive amount on NO. For the lower equivalence ratios the fuel air unmixedness in premixer could effect NO_x more than at the rich end of the range. The zones with higher local equivalence ratio would create hot pockets of gas and thus more NO_x would be produced. Since this effect was not modeled the CFD simulation would predict lower NO concentrations when compared with the experimental data.

Item	Discussion of differences and similarities
Temperature	The 8-step global mechanism predicts the peak temperature of 1967 K in the recirculation zone of the combustor. The 5-step, 8-atm global mechanism predicts the peak temperature of 1966 K. See figures 4.20 and 4.21
Carbon Monoxide	The concentration fields of monoxide are similar for the 5-step and 8-step mechanisms. The maximum levels of CO are 1.25% and 1.4% for 5-step and 8-step mechanism. Due to the faster reaction of the CO oxidation in 5-step mechanism, the area with high carbon monoxide concentration is smaller. See Figures 4.22 and 4.23. CO exit-plane emissions are 0.5 ppm for the 5-step and 0.8 ppm for the 8-step mechanism. In the case of the 8-step, the exit-plane CO concentration has two a peaks: at the centerline of the combustor it is about 2.3 ppm, the other at the combustor wall the CO mole fraction is about 0.9 ppm. The 5-step mechanism predicts the peak CO concentration of 1.5 ppm near the centerline. The CO mole fraction at the combustor wall is about 0.3 ppm.
NO Formation Rate	Figures 4.26, 4.27, and 4.28 show the rates of non-thermal NO formation. The 8-step global predicts a high rate of NO formation via prompt global reaction near the inlet of the combustor where the hot recirculation gas mixes with the fresh fuel-air mixture. In both the 5 and 8-step mechanisms, most of NO formed via the non-thermal N_2O and Zeldovich pathways occur at the lower edge of the jet. The zone of NO formation via N_2O and Zeldovich is lager than the zone of prompt NO formation, however the maximum rate of prompt reaction is ten times as high as the non-thermal N_2O and Zeldovich rate. When default values of A and B coefficients are used for both reaction 1 and 2 most of non-thermal NO is formed in the zone immediately following the flame brush. See Malte et al. (2000).
NO	Figures 4.24 and 4.25 depict the NO mole fractions in the combustor. The 8-step mechanism predicts NO mole fraction of 72 ppm in lower part of the jet and about 45 ppm in the center of the recirculation zone. The 5-step mechanism predicts the maximum NO level in the recirculation zone of 31 ppm. The exit plane NO are 11 ppm and 18.5 ppm for the 5-step and the 8-step mechanisms.

Table 4.4 Main characteristics of CFD simulation using 5-step and 8-step global mechanisms for Combustor A with fuel-air equivalence ratio of 0.61.

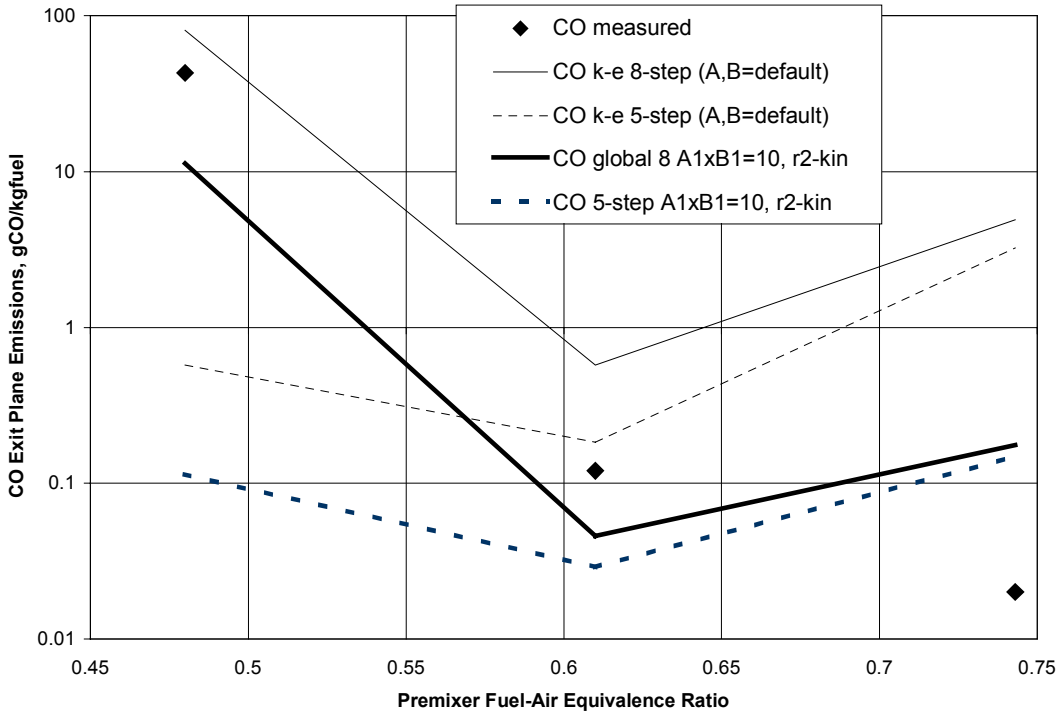

Figure 4.18 Carbon monoxide emissions at the exit plane of Combustor A. Operating conditions: pressure – 10 atm, inlet temperature - 650 K.

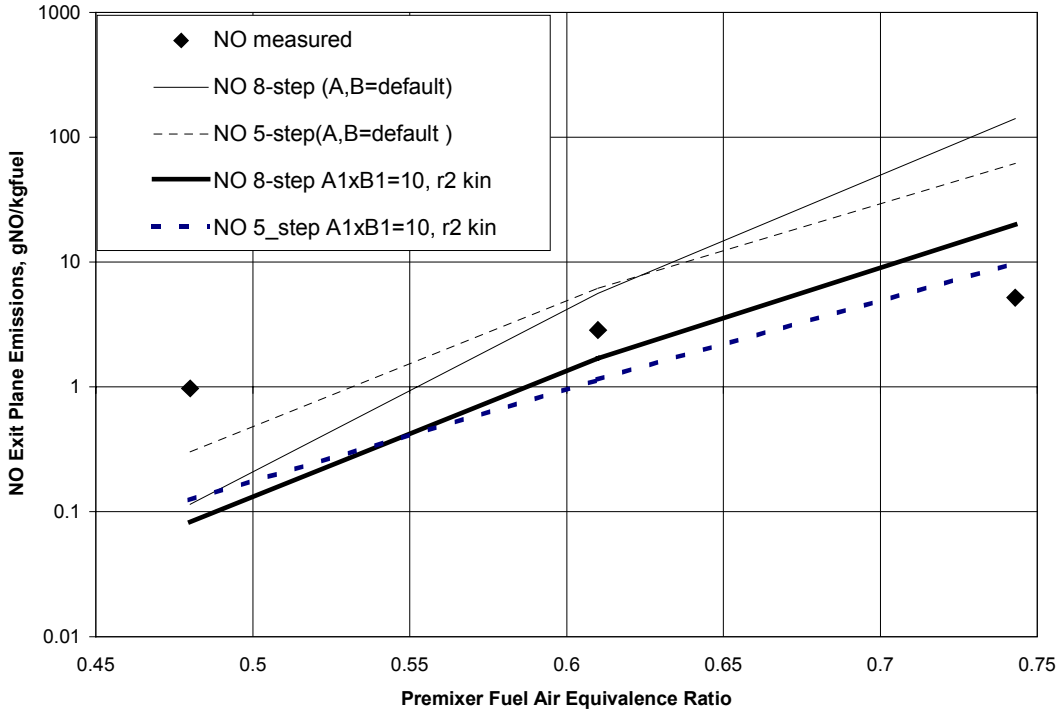

Figure 4.19 NO emissions at the exit plane of Combustor A. Operating conditions: pressure – 10 atm, inlet temperature - 650 K.

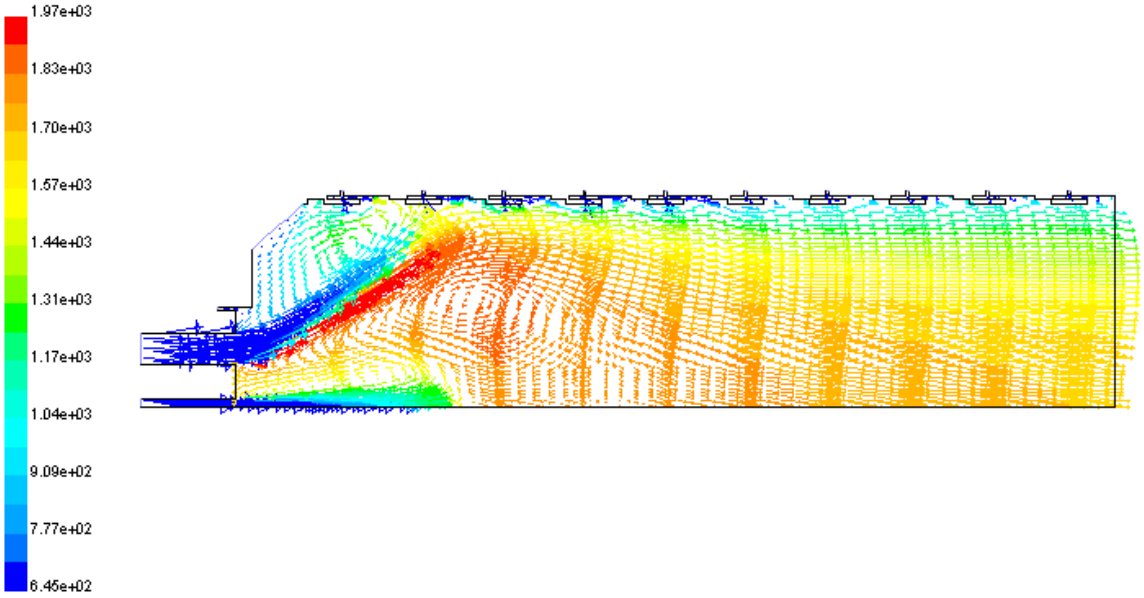

Figure 4.20 Velocity vectors colored by temperature for the CFD simulation using k-epsilon momentum closure model, 8-step global kinetic mechanism. Operating conditions: Pressure = 9.9 atm, Inlet temperature = 650 K, Fuel-Air equivalence ratio premixer = 0.61. Eddy break up model coefficients for reaction 1 are A=1000, B=0.01. Maximum temperature in the combustor = 1967 K.

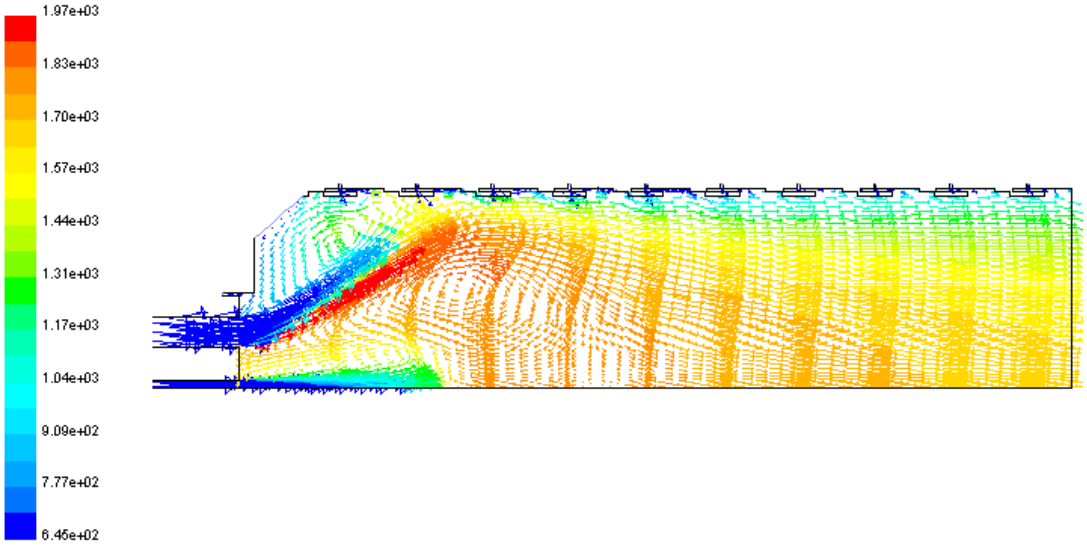

Figure 4.21 Velocity vectors colored by temperature for the CFD simulation using k-epsilon momentum closure model, 5-step, 8-atm global kinetic mechanism. Operating conditions: Pressure = 9.9 atm, Inlet temperature = 650 K, Fuel-Air equivalence ratio premixer = 0.61. Eddy break up model coefficients for the reaction 1 are A=1000, B=0.01.Maximum temperature in the combustor = 1966 K.

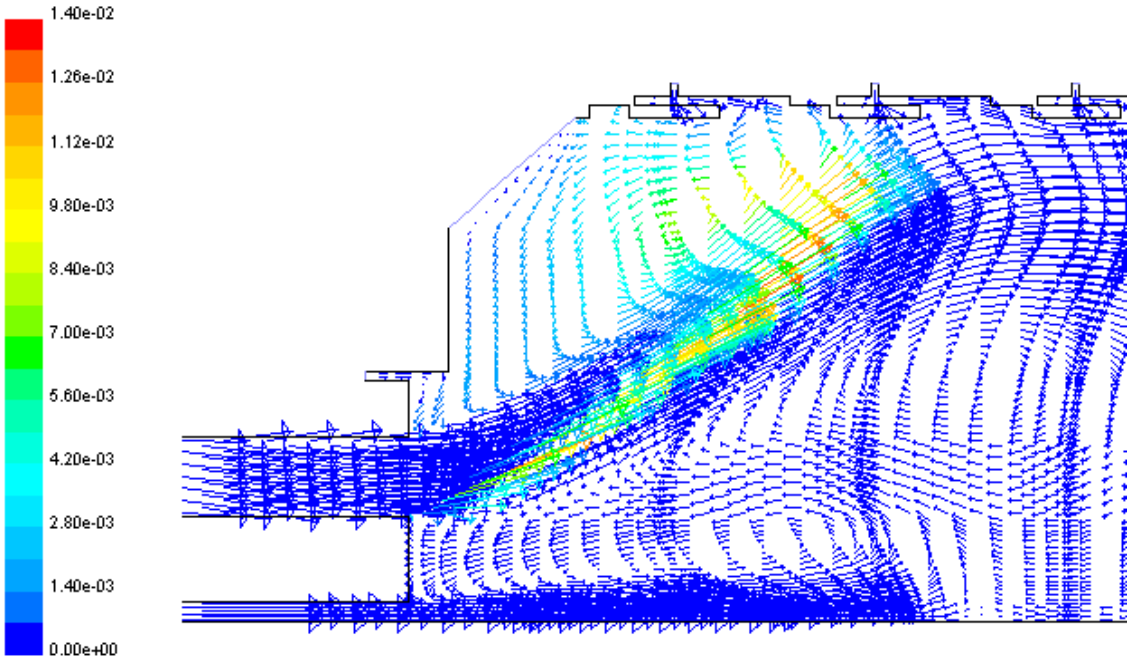

Figure 4.22 Velocity vectors colored by CO mole fraction for Fig. 4.20 (8-step global).). Maximum CO mole fraction = 1.4%

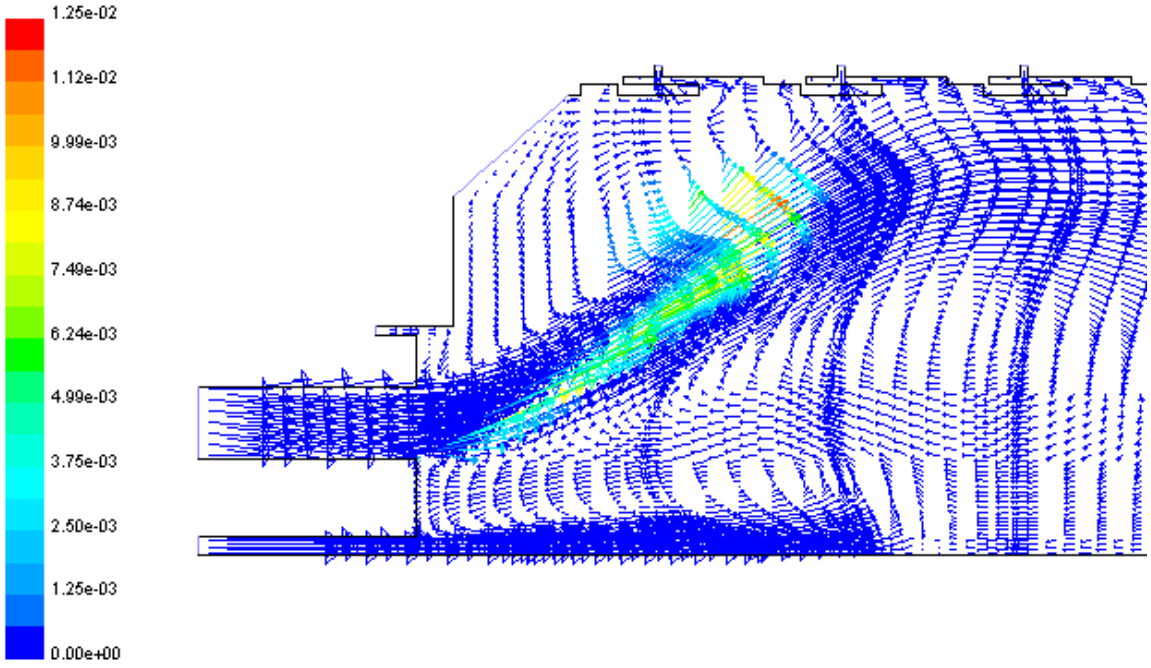

Figure 4.23 Velocity vectors colored by CO mole fraction for Fig. 4.21 (5-step global). Maximum CO mole fraction = 1.25%

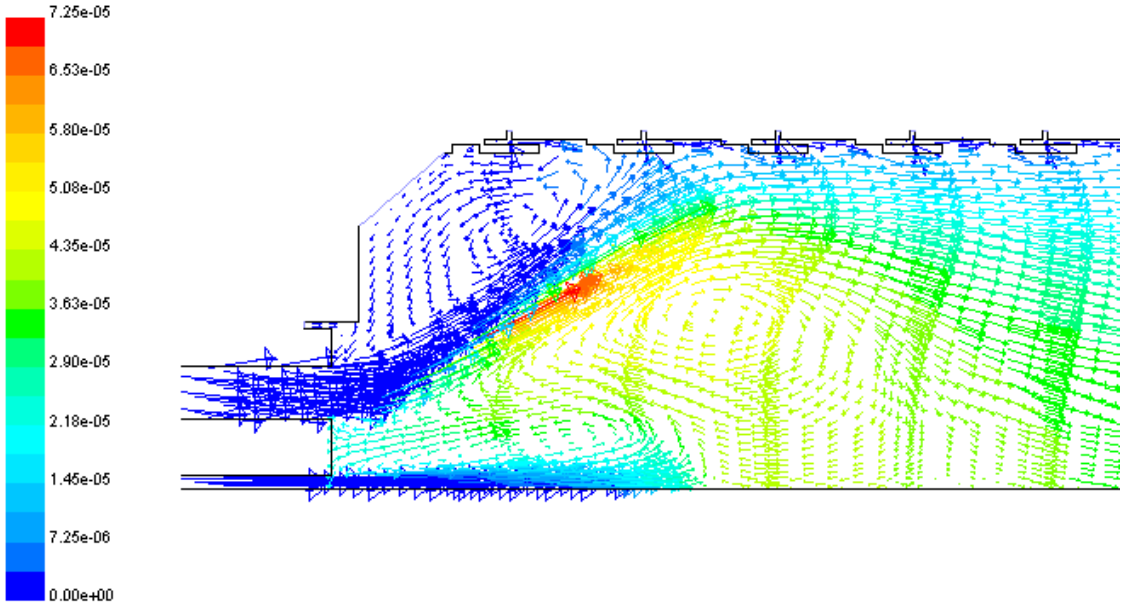

Figure 4.24 Velocity vectors colored by NO mole fraction for Fig. 4.20 (8-step global). Maximum NO mole fraction = 7.25e-5

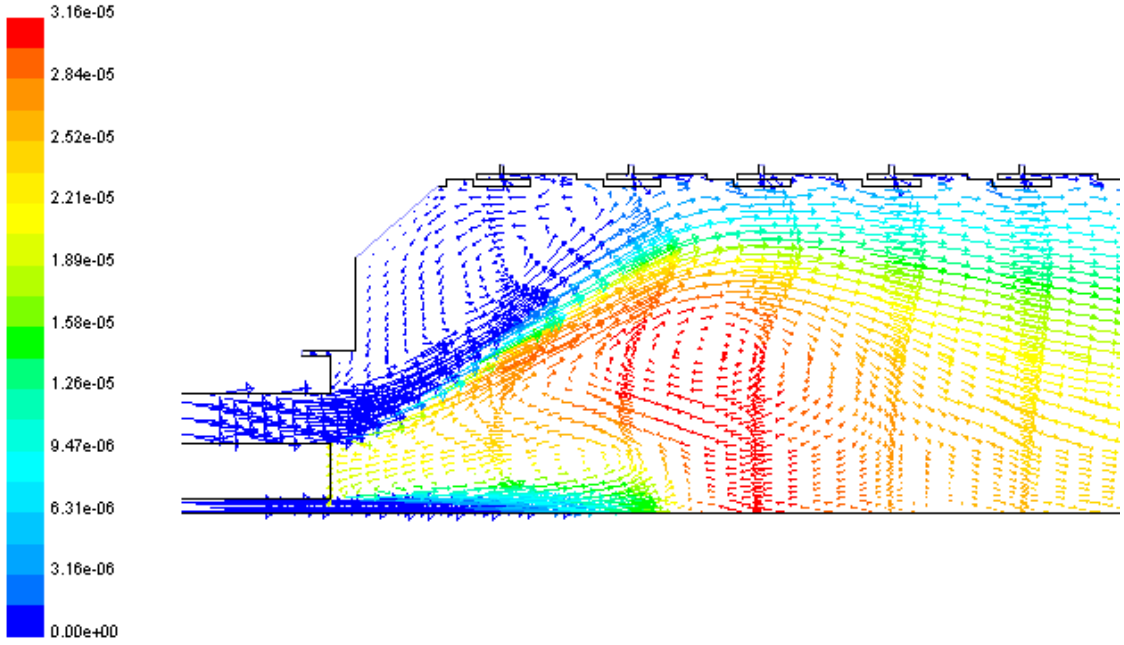

Figure 4.25 Velocity vectors colored by NO mole fraction for Fig. 4.21 (5-step global). Maximum NO mole fraction = 3.16e-5

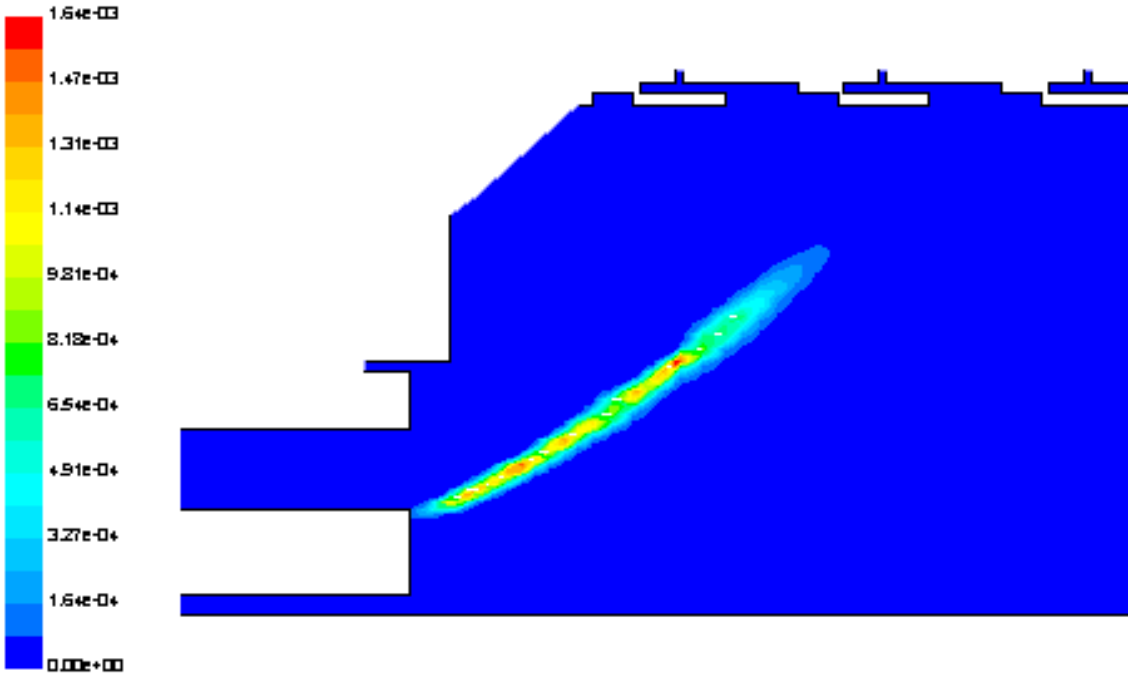

Figure 4.26 Contours of rate reaction 4 of 8-step global mechanism – NO formation via non-thermal N_2O and Zeldovich for Fig. 4.20

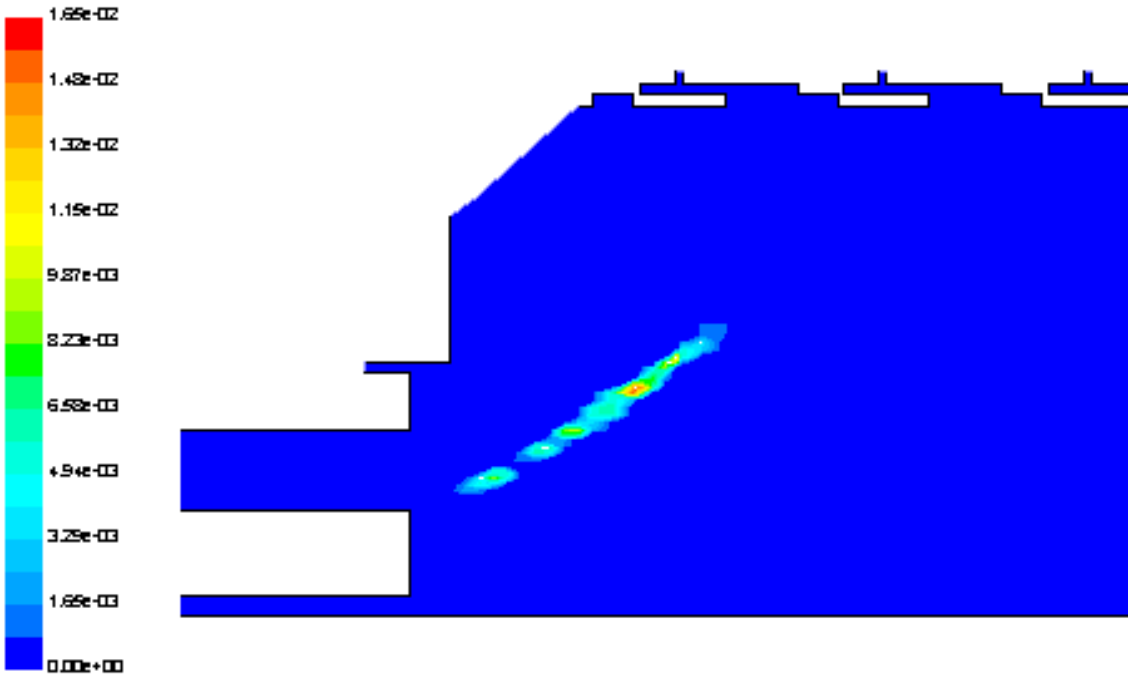

Figure 4.27 Contours rate reaction 5 of 8-step global mechanism – NO formation via prompt and NNH mechanisms for Fig. 4.20

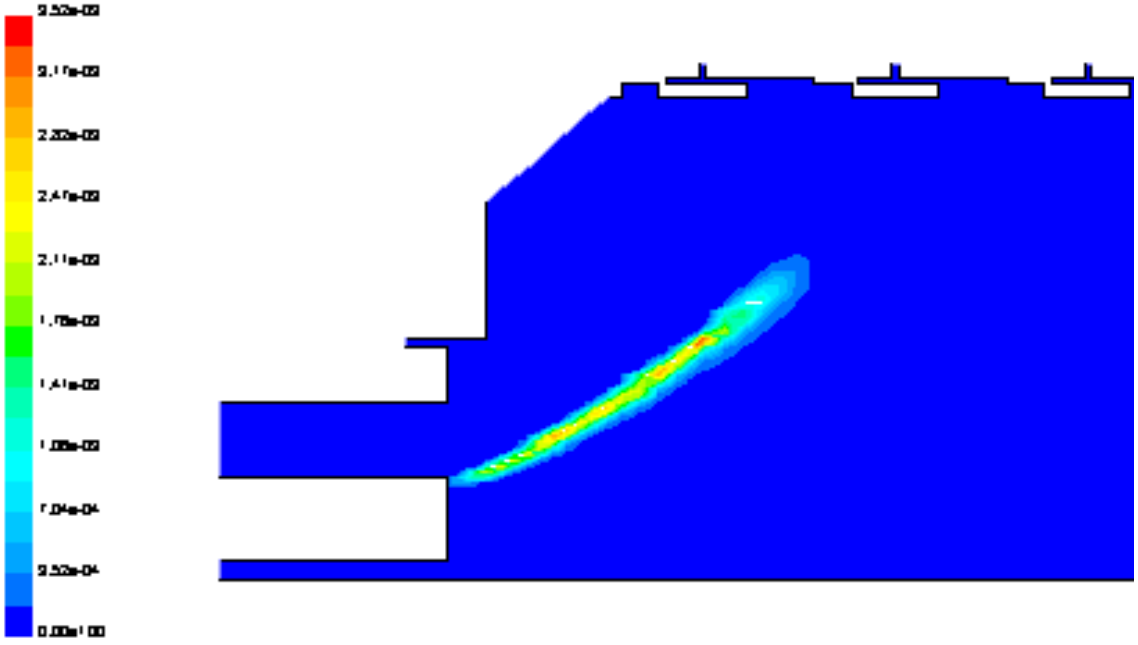

Figure 4.28 Contours of rate of non-thermal NO formation of 5-step global mechanism for Fig 4.21

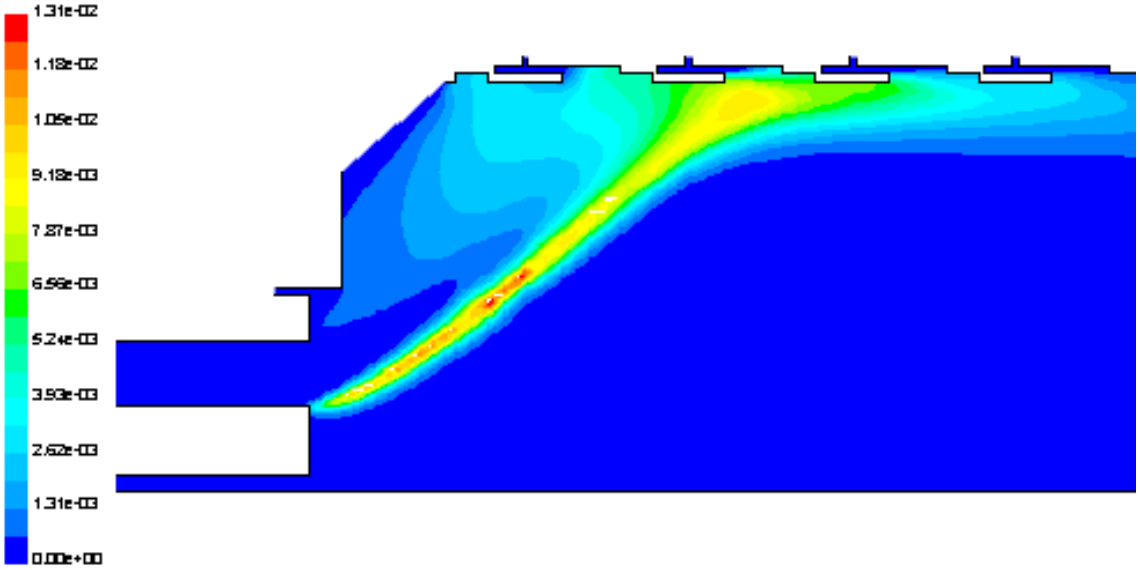

Figure 4.29 Velocity vectors colored by CO mole fraction for the CFD simulation using k-epsilon momentum closure model, 8-step global kinetic mechanism. Operating conditions: Pressure = 9.9 atm, Inlet temperature = 650 K, Fuel-Air equivalence ratio premixer = 0.48. Eddy break up model coefficients for reaction 1 are A=1000, B=0.01. Maximum CO mole fraction = 1.61%

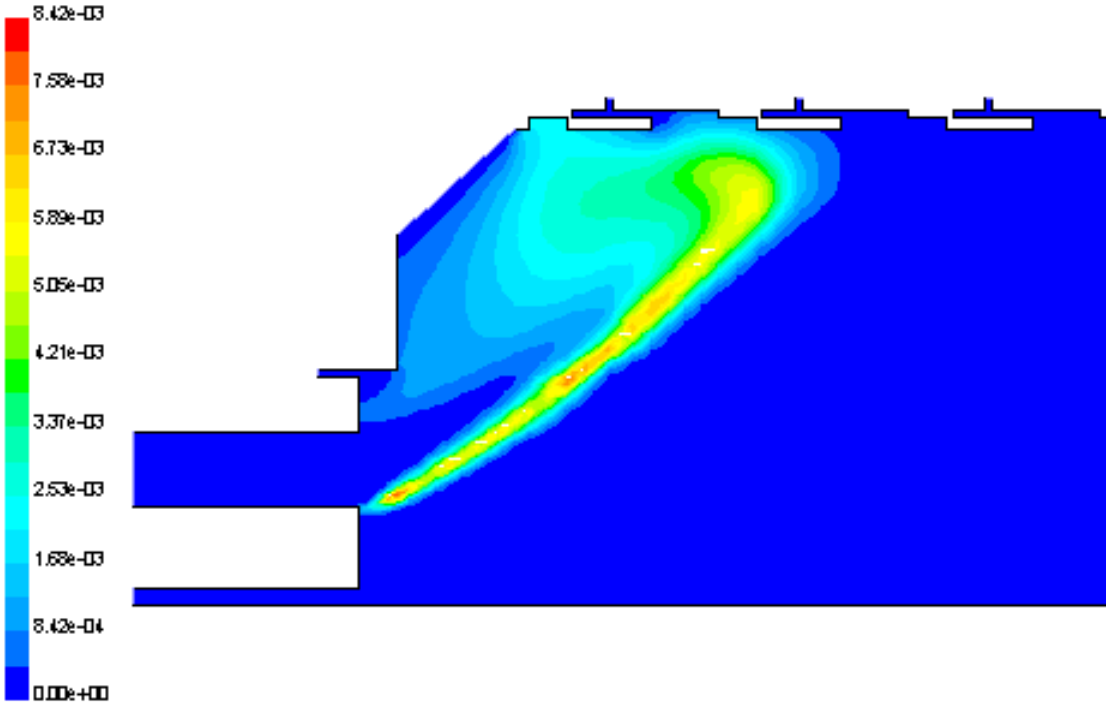

Figure 4.30 Velocity vectors colored by CO mole fraction for the CFD simulation using k-epsilon momentum closure model, 5-step global kinetic mechanism. Operating conditions: Pressure = 9.9 atm, Inlet temperature = 650 K, Fuel-Air equivalence ratio premixer = 0.48. Eddy break-up model coefficients for reaction 1 are A=1000, B=0.01. Maximum CO mole fraction = 1.44%

Chapter 5

Conclusion and Recommendations

5.1 Conclusions

An eight-step, pressure-sensitive global mechanism for methane oxidation with nitric oxide formation for CFD simulation of lean-premixed combustors used in advanced power generation gas turbine engines is developed and validated against the experimental databases. The global mechanism is based on the detailed chemical kinetic mechanism GRI 3.0 and covers the pressure range from 5 to 20 atmospheres and the fuel-air equivalence ratio range from 0.45 to 0.8.

The mechanism includes: one reaction for methane oxidation to CO and H_2O, one reaction for carbon monoxide oxidation, one reaction for carbon dioxide dissociation, two reactions for nitric oxide formation via non-equilibrium free radical chemistry, and three reactions for NO formation in zones of the equilibrium free radicals chemistry. Four major pathways of NO formation are considered in the development of the global: NNH, prompt, nitrous oxide, and Zeldovich.

Validation of the new eight step global mechanism is conducted by comparing results obtained with it in chemical reactor modeling against the experimental data of Rutar (2000) and Bengtsson (1998) for high-pressure jet-stirred reactors. The comparison shows that the eight-step global mechanism has a good agreement with GRI 3.0 and the experimental data for the cases with preheated inlet, an assumption was made in the development of the global mechanism. The cases with an unheated inlet show that the new global mechanism under-predicts the CO levels and NO formed via the nitrous oxide and Zeldovich mechanisms. The relative error in these cases is up to 15 %.

The CO_2 dissociation reaction of the global mechanism is tuned to match conditions in the post-flame zone as the gases approach the chemical equilibrium. Because of that the global mechanism under-predicts the rate of CO_2 dissociation in the non-equilibrium zones of combustion. While in the flame zone this effect seems to be negligible and mechanism predicts the correct amount of CO, just after the flame zone as the gases began to relax toward equilibrium the global mechanism reaches the CO-CO_2 equilibrium point faster than GRI 3.0.

Due to the absence of hydrocarbon radicals in the global mechanism and thus the absence of endothermic chemistry in the methane oxidation, the global mechanism tends to predict a higher flame zone temperature than GRI 3.0 when the residence time is close to the blowout condition. The blowout residence time predicted with the global mechanism is slightly lower than that found by GRI 3.0.

Additional validation of the eight-step global mechanism is obtained by employing it in a chemical reactor model simulation of a gas turbine combustor, and comparing the results

to the simulation using the full GRI 3.0 mechanism. The agreement between the global mechanism and GRI 3.0 is very close in this test

The new global mechanism is also tested in the commercial CFD code FLUENT 5 for modeling the gas turbine combustor. The can-type combustor is represented as a 2-D axi-symmetric flow with swirl. The momentum equations are closed using the standard k-epsilon closure model. The results of the CFD modeling of Combustor A with the eight-step global mechanism show good agreement of CO and NO exit plane emission with the experimental data for premixer fuel-air equivalence ratio of 0.6. More modeling efforts are required to find the agreement for cases significantly leaner and richer than the ϕ of 0.6.

5.2 Recommendations

The eight-step global mechanism should be used for modeling LP combustion, where the local fuel-air equivalence ratio is less that about 0.8. Generally, the mechanism predicts the CO and NO emissions most accurately for the cases with an operating pressure of 10 to 20 atm and a premixer fuel-air equivalence ratio of 0.5-0.65.

A more rigorous examination of the mechanism should be conducted in the CFD applications. The global mechanism should be tested using different CFD packages. A momentum closure model of higher order than k-epsilon, that does not assume isentropic turbulence, should be used. A different diffusion controlled reaction rate model should be used for the simulation or at least the coefficients A and B of the eddy break-up model should be adjusted.

Bibliography

Bengtsson K.U.M., Benz, P., Schareren, R., and Frouzakis, C.E. "NyOx Formation in Lean Premixed Combustion of Methane in a High Pressure Jet-Stirred Reactor." *Twenty-Seventh Symposium (International) on Combustion*, The combustion institute, (1998): 1393-1401.

Borghi, R. " Turbulent Combustion Modeling*". Progress in Energy and Combustion Science,* 14, (1988): 245-292.

Boussinesq, J. Theorie de l'ecoulement tourbillant. Mem. Presentes par Divers Savants, 1877.

Bozzelli, J.W., Chang, A.Y., and Dean, A.M. "Analysis of the Reactions H + N2O and NH + NO: Pathways and rate Constants Over a wide Range of Temperature and Pressure." *Twenty-Fifth Symposium (International) on Combustion*, The combustion institute, (1994): 965-974.

Chen, J.C., and Lin, C. A. "Computations of strongly swirling flows with second-moment closures." *Int. J. Numer. Meth. Fl.,* 30 (5), (1999): 493-508.

Dryer, F. L., and Glassman I. *Fourteenth Symposium International on Combustion,* The Combustion Institute, Pittsburg, PA, 1973, p. 987.

DuPont, V., Pourkashanian, M., and Williams. *A. Journal of the Institute Of Energy*, 66:20, (1993).

Glassman, I. *Combustion*, Academic Press, 1996.

GRI MECH 2.11. World Wide Web Site http://www.me.berkley.edu/gri_mech/, 1995.

GRI MECH 3.0. World Wide Web Site http://www.me.berkley.edu/gri_mech /, 1997.

Hogg, S. and M. A. Leschziner. "Computation of highly swirling confined flow with a Reynolds stress turbulence model." *AIAA J. 27 (1),* (1989): 57-63.

Jones, W. P., and Lindstedt, R.P. *Combustion and Flame*, 73:233, (1988).

Malte, P.C., Nicol, D.G. "CFD Modeling of Combustor A with Evaluation of the Five-Step Mechanism for Methane Oxidation with Nitric Oxide Formation." *Report to Solar Turbine, Inc., San Diego, California* (2000).

Mellor, A.M., Editor. "NO_x and CO Emissions Models for Gas-Fired, Lean Premixed Combustion Turbine: Final Report", Vanderbilt University (1996).

Miller, J.A. and Bowman, C.T. *Prog. In Energy and Combust. Science,* 15:287 (1989).

Nicol, D.G. "A Chemical and Numerical Study of NOx and Pollutant Formation in Low-Emission Combustion." *Ph.D. Dissertation*, University of Washington, Seattle, WA, 1995.

Peters, N. (2000). *Turbulent Combustion*. Cambridge University Press.

Pope, S. "PDF methods for turbulent reactive flows." *Progress in Energy and Combustion Science* 11, (1985): 119-192.

Rutar-Shuman, T. " NOx and CO Formation for Lean-Premixed Methane-Air Combustion in a Jet-Stirred Reactor Operated at Elevated Pressure," *Ph.D. Dissertation*, University of Washington, Seattle, WA, 2000.

Rutar, T., Malte P.C. "NOx Formation in High-Pressure Jet-Stirred Reactors with Significance to Lean-Premixed Combustion Turbines." *2001-GT-0067,* (2001)

Steele R.C. "NO_x and N_2O in Lean-Premixed Jet Stirred Reactors Operated from 1 to 7 atm." *Ph.D. Dissertation*, University of Washington, Seattle, WA, 1995.

Turns, S.R. *An Introduction to Combustion*. McGraw-Hill, 2000.

Westbrook, C.K., and Dryer, F.L. *Prog. Progress in Energy and Combustion Science,* 10:1, (1984).

Wilcox, D. C. (1993). *Turbulence Modeling for CFD*. La Canada, California: DCW Industries, Inc.